CHARACTERIZATION OF COUPLED AGING-MOISTURE DEGRADATION FOR HOT MIX ASPHALT CONCRETE

A Dissertation

by

MONA NOBAKHT

Submitted to the Office of Graduate and Professional Studies of
Texas A&M University
in partial fulfillment of the requirements for the degree of

DOCTOR OF PHILOSOPHY

Chair of Committee,	Maryam S. Sakhaeifar
Co-Chair of Committee,	Robert L. Lytton
Committee Members,	Nasir Gharaibeh
	Anastasia Muliana
Head of Department,	Robin Autenrieh

December 2018

Major Subject: Civil Engineering

ABSTRACT

Durability of asphalt concrete is significantly influenced by *aging* and *moisture damage*. These two phenomena occur simultaneously in the field, resulting in early degradation of asphalt pavements. Although there exists a significant number of studies in the literature addressing these phenomena individually, research efforts to characterize the coupling effect of aging-moisture degradation in asphalt concrete are very limited. This was the main motivation for conducting the study presented in this dissertation.

The focus of this study is to formulate an Integrated Aging-Moisture Predictive model (IAMP) for dynamic modulus of asphalt concrete as a function of aging temperature, loading frequency, and exposure time. The integrated model combines a predictive kinetic-based aging model with a moisture damage one. The aging model characterizes the dynamic modulus master curve of an aged asphalt concrete based on aging properties (i.e., activation energies and pre-exponential), temperature, and exposure time. This model is then modified by incorporating the moisture damage model, which is developed based on intermolecular bond energy/force, and the mechanisms of cohesive and adhesive failures. The moisture damage model assumes water vapor diffusion, which is the dominant moisture transport mode in asphalt pavements. Parameter calibration and model validation for a Superpave mixture is done through performing dynamic modulus tests (on fine-aggregate and full mixture specimens), as well as Bitumen Bond Strength test (on the adhesive bond between aggregate and asphalt binder). Validation results show the competence of the proposed model in predicting the dynamic modulus of asphalt concrete under simultaneous effect of aging and moisture damage.

DEDICATION

To my dearest parents for their endless love and unconditional support

In memory of my beloved brother

ACKNOWLEDGEMENTS

I am sincerely grateful to people who helped me to accomplish this achievement. First of all, I would like to thank my husband, Mohammad, not only for his support throughout this journey but also for his constructive comments and technical advice, specifically on the mathematical aspect of my work. Also, I would like to thank my committee co-chairs, Drs. Robert Lytton and Maryam Sakhaeifar, for providing me with the opportunities and for their precious guidance and support throughout the course of this research. Thanks also go to my advisory committee members, Drs. Nasir Gharaibeh and Anastasia Muliana, for their pertinent comments and support. Appreciation is extended to Drs. David Newcomb, Amy Epps Martin, Bjorn Birgisson, and Charles Gurganus for their contribution to my professional development. I would also like to express my gratitude toward Dr. Derun Zhang for his instructive comments during the last stages of this work.

CONTRIBUTORS AND FUNDING SOURCES

This work was supervised by a dissertation committee consisting of Dr. Maryam Sakhaeifar (advisor), and Dr. Robert Lytton (co-advisor) and Dr. Nasir Gharaibeh of the Department of Civil Engineering, and Dr. Anastasia Muliana of the Department of Mechanical Engineering. All work for this dissertation was completed independently by the student. Assistantships and fellowship awarded to the student over the course of this research are listed as follows:

1. Graduate Research/Teaching Assistantship Awarded by Civil Engineering Department
2. Graduate Teaching Fellowship Awarded by Dwight Look College of Engineering

TABLE OF CONTENTS

LIST OF FIGURES

Page

LIST OF TABLES

Page

1. INTRODUCTION

Asphalt Concrete (AC) is one of the oldest composite materials used in pavements, which is composed of two distinct phases; namely coarse aggregates and Fine Asphalt Matrix (FAM). Coarse aggregate is the portion larger than No. 16 sieve, and FAM is the combination of asphalt binder and fine aggregate passing No. 16 sieve. Coarse aggregate has the main contribution in compressive strength of the mixture, while FAM binds coarse aggregates and supports tensile strength of the mixture. The mechanical characteristics of AC depend not only on the properties of FAM and aggregates but also on the strength of interfacial bond between them (i.e., aggregate and asphalt). The interfacial bond is responsible to transmit loads from FAM to aggregate. In other words, the degree to which a load is transferred from FAM to aggregate is controlled by the strength of the interfacial bond.

Durability of AC is mainly affected by environmental changes such as aging and moisture transport within AC pavements. The combined effect of these changes and traffic loading results in the formation of various types of distresses in AC pavements, such as pothole, stripping, fatigue cracking, and so on. In fact, aging and moisture accelerate the evolution of pavement distresses under the traffic loading. However, even in absence of traffic loading, the environmental effects deteriorate properties of AC, resulting in the reduction of in-service life of pavements and need for early rehabilitation.

Degradation of mechanical properties of AC due to aging and moisture occur through separate mechanisms. Aging is the process of stiffening asphalt mixture due to oxidation, volatilization and molecular agglomeration (Newcomb et al. 2015), resulting in the brittleness of AC and acceleration of cracking. Aging of asphalt mixture consists of two chronological stages;

a fast-rate reaction that results in an initial jump in the stiffness in a short time, and a constant-rate reaction which causes a constant increase in the stiffness at a much slower rate. Degradation of AC due to presence of moisture, referred to as moisture damage, is a complex phenomenon involving thermodynamic, chemical, physical and mechanical components (Caro et al. 2008). In general, moisture degrades AC in two ways: 1) adhesive failure and 2) cohesive failure. Adhesive failure occurs when water enters the interface between aggregate and asphalt via the air voids or by diffusion through the asphalt binder, causing the deterioration of interfacial bond strength. Cohesive failure happens when water diffuses into FAM, resulting in the reduction of its cohesive strength and stiffness.

Moisture damage starts when water – in the form of liquid or vapor – transports into the AC pavements. Water transport happens through three main mechanisms; namely permeability, capillary rise and diffusion (Caro et al. 2008). Permeability and capillary rise are mostly controlled by the air void system of asphalt pavements while diffusion is affected by the diffusivity of water molecules in the asphalt binder and its molecular structure. Water vapor diffusion in the AC pavement is the main contributor in the moisture damage (Luo et al. 2018). It occurs because of the Relative Humidity (RH) differential that exists between atmosphere above the asphalt layer and the subgrade below the pavement structure. RH of the atmosphere changes with location and weather. However, RH in the subgrade is always near 100% and so it serves as a reservoir beneath the pavement, resulting in a diffusive motion of water vapor toward the pavement. Several research studies have reported the moisture damage in pavements located in the region with desert/semiarid climate such as Arizona (Hicks 1991; Tong 2013). This further implies the pivotal role of subsurface vapor diffusion in formation of the moisture damage.

Over the in-service life of pavements, age-hardening and moisture damage occur simultaneously at different intensities and rates, which depends on their aging characteristic and moisture sensitivities. There has been extensive research efforts about the individual impact of aging and moisture damage on properties of AC and performance of asphalt pavements. However, there has been limited research looking at the combination of aging and moisture damage, and the coupling effect of them on mechanical properties of AC. In order to investigate the detrimental effects of environmental condition, one should consider the combined effects of aging and moisture damage as it happens in the field during the service-life of a pavement. Development of an analytical model that quantifies such a coupling effect on mechanical properties of AC provides valuable information for pavement design. This dissertation proposes an analytical model to predict the dynamic modulus of asphalt concrete based on the interaction between aging and moisture diffusion, and the mechanisms involved in age-hardening and moisture damage of AC. Dynamic modulus is one of the major material properties used for pavement design. Therefore, development of such a predictive model will help with designing asphalt pavements that perform better in the field and preventing environmental-related premature failures.

1.1 Research Objectives

The main objectives of this study include:

- Developing a predictive aging model to construct the dynamic modulus master curve of asphalt concrete;
- Quantification of the detrimental effect of water vapor diffusion on dynamic modulus of aged asphalt concrete through formulating a moisture damage model;

- Developing an integrated aging-moisture model to predict the dynamic modulus of asphalt concrete;

1.2 Literature Review

This section gives an overview on the related works reported in the literature. The focus here is on drawing a big picture rather than technical details. More details regarding existing aging and moisture models will be given later in the corresponding sections.

1.2.1 Moisture Damage

Moisture damage in asphalt concrete is defined as degradation of mechanical properties due to the presence of moisture (Caro et al. 2008). It is a progressive deterioration which happens when water in a liquid or vapor state transports into the asphalt pavements, and deteriorates the adhesive bond between the aggregate surface and asphalt binder, referred to as the *adhesive damage,* and the cohesive resistance within the asphalt binder, known as the *cohesive damage* (Kiggundu and Roberts 1988). Moisture damage comprises two steps, first, moisture transports into the asphalt pavements through permeability, diffusion and/or capillary rise. Second, it causes the adhesive and cohesive damages, which are considered as the responses of pavements to the presence of water. The modes of water transport are controlled by the components of mixture such as air void sizes and their connectivity, diffusivity of water molecules in mixture and asphalt binder, aggregate absorption capacity and so on. Permeability of surface water is mostly related to rainfall and drainage condition (Caro et al. 2008). However, the field evaluations of pavements located in some regions with low levels of annual rainfall, like Arizona and New Mexico, show the severe moisture damage (Hicks et al. 2003). This suggests that subsurface vapor diffusion and capillary rise are as important as permeability to induce the moisture damage.

The amount of water vapor diffused into the asphalt binder is dependent on the water holding capacity of the binder, diffusivity of water vapor into the asphalt binder, and relative humidity. The two former factors are controlled by the thermodynamic and chemical characteristic of binder, but the latter one depends on the environmental condition. Kassem et al. (2006) measured the diffusivity of water vapor in three mastics (combination of asphalt binder and fillers smaller than 0.075 mm) by measuring the rate of change in suction with time using the thermocouple psychrometers. They found a correlation between diffusion coefficients and moisture damage observed in the field for asphalt pavements corresponding to the mastics; a high diffusion coefficient was associated with a poor moisture resistant pavement. In another study, Cheng et al. (2002) demonstrated that the mixtures composed of asphalt binders with high water holding capacity are more susceptible to moisture damage.

The adhesion properties of an asphalt-aggregate bond is affected by moisture. Three main interactions are involved in the adhesive bond (Hefer et al. 2005). The first interaction is related to electrostatic forces between the ions in aggregate and binder, resulting from the Coulomb forces. The second one corresponds to electrodynamic forces between molecules, which results from Van der Waals intermolecular bonding. Combination of first and second interactions, referred to as *Physico-chemical* interaction, is related to a thermodynamic property of the material known as the *surface free energy* (Caro et al. 2008). The third interaction pertains to the covalent bond, resulting from creation of a new compound due to the reaction of asphalt binder with mineral aggregate. Work of adhesion between materials is calculated from the surface free energy of each material involved in the bond. Moisture impacts on the cohesion of asphalt binder as well as the adhesion bond. Water molecules diffuse within asphalt binder's molecular chains, resulting in 'softening.

With regard to the characterization of moisture damage, extensive analytical and experimental efforts have been made to quantify the moisture damage based on the thermodynamics and mechanics. The quantification of moisture damage in most of the studies in literature include three steps : 1) defining a moisture conditioning method, 2) defining a performance measure obtained by conducting a performance test, and 3) calculating the damage factor as the ratio of performance measure in dry and wet conditions. AASHTO T283, Copeland et al. (2007), Song et al. (2005), Masad et al. (2006c), Birgisson et al. (2003), Arambula et al. (2007) and Lytton et al. 2005 are several examples of the works conducted in this area. For more information on the abovementioned approach, refer to the review paper by Caro et al. (2008). Such a quantification method provides a valuable tool that can also be used in mix design specifications. A threshold value can be assigned to the damage ratio to separate moisture resistant mixtures from those susceptible to the moisture.

Moisture damage is due to the moisture transport within the asphalt pavement. Numerical modeling can be used to simulate the moisture transport. Masad et al. (2007) and Kutay (2007a; 2007b) developed numerical models to simulate the water flow in porous asphalt mixtures. In another study, Kringos et al. (2008b; 2008c) developed a finite element program to simulate the transport of water flow and vapor diffusion in the pavement, and model moisture damage based on coupling physical and mechanical processes contributing to the moisture damage. They conducted an extensive parametric analysis to investigate the effect of moisture damage on the asphalt mixture response (i.e. stress and strain). In a similar study, Caro et al. (2010), developed a micromechanical finite element modeling to show the impact of material properties and loading condition on the response of asphalt mixtures subjected to moisture diffusion. Their

models incorporate the water diffusion and fracture mechanics to study the deterioration of mixtures.

1.2.2 Age-hardening

Aging of asphalt pavement has been recognized to be one of the key factors affecting the pavement performance. It happens due to the reaction of asphalt binder with oxygen and loss of volatile oils. As a result, the brittleness and stiffness of binder increase, which in some cases leads to higher cracking-susceptibility and shorter service life of an asphalt concrete. Extensive research efforts have been conducted to study the effect of aging on the rheological properties of asphalt binders (Mirza and Witczak 1995; Peterson 1998; Ruan et al. 2003; Glover et al. 2005; Ling et al. 2017). While most of these works aim to quantify the effect of aging on the fundamental characteristics of asphalt binder, there is a need for conducting research studies to directly model changes in physical properties of asphalt mixtures due to aging.

The Global Aging (GA) Model (Mirza and Witczak 1995), which is currently included in the Pavement ME (Mechanistic-Empirical) Design, is a binder-based model. This model considers the asphalt binder as the only contributing factor to age-hardening characteristic of the asphalt mixture. To consider the effect of aging, GA model predicts the viscosity of an aged binder, and then uses it in a statistically-developed dynamic modulus predictive model. It has been agreed upon that other factors such as antistripping additives, warm mix asphalt technology, aggregate types, air void and use of Reclaimed Asphalt Pavement (RAP) have impacts on aging characteristic of asphalt mixtures (Yin et al. 2017; Garcia Culalon 2016). In some mixtures, aggregate fraction can act as a catalyst in the oxidation process (Barbour et al. 1974, Petersen et al. 1974). Also, the adhesion between aggregate and asphalt binder alters aging susceptibility of asphalt mixtures (Bell and Sosnovske 1994). The strength of this adhesion

depends on the aggregate, mixing technologies, and additives. Some mineral aggregates adsorb polar components of the asphalt binder, resulting in a reduction in the amount of oxidation products (Petersen et al. 1974). Also, the air void content and aggregate morphology play important roles on the aging progress as they control accessible air for oxidation. Therefore, in order to have a realistic prediction of hardening performance of each asphalt mixture, its unique aging characteristic should be taken into account.

One of the mechanical properties of asphalt mixture impacted by aging is dynamic modulus. Dynamic modulus captures linear viscoelastic behavior of asphalt concrete, and is recognized as one of the most important material properties in the mechanistic-empirical pavement design and continuum damage models. Thus, developing a model to predict the changes of dynamic modulus due to oxidative aging based on mixture characteristics (not only binder) will be of a significant importance. Along this line of research, Luo X. et al. (2015; 2017) developed a kinetic-based aging predictive model to estimate the modulus of field cores. Their model inputs aging temperature and aging time, but it does not take into account the variation of loading temperature and loading frequency. This study aims to improve their model by incorporating the latter factors (i.e., loading temperature and frequency)

1.2.3 Coupling Aging with Moisture Damage

With regard to the coupling effect of aging and moisture, related works in the literature can be divided into three groups. 1) Those that study the impact of the presence of moisture on the aging process. 2) Research works that examine the effect of aging on the moisture damage. 3) Studies that look into the effects of coupling aging with moisture damage on the thermodynamic and mechanical properties of asphalt binder and asphalt mixture. Works that fit into the first and

second groups are detailed in Section 2 as they are considered as the basis for development of an integrated model. This section focuses on the third group. However, as mentioned earlier in the introduction, limited research has been conducted on this area.

Pan et al. (2016) studied the moisture impact on asphalt binder before and after oxidation using molecular dynamic simulations, which is a numerical approach for the simulation of the physical movement of atoms and molecules. They compared bulk modulus, density and viscosity of unaged and aged binder under various moisture content, and observed that bulk modulus and viscosity of aged binder decreased faster than unaged binder with moisture content. They concluded that aged asphalt binder is more susceptible to moisture damage. In another study, Copeland et al. (2007) evaluated the impact of aging combined with moisture on bond strength between asphalt binder and aggregate, which was measured using pneumatic adhesion tensile testing instrument (PATTI). They observed that aging increases the cohesive strength of asphalt binder, but aging combined with moisture decreases the adhesive strength. Also, their results suggest that moisture conditioning combined with aging decreases the bond strength more than moisture conditioning alone. Similar observation was reported by Aguiar-Moya et al. (2015). They characterized the bond strength between the RTFO and PAV-aged asphalt binder and several aggregates using bond strength test under dry and wet conditioning, and observed that the loss of adhesion for PAV-aged binder are greater than unaged and RTFO-aged samples when they are subjected to water.

1.3 Dissertation Outline

This dissertation contains 8 sections. The current section explains the statement of need, research objectives and outline of the document. Section 2 provides a summary of research studies conducted on oxidative aging and moisture damage. Section 3 focuses on the research

methodology, conditioning approach, and experimental plan adopted in this study to fulfill the objectives. This section also includes a comprehensive literature review on the interaction between the mechanisms of aging and moisture damage. The aging model is developed and validated in Section 4. Section 5 and 6 focus on the formulation of moisture damage model based on two separate mechanisms, i.e., cohesive and adhesive, involved in moisture damage. The integrated aging-moisture predictive model is formulated, calibrated and validated in Section 7. Finally, Section 8 concludes this study and presents some recommendations for future work.

2. RESEARCH METHODOLOGY

In order to develop a model that takes into account the effects of coupling moisture and aging on dynamic modulus of asphalt concrete (AC), the interaction between age-hardening and moisture damage needs to be comprehended. In other words, the impact of age hardening on moisture damage, and the effect of moisture diffusion on oxidative aging rate should be evaluated. Understanding this interaction will help to formulate a proper predictive model that captures the changes of dynamic modulus for the AC subjected to both aging and moisture diffusion.

2.1 Effects of Moisture Diffusion on Oxidative Aging

A comprehensive literature review was performed to study the effect of moisture diffusion on oxidative aging. The purpose of this section was to explore whether presence of water in the vapor or liquid state has significant impact on aging kinetic or not. It has been agreed upon that oxidative aging is influenced by factors such as aging temperature, asphalt aging characteristic (i.e., activation energy, pre-exponential factor) and oxygen diffusion rate into the asphalt binder. Another factor to be investigated is the presence of moisture during aging, and potential change in the chemical composition of a binder. Obviously, moisture in the form of liquid or vapor exists in the field, and comes from different sources such as ground water, snow and rain. Therefore, its impact on aging-hardening characteristic of AC need to be studied in laboratory aging procedures and aging models. There have been several research efforts aimed to study this matter. Thomas (2002) studied the effect of water during the laboratory aging of asphalt binder. He used the pressure aging vessel (PAV) to age a set of asphalt binders used in Strategic Highway Research Program (SHARP) at 60 and 80°C in the

presence or absence of water for various time periods. Asphalt binders were first aged using the Rolling Thin-Film Oven (RTFO) test (AASHTO T 240), and then RTFO aged binders were further aged using the PAV test (AASHTO PP1). Samples were aged either at 60 or 80°C for 144, 240 and 480 hours. For those aged in the presence of water, 15 ml of water in a glass dish container was put in the pressure vessel. The air pressure in the vessel was 2.1 MPa, and the partial pressure of water in the vessel was 0.02, and 0.047 MPa at 60 and 80°C, respectively. The chemical properties of the aged binders were determined by measuring the concentrations of carbonyl and sulfoxide using infrared spectroscopy, and the rheological properties were estimated using a Dynamic Shear Rheometer (DSR) test. It was concluded that PAV aging in the presence of moisture accelerates the aging kinetic process, and that binders which were PAV-aged in the presence of water has more carbonyl compounds compared to those PAV-aged in a dry vessel. Also, the presence of water resulted in the average stiffness increase of 18% for all binders. Thomas (2002) explained the observation by this theory that at high pressure, water disrupts the colloidal structure of asphalt, resulting in generating additional compounds to react with oxygen.

The effect of supercritical water on changing the chemical structure of asphalt binder has been widely used in the oil generation process (Hu et al. 1999; Sato et al. 2003; Schlepp et al. 2001). Supercritical water is the water at a pressure and temperature above its liquid-vapor critical point, where phase boundaries disappear, and water liquid and vapor can coexist. The critical point of water occurs at 647 K (705° F or 374° C) and 22.064 MPa (218 atm) (Cooper et al. 2007). Supercritical water, known as dense steam, can be employed for upgrading asphalt and converting asphaltene to maltene fractions. Hydrogen atoms in supercritical water are able to cap the free radicals produced during the thermolysis of asphalt, resulting in an increased asphaltene

conversion (Sato et al. 2003). Therefore, it can be concluded that at high pressure and temperature, water is able to change the extent of chemical aging of an asphalt bindet given that it apparently participates in the oxidative reaction and alters the chemical composition of binders.

PAV laboratory aging has been used to simulate long-term field aging in the lab. However, it has been argued that PAV aging might not be a realistic method to simulate field aging because field aging occurs at the atmospheric pressure all along (Huang et al. 2012). Huang et al. (2012) conducted a comprehensive study to determine whether the presence of moisture during aging at temperature and pressure happening in the field had any significant impacts on the oxidation rates of thin asphalt binders. Therefore, he aged five binders at a pavement service temperature of 60°C and atmospheric pressure for varying time lengths in the dry and humid conditions. For samples aged in the presence of water, a humid environment was prepared by including a 2800-mL water dish in the oven. Humidity of the oven was controlled to be at 99% during aging. The chemical composition and rheological properties of the dry-aged and moisture-aged samples were determined by Fourier Transform Infrared Spectroscopy (FTIR) and DSR. The properties of dry-aged samples were compared with those of moisture-aged samples to determine whether the presence of moisture has any significant impacts on the oxidation rate at 1 atmospheric pressure. The results showed that moisture does not affect the oxidation rate at the ambient pressure, and that dry-aged and moisture-aged samples had almost the same carbonyl compound concentrations over the aging time. Also, complex modulus and phase angle master curves for dry-aged and moisture-aged samples were almost similar, and fell on top of each other. The results implied that the presence of moisture during aging at ambient pressure and temperature does not affect the rheological properties of asphalt binders.

Saturation Aging Tensile Stiffness (SATS) test was developed in UK to evaluate the resistance of asphalt mixtures to moisture damage (Collop et al. 2004). SATS is a combined aging/moisture sensitivity laboratory test which consists of saturating AC samples, and subjecting them to high temperature and pressure for a certain time period. The modulus of AC samples measured after conditioning divided by the initial modulus is defined as an indicator of the moisture sensitivity of asphalt mixture to the combination of moisture and aging. SATS test procedure was developed after conducting a set of preliminary experiments focused on combining the various aging and moisture conditioning approaches. The purpose of the preliminary works was to develop a conditioning method that accounts for the effect of aging and moisture together on the resistance of asphalt mixture to moisture damage. Six various aging/moisture procedures were examined in the preliminary studies. In one of the procedures, which resulted in a most severe moisture damage and reduction in initial stiffness, AC samples were placed in a partially saturated pressure aging vessel at 85°C and 2.1 MPa for 65 hours. Then, asphalt binder was recovered from specimens and tested by DSR. The complex shear modulus and phase angle master curves for the recovered binder were compared with those for the same binder subjected to long term PAV aging (referred to as PAV-aged binder). It was observed that the recovered binder and PAV-aged binder had similar master curves falling on top of each other. The results indicate that the aging level of PAV-aged binder is similar to that of a recovered binder, and that the presence of moisture in the pressure aging vessel even at high pressure does not have any significant effects on the aging rate.

As mentioned earlier, the results of study conducted by Thomas (2002) suggests that the presence of moisture during PAV aging affects the aging kinetic of asphalt binders. However, the results obtained by Collop et al. (2004) suggests that once AC is aged in the pressure aging

vessel in the presence of water, water does not influence the aging rate. It should be noted that Thomas subjected thin asphalt binder to oxygen and moisture under high temperature and pressure while in the study conducted by Collop and his colleagues compacted mixtures were subjected to the oxygen and moisture under high temperature and pressure. One possible explanation is that 65 hours might be sufficient time for water vapor at 2.1 MPa and 85°C to diffuse in thin asphalt binder and change the colloidal structure, which results in the production of more oxidized binder. However, under the same pressure and temperature, a longer conditioning period is needed for compacted mixture to reach to the same aging level as thin binder.

Water has been employed as a foaming agent in the production of warm mix asphalt (WMA). WMA technologies are aimed to reduce mixing and compaction temperatures for asphalt mixtures by adding warm mix additives or mechanical foaming processes (Yin et al. 2016). WMA technologies offer a number of benefits over Hot Mix Asphalt (HMA) such as improved workability, extended hauling distance, decreased fuel consumption and emissions (Cucalon et al. 2015). However, there has been some concerns about the performance of WMA mixtures with regard to the moisture susceptibility and age hardening properties as a result of adding water in the production process (Yin et al. 2016). Yin et al. (2011) conducted a study on the laboratory aging conditioning of WMA and HMA. He showed that the initial stiffness of HMA is more than the initial stiffness of WMA given that WMA is produced at the lower mixing and compaction temperatures. However, the difference in stiffness reduces with long-term aging, and eventually stiffness of WMA reaches to the stiffness of conventional HMA after being in-service for certain times (Yin et al. 2017). This suggests that the additional moisture

introduced by some WMA technologies does not have any significant effect on the long-term aging rate of mixtures.

With regard to the interaction between moisture diffusion and oxidative aging, the review of research efforts in the literature indicates that the presence of water during aging does not affect the oxidation rate of asphalt mixtures if aging occurs at the ambient pressure and pavement temperature in the field. The following section evaluates this interaction with regard to the effect of oxidative aging on moisture damage.

2.2 Effects of Oxidative Aging on Moisture Damage

To evaluate the effect of aging on moisture damage, a complete understanding of mechanisms including moisture damage is needed. These mechanisms are explained in details in Section 1.2.2. Adhesive and cohesive failure are two major mechanisms of moisture damage that occur in the field or laboratory moisture conditioning approaches. Adhesive failure occurs when water enters the interface between aggregate and asphalt via the air voids or by the diffusion through the asphalt binder, causing the deterioration of aggregate-asphalt bond. Cohesive failure happens when water diffuses into the asphalt film, resulting in the reduction of cohesive strength and stability of mixtures (Lytton et al. 2005). In general, water transports into the AC pavements through three main mechanisms including permeability, capillary rise and diffusion (Caro et al. 2008). Permeability and capillary rise are mostly controlled by the air void system of asphalt pavements while diffusion is affected by the diffusivity of water molecules in the asphalt binder and its molecular structure.

Surface energy measurement of aggregate and asphalt binder are recognized as effective tools to evaluate the moisture damage potential in asphalt mixtures (Kim et al. 2004). A nonpolar

component and an acid-base component compose surface energies of an aggregates asphalt binder. Total surface energy of a component is defined in Equation (1) (Cheng et al., 2003):

$$\gamma = \gamma^{LW} + \gamma^{AB} \quad (1)$$

where,

γ = surface energy of asphalt or aggregate (FL/L^2);

γ^{LW} = Lifshiz-van der Waals components of surface energy (FL/L^2);

γ^{AB} = acid-base component of surface energy (FL/L^2).

Lifshiz-van der Waals force is related to the dipole to dipole interactions, and acid-base components pertain to interactions of electron donor to electron accepter (Cheng et al., 2003). Acid-base component is calculated by Equation (2):

$$\gamma^{AB} = 2\sqrt{\gamma^{+}\gamma^{-}} \quad (2)$$

γ^+ is the Lewis acid component and γ^- is the Lewis base component of surface energy. Adhesive bond energy between aggregate and asphalt binder is affected by surface energies of components and described in Equation (3)-(5):

$$\Delta G_{12}^{a} = \Delta G_{12}^{aLW} + \Delta G_{12}^{aAB} \quad (3)$$

$$\Delta G_{12}^{aLW} = 2\sqrt{\gamma_1^{LW}\gamma_2^{LW}} \quad (4)$$

$$\Delta G_{12}^{aAB} = 2\sqrt{\gamma_1^{+}\gamma_2^{-}} + 2\sqrt{\gamma_1^{-}\gamma_2^{+}} \quad (5)$$

ΔG_{12}^{aLW} and ΔG_{12}^{aAB} are the nonpolar and polar parts of adhesive strength, respectively. Subscripts 1, 2 denote asphalt binder and aggregate, respectively. In the presence of water, the adhesive strength of aggregate and binder in contact with water is calculated by Equations (6) and (7):

$$\Delta G_{132}^{a} = \Delta G_{33} + \Delta G_{12} - \Delta G_{13} - \Delta G_{23} \tag{6}$$

$$\begin{aligned}\Delta G_{132}^{a} = {} & 2\gamma_3^{LW} + 2\sqrt{\gamma_1^{LW}\gamma_2^{LW}} - 2\sqrt{\gamma_1^{LW}\gamma_3^{LW}} - 2\sqrt{\gamma_2^{LW}\gamma_3^{LW}} + 4\sqrt{\gamma_3^{+}\gamma_3^{-}} \\ & -2\sqrt{\gamma_3^{+}}(\sqrt{\gamma_1^{-}} + \sqrt{\gamma_2^{-}}) - 2\sqrt{\gamma_3^{-}}(\sqrt{\gamma_1^{+}} + \sqrt{\gamma_2^{+}}) + 2\sqrt{\gamma_1^{+}\gamma_2^{-}} + 2\sqrt{\gamma_1^{-}\gamma_2^{+}}\end{aligned} \tag{7}$$

Subscripts 1, 2, 3 denote asphalt binder, aggregate and water, respectively. ΔG_{132}^{a} has a negative value, implying that debonding between aggregate and binder in the presence of water is thermodynamically favourable. For a mixture to be least susceptible to the moisture, ΔG_{132}^{a} and ΔG_{12}^{a} should have least negative and most positive values, respectively.

Cohesive bond energy is the energy required to create a unit area crack in the binder, and determined by Equation (8):

$$\Delta G_{11}^{c} = 2\gamma_1 = 2(\gamma^{LW} + \gamma^{AB}) = 2\gamma_1^{LW} + 4\sqrt{\gamma_1^{+}\gamma_2^{-}} \tag{8}$$

In the presence of water, the formula for cohesive bond energy is derived by replacing γ_2 with γ_1 in Equation (7). Diffusion of the water in asphalt binder reduces the cohesive bond, which results in asphalt softening.

As mentioned in Section 1.2.1, oxidative aging affects the molecular structure and polarity of the asphalt binder, consequently changing the acid-base components of the surface energy. Furthermore, when asphalt binder reacts with the oxygen, the number of high molecular weight components increases. This results in changes in values of Lifshiz-van der Waals component of the surface energy. Cheng (2003) measured the surface free energy for several unaged and aged asphalt binders, and aggregates by conducting the Wilhelmy plate and universal gas adsorption test methods. The surface free energy of asphalt binder was measured in wetting and dewetting modes, related to healing and fracture process, respectively. The above-mentioned

equations is used here to calculate the cohesive and adhesive bond strength values with and without the presence of water for materials, the surface free energy of which were measured by Cheng (2003). The calculation results are illustrated in Table 1 and 2, respectively. The results in Table 1 suggests that aging reduces both cohesive and adhesive bond strength.

Table 1 Cohesive and Adhesive Bond Energy

Cohesive Energy (ergs/cm^2)	Asphalt	Adhesive Energy (ergs/cm^2)	
		Georgia Granite	Texas Limestone
111.00	Unaged HCR[1]	211.54	189.23
104.12	3 Month Aged HCR	180.19	175.63
67.36	6 Month Aged HCR	171.31	164.80
83.60	Unaged Rubber Asphalt	191.40	183.75
78.97	3 Month Aged Rubber Asphalt	179.80	181.50
74.14	6 Month Aged Rubber Asphalt	174.36	184.32

[1] High Cure Rubber Asphalt

As shown in Table 2, when water is present, for some aggregate-binder combinations, aging decreases the adhesive strength (i.e., resulting in a more negative value), and for some combinations results in an improvement in the work of adhesion (i.e. less negative value). The net result of aging on adhesive strength in the presence of water is controlled by the adhesion work between aggregate and aged binder (i.e., ΔG_{12}^{a}) and the interaction adhesion work between aged binder and water (i.e., ΔG_{13}^{a}). The adhesive strength between aggregate and water (i.e., ΔG_{23}^{a}) and water cohesive energy (i.e., ΔG_{33}^{a}) are not influenced by aging. ΔG_{12}^{a} and ΔG_{13}^{a} both decrease with aging; depending on the amount of reduction, the value of ΔG_{132}^{a} can become either less negative or more negative, implying that aging might either improve or worsen adhesive

bond strength in the presence of water. If the reduction of ΔG_{12}^{a} is higher than the reduction of ΔG_{13}^{a}, then ΔG_{132}^{a} becomes more negative due to aging. The amount of reduction in ΔG_{12}^{a} and ΔG_{13}^{a} with aging are dictated by the change of Lifshiz-van der Waals and acid-base components of aged binders.

Table 2 Adhesive bond energy components with the presence of water

Asphalt	Georgia Granite					Texas Limestone				
	ΔG_{33}	ΔG_{12}	ΔG_{13}	ΔG_{32}	ΔG_{132}	ΔG_{33}	ΔG_{12}	ΔG_{13}	ΔG_{32}	ΔG_{132}
Unaged HCR	145	211.5	131.2	255.8	-30.3	145	189.2	131.2	263.5	-60.3
3Month Aged HCR	145	180.2	119.1	255.8	-49.5	145	175.6	119.1	263.5	-61.8
6Month Aged HCR	145	171.3	99.6	255.8	-38.9	145	164.8	99.6	263.5	-53.1
Unaged Rubber Asphalt	145	191.4	110.9	255.8	-30.2	145	183.8	110.9	263.5	-45.5
3Month Aged Rubber Asphalt	145	179.8	106.8	255.8	-37.7	145	181.5	106.8	263.5	-43.6
6Month Aged Rubber Asphalt	145	174.4	102.8	255.8	-39.0	145	184.3	102.8	263.5	-36.8

To further evaluate the effect of aging on moisture damage characteristic for the aggregate-asphalt combination used in this study, a Bitumen Bond Strength (BBS) test was conducted by using the Pneumatic Adhesion Tensile Testing Instrument (PATTI). In the BBS test, the adhesive characteristic of asphalt-aggregate system is determined by measuring the bond strength between asphalt and aggregate, referred to as Pull-off Tensile Strength (POTS) (Copeland et al. 2007). POTS is defined as the tensile stress at failure and calculated as follows:

$$POTS = \frac{(BP \times A_g) - C}{A_{ps}} \quad (9)$$

where,

C = Piston constant;

BP = Burst pressure (kPa);

A_g = Contact area of piston with reaction plate (mm^2);

A_{ps} = Area of the pull-stub (mm^2).

The details of specimen preparation and test procedure will be explained in Section 5. Figure 1 shows the experimental setup. In order to properly characterize the asphalt-aggregate adhesion, the substrate surface was prepared by cutting few thin slices (2 cm thickness) from AC specimens fabricated using limestone aggregates. Aged and unaged PG 64-22, PG 70-28 and PG 76-28 were used as adhesive materials. RTFO and PAV-aged binders were prepared in accordance with AASHTO T24 and AASHTO PP1, respectively, to simulate short-term and long-term aging. The influence of aging combined with the moisture condition on adhesive characteristic of aggregate-asphalt system was determined by measuring POTS in both dry and wet conditions.

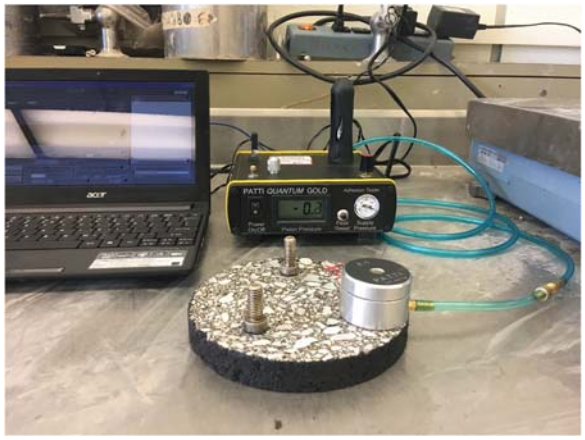

Figure 1 Experimental setup for BBS test

Dry samples were tested 24 hours after attaching stubs to the substrate. For moisture conditioning, samples were kept at room temperature for 2 hours to assure that stubs were adhered firmly to the substrate. Then, the samples were submerged in a water bath at 25°C for 48 hours, and tested immediately after being removed from the bath. The measured POTS for dry and moisture conditioned samples are denoted by $POTS_{dry}$ and $POTS_{wet}$, respectively. A minimum of three replicates were tested for each aging-moisture combination. The percent loss in POTS caused by immersing the samples in water bath is calculated by Equation (10), and is defined as loss of adhesion:

$$\%\,\text{Loss} = \frac{POTS_{dry} - POTS_{wet}}{POTS_{dry}} \times 100 \tag{10}$$

Figure 2 shows the loss of adhesion for the original and aged binders. It is observed that moisture conditioning results in the loss of adhesion for all aged and unaged binders, and that PAV-aged binders have the highest percent loss compared to the unaged and RTFO aged binders. This implies that moisture affects the POTS of PAV-aged binders more negatively, and that aged binders especially PAV-aged binders are more susceptible to moisture damage. Also, It was observed that, as reported in other research studies (Kanitpong and Bahia 2005; Moraes et al. 2011), moisture conditioning results in a change in failure mode from cohesive to adhesive or combination of both. Therefore, it can be concluded that aging exacerbates the moisture damage for aggregate-asphalt combinations that will be studied in this study.

The driving factor controlling the cohesive and adhesive failure is the water transport mode through the AC. In fact, the initial step to estimate the moisture sensitivity of a mixture is to characterize the dominant moisture transport mode. As mentioned earlier, water transport at the interior of asphalt mixture is controlled by permeability, capillary rise and moisture diffusion.

Water vapor diffusion in asphalt layer is recognized as the primary process that contributes in the moisture damage of asphalt pavements (Tong 2013). The moisture diffusion through the asphalt binder is a complex process affected by several factors including its molecular structure and temperature. Oxidative aging changes the molecular structure of the binder; polar functional groups formed during aging are associated to other molecules to form high molecular weight components. These associated large molecules lose sufficient mobility to flow on each other, resulting in an increase in asphalt viscosity (Petersen 2009). The diffusive motion of water molecules within large molecular chains of an aged binder is slower than that within the small molecular chains of an unaged binder. Furthermore, an aged binder has more crystalline regions than an unaged binder, which causes the reduction of its water diffusivity given that the diffusion rate is higher through amorphous regions than crystalline structure. The structure of amorphous regions is more open and so it contains more vacancies to be filled by the diffusive molecules (Callister Jr and Rethwisch 2012).

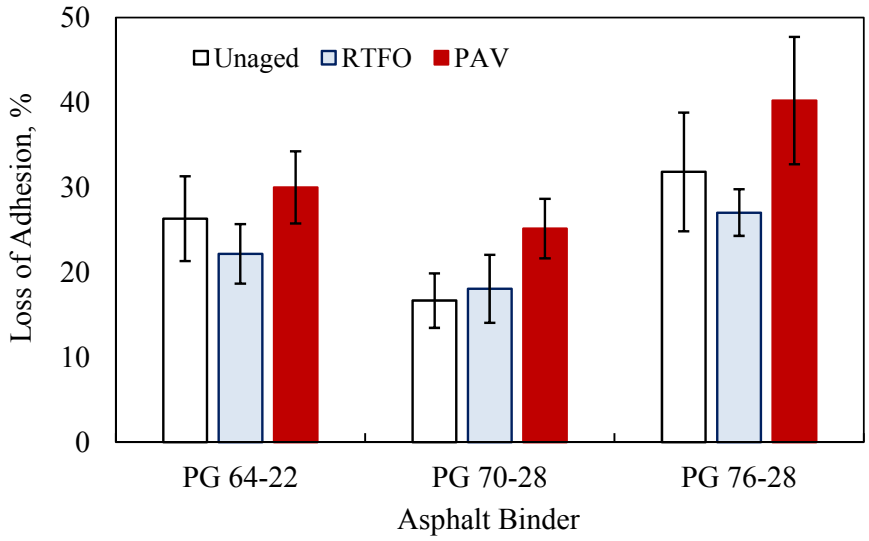

Figure 2 Loss of adhesion for unaged, RTFO and PAV-aged binders

Therefore, with regard to the interaction between aging and moisture damage, it can be concluded that aging has significant effects on the development of moisture damage through changing asphalt binders' surface free energy and moisture diffusion coefficient. This interaction should be taken into account when developing models predicting mechanical properties of AC subjected to the aging and moisture at the same time. The following section describes the methodology adopted in this study to develop an integrated aging-moisture predictive model.

2.3 Integrated Aging-Moisture Predictive (IAMP) Model

This study is aimed to develop an integrated aging-moisture predictive model, referred to as IAMP model hereinafter, that accounts for the effects of coupling oxidative aging and moisture diffusion on dynamic modulus, $|E^*|$, of asphalt mixtures. Dynamic modulus is recognized as the primary material property in mechanistic-empirical pavement design methods and performance prediction models. Therefore, development of a model that predicts the changes of dynamic modulus due to the aging coupled with moisture conditioning deems vital. The IAMP model is developed by providing links to the underlying causes of deterioration, and considering the interactions among chemical and physical properties influenced by aging and moisture. A key to develop such a model is to: 1) account for physical, chemical and mechanical changes happened during conditioning, 2) properly conditioned asphalt mixtures as it occurs in the field.

As depicted in Figure 3, the IAMP model is composed of a predictive aging model and a Moisture Damage model, referred to as MD model hereinafter. The models are developed based on the interaction between aging and moisture damage, discussed in sections 2.1 and 2.2, and mechanisms involved in age-hardening and moisture damage of AC. AC is considered as a composite material containing Fine Asphalt Matrix (FAM) (mixture of an asphalt binder and

aggregate portion passing No. 16 sieve), large aggregates (portion retaining on No. 16 sieve) and air void. The aging model predicts the dynamic modulus master curve of aged AC based on aging properties of asphalt mixture, aging temperature and time. The MD model consists of a Cohesive Damage (CD) model and an Adhesive Damage (AD) model. When water vapor diffuses into asphalt layer from subgrade or air, it reduces dynamic modulus in two ways: 1) weakening the FAM; 2) deteriorating asphalt-aggregate bond. The CD model is the function of gravimetric moisture content of FAM to model weakening of FAM as water vapor is absorbed while AD function models the deterioration of aggregates-asphalt bond as the function of moisture concentration in the interface.

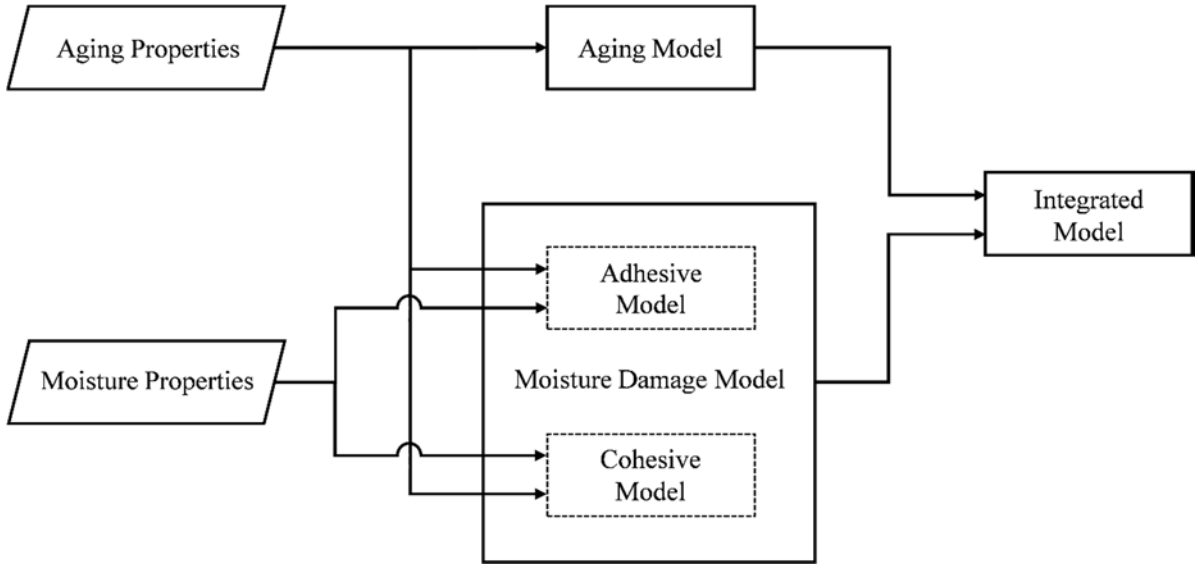

Figure 3 IAMP model framework

CD and AD models are formulated based on the concepts of intermolecular bond energy and force (i.e., Lennard-Jones Potential), and parameters of the model are determined from the

experiments. FAM is considered as an individual material and not a composite one. In fact, asphalt softening as well as deterioration of fine aggregate-asphalt bond are integrated as one damage mechanism in CD model, which is captured by conducting $|E^*|$ test on FAMs. Also, BBS tests were conducted on asphalt-aggregate samples to provide the required data for AD model. All Samples are subjected simultaneously to aging and relative humidity so that the parameters of the models can capture the interaction between aging and moisture damage.

As illustrated in Equation (11), the integrated model modifies the aging model by incorporating MD model. Inputs in the MD model include the amount of absorbed water in FAM, water concentration at the interface of aggregate and binder, loading temperature, *T,* and frequency, *f*. The MD model outputs a damage value between 0 and 1. The maximum damage value for a certain mixture is controlled by its diffusion coefficient, maximum water uptake, adhesive and cohesive property; when water is not present in the mixture, the damage value is 0 and so the integrated model outputs the aging model. The development of the aging predictive model is detailed in Section 3. Section 4 and 5 describes the derivation of the CD and AD model, respectively. In order to account for the impact of aging on moisture induced damage, parameters of CD and AD models are determined by conducting the required tests on samples subjected to aging and moisture at the same time. Finally, in Section 6, CD and AD models are integrated to develop MD model. Also, calibration and validation of IAMP model is performed in Section 6.

$$\left|E^*\right|_{Aging+Moisture} = \left|E^*(\mathrm{t},\mathrm{T})\right|_{aging} \times (1 - d_{MD}(T, f, C_m(\mathrm{t}), w(t))) \tag{11}$$

2.4 Conditioning Approach

This section explains the conditioning procedure adopted in this study. Most of the AASHTO and ASTM standard procedures pertaining to the moisture conditioning have been

established to condition asphalt mixtures for the purpose of evaluating their moisture sensitivity. These procedures are helpful for ranking the mixtures in the order of moisture susceptibility. However, they are not necessarily able to simulate what actually occurs in the field. For instance, AASHTO T283, which is the standard method to investigate the resistance of compacted asphalt mixture to moisture damage, suggests to submerge compacted mixtures in vacuum container filled with water for 5 to 10 minutes, and apply partial vacuum (10 to 26 in) in order to prepare the saturated samples. However, in the field, diffusion of water vapor through the asphalt pavement from both air and subgrade is the main mechanism of water transport, which induces moisture damage. Obviously, moisture damage induced by applying a vacuum saturation approach is different than that induced by water vapor diffusion (Tong 2013).

Under the context of aging, it has been long argued that PAV aging might not be a realistic method to simulate field aging because field aging occurs at atmospheric pressure at all time (Huang et al. 2012). The interaction between moisture and aging is highly influenced by the conditioning approach. As mentioned in Section 2.2, water is not able to change the aging process at atmospheric pressure whereas at high pressure, water disrupts the colloidal structure of asphalt binder that results in generating additional compounds to react with oxygen. Therefore, the first step towards developing the predictive model is to identify the in-service pavement condition and simulate it properly in the laboratory.

Water vapor diffusion in AC layer is the primary process contributing in the moisture damage of asphalt pavements (Tong 2013). This occurs because of the Relative Humidity (RH) differential that exists between atmosphere above the asphalt layer and subgrade below the pavement structure (Luo et al. 2018). RH in the subgrade is always near 100% and so it serves as a reservoir beneath the pavement. Tong (2013) developed a diffusion model to characterize the

water vapor transport in pavement. His modeling results showed that RH in the surface layer of a newly constructed pavements (with initial RH=0) reaches 95% in almost 180 days, and remains at this level during the pavement service life. This high RH level accelerates the pavement deterioration and so it should be included in the laboratory conditioning procedures.

In this study, to consider the effect of aging coupled by moisture, asphalt mixtures are conditioned in a moisture room with 100% RH and aging temperature of 35°C for varying time periods to simulate the in-service pavement condition. The temperature of an asphalt pavement in field varies with depth, time and pavement location. According to data extracted from a LTPP pavement section located in Texas, temperature at 25 mm below the surface changes within the range of -25 to 65°C approximately. Therefore, aging temperature of 35°C is selected for conditioning since it can reasonably represent the pavement temperature for a long period of time during a year.

2.5 Experimental Plan

The experimental plan to accomplish the objectives is shown in Figure 4. In order to establish the aging predictive model, $|E^*|$ test is conducted on two types of HMA mixtures (S4 PG 76-28 and S3 PG 64-22) aged under 9 different levels. A S3 PG 64-22 HMA mixture is used for calibration of the IAMP (Integrated Aging-Moisture Predictive) model. The mixture is a 19 mm Superpave mixture composed of limestone aggregates and PG 64-22 binder. To calibrate the CD model, dynamic modulus testing was conducted on the FAM portion of mixture, referred to as S3 PG 64-22 FAM. FAM specimens were subjected to 8 aging conditioning, and 8 aging-moisture conditioning levels. The parameters in AD model is adjusted by the data measured in BBS test. The substrate surface was prepared by cutting thin slices from S3 PG 64-22 HMA mixture. RTFO-aged PG 64-22 was adhered to the aggregates appearing on the surface of

prepared slices. Samples were then placed in 100% RH and 35°C temperature, and the bond strength was measured at varying times. To verify the IAMP model, |*E**| testing was also conducted on S3 PG 64-22 HMA specimens subjected to 5 aging-moisture conditioning levels.

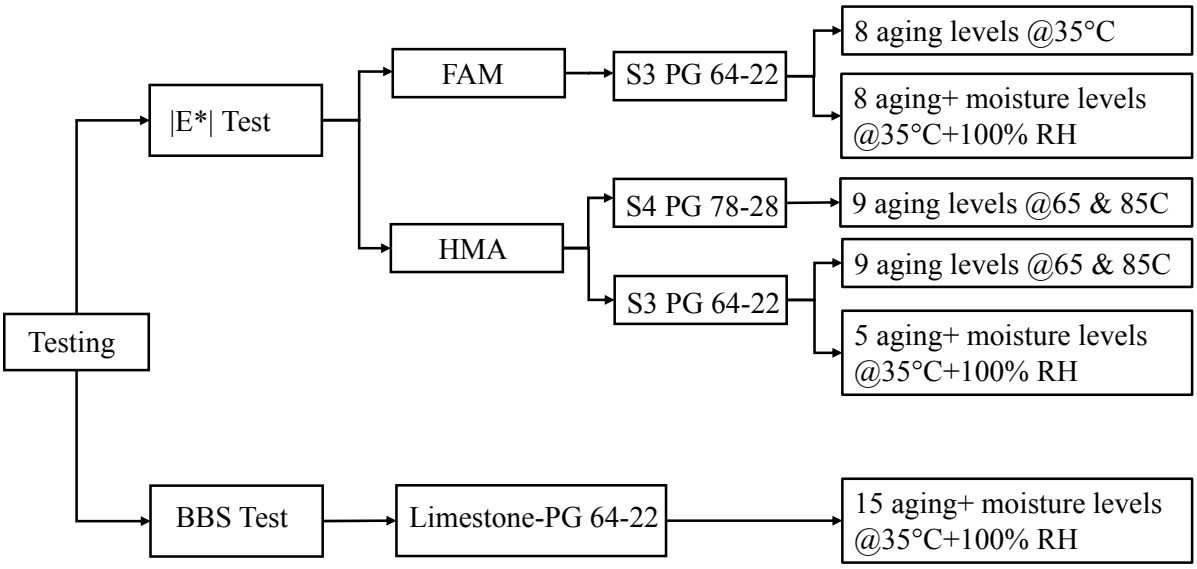

Figure 4 Experimental plan

3. PREDICTIVE AGING MODEL*

Aging in asphalt pavements has been recognized to be one of the key factors affecting the pavement performance. One of the mechanical properties of asphalt mixture impacted by aging is dynamic modulus. Developing a model to predict the changes of dynamic modulus due to the oxidative aging based on mixture characteristics (not only binder) will be of significant importance. Such a model can be used in pavement design methods to account for the age-hardening in the pavement performance prediction models. Along this line of research, Luo X. et al. (2015; 2017) developed a kinetic-based aging prediction model to estimate the modulus of field cores. This model inputs aging temperature and aging time, but does not take into account the variation of loading temperature and frequency. This study aims to improve their models by incorporating the latter factors in developing a model that predicts $|E^*|$ master curves.

3.1 Kinetic-Based Aging Prediction Model

Asphalt binder is composed of molecules containing carbon, hydrogen, nitrogen, and sulfur. The asphalt composition has been recognized by separation and characterization of its components based on reactivity and/or polarity of different molecules (Petersen 2009). According to the separation scheme developed by Corbett, asphalt binder is composed of four fractions. These fractions, sorted in an increasing order of polarity, are saturates, naphthene

* This chapter contains materials from the article "Dynamic modulus and phase angle prediction of laboratory aged asphalt mixtures" by Mona Nobakht and Maryam S. Sakhaeifar, published in Construction and Building Materials Journal, volume 190, pages 740-751, November 2018. DOI: https://doi.org/10.1016/j.conbuildmat.2018.09.160, reprinted with permission.

aromatics, polar aromatics, and asphaltenes. Reaction with oxygen increases the polarity of asphalt components given that polar functional groups are created in the asphalt molecules. Carbonyl and sulfoxide compounds are the main polar functional groups formed during the oxidation (Petersen 1989). The formation of polar functional groups impacts physical properties of asphalt binder, and results in an increase in the asphalt viscosity. Herrington (1998) showed that the oxidation of asphalt binders consists of a group of fast rate reactions involving carbonyl and sulfoxide formation, which is followed by a group of slower rate reactions involving only carbonyl formation. Equation (12), referred to as the kinetic model, has been reported by different researchers to determine the oxidation product concentration for a film of asphalt binder saturated by oxygen. (Branthaver et al. 1993; Herrington 1998; Van Gooswilligen et al. 1985):

$$P = P_f + P_s = P_{f\infty}(1 - e^{-k'_f t}) + k'_c t \tag{12}$$

where,

P = oxidation product concentration;

P_f = product concentration for fast-rate reaction phase;

P_s = product concentration for constant-rate reaction phase;

$P_{f\infty}$ = Product concentration at the completion of fast-rate reaction phase;

k'_f and k'_s = fast and constant-rate reaction constant, respectively.

Herrington (1998) showed that Equation (12) can be used to derive a similar equation to predict the changes in asphalt binder viscosity resulting from oxidation as shown in Equation (13):

$$P = M(1 - e^{-k''_f t}) + k''_c t \tag{13}$$

Where, P is the change of logarithmic viscosity; k''_f and k''_c are reaction constants for the fast and constant-rate reaction phase, respectively; and, M is the maximum or long-term change of logarithmic viscosity due to the fast-rate reaction. As illustrated in Equation (14) and (15), reaction constants (i.e., k''_f and k''_c) follow an Arrhenius equation. A_f, A_c, E_f and E_c are binder-specific parameters varying upon binder source and grade.

$$k''_f = A_f e^{-E_f/RT} \tag{14}$$

$$k''_c = A_c e^{-E_c/RT} \tag{15}$$

where,

A_f and A_c = fast and constant-rate pre-exponential factor, respectively (1/day, Log Pa.s/day)

E_f and E_c = fast and constant-rate activation energy of asphalt binder (kJ/mol);

R = universal gas constant (8.314 J/mol.K);

T = aging absolute temperature (Kelvin).

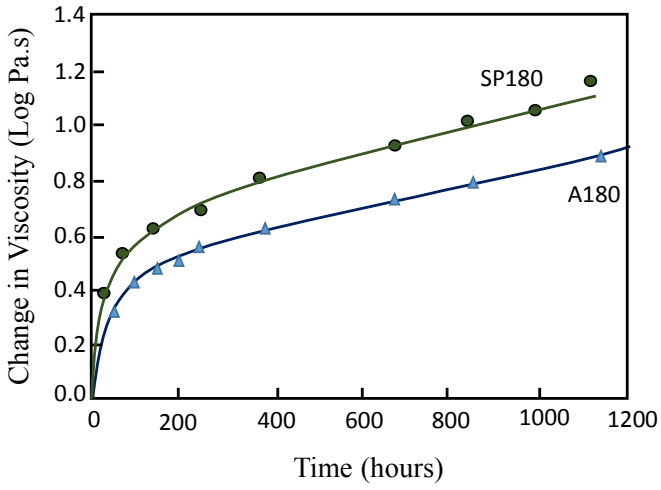

Figure 5 Viscosity change of two asphalt binders (SP 180 and A180) aged by Herrington (1998) in the laboratory

Figure 5 shows the viscosity change of two asphalt binders aged by Herrington (1998) in laboratory. Asphalt samples were subjected to 300 psi air pressure at 60° C for up to 1500 hours. It can be seen in the figure that a fast-rate oxidation phase is followed by a constant-rate oxidation stage.

Asphalt binder is the main constituent of an asphalt mixture which is affected by aging. Viscosity of an asphalt binder increases with aging, resulting in an increase in the stiffness of asphalt mixture. On the other hand, aggregates, additives, reclaimed asphalt pavement (RAP), air void content, and other mixture attributes also impact age-hardening properties of asphalt mixtures given that they alter binder-aggregate adhesion and oxygen diffusion coefficient of AC. Analogous to the asphalt binder aging kinetic model, Equation (16) is formulated by Luo X. (2015) to predict the dynamic modulus of asphalt mixture aged at temperature T for time duration t:

$$|E^*| = |E^*|_i + (|E^*|_M - |E^*|_i) \times (1 - e^{-k_f t}) + \mathrm{k}_c\, t \tag{16}$$

$$k_f = A_f e^{\frac{-E_f}{RT}} \tag{17}$$

$$k_c = A_c e^{\frac{-E_c}{RT}} \tag{18}$$

where,

$|E^*|$ = dynamic modulus of aged AC at aging temperature *T*, and frequency *fr*, MPa;

$|E^*|_i$ = initial dynamic modulus of unaged AC at aging temperature *T* and frequency *fr*, MPa;

$|E^*|_M$ = dynamic modulus of aged AC at completion of the fast-rate reaction phase, MPa;

T =aging temperature, Kelvin;

t = aging time, hour;

k_f and k_c = fast-rate and constant-rate reaction constants, respectively;

A_f = fast-rate pre-exponential factor, 1/hour;

A_c =constant rate pre-exponential factor, MPa/hour;

E_f, E_c =fast rate and constant rate aging activation energy, respectively, kJ/mol.

A_f, A_c, E_f, E_c, and $|E^*|_M$ are the parameters used in model which account for the effect of RAP, additives, mixing technologies, and volumetric properties on the age-hardening characteristic of each specific asphalt mixture. This kinetic model is used in this study to predict the dynamic modulus of lab-mixed lab-compacted specimens that are subjected to long-term oven aging. To accelerate the oxidative aging in most of the laboratory aging simulation procedures, asphalt mixtures are conditioned at a high temperature (e.g. 85°C). Duration for which mixtures need to be exposed to high temperature in order to simulate a given in-service aging depends upon the mixture characteristic. For a desired aging temperature, Equation (16) can be used to find the required laboratory aging duration corresponding to field cores. Dynamic modulus of field cores should be set to the right side of Equation (16) to estimate the laboratory aging duration equivalent to the given in-service aging. A series of upfront testing is needed to determine the model parameters for a certain asphalt mixture with a certain air void content.

This study takes a further step in the prediction of $|E^*|$ master curve of an aged mixture. Dynamic modulus is a function of loading frequency and temperature, aging temperature and aging duration. Equation (16) has only two variables of aging temperature and aging time, and does not account for the variation of loading frequency and temperature. In fact, the kinetic model is able to predict the modulus of asphalt mixture aged at a selected aging temperature (e.g.

85˚C in case of simulating based on AASHTO R30) and a constant frequency (e.g., 1 Hz) for which the parameters in model are determined. Parameters A_c, $|E^*|_M$ and $|E^*|_i$ are frequency-dependent while other parameters involved in the kinetic model are independent to the loading frequency. To incorporate the effect of aging in pavement design, dynamic modulus of mixtures aged at a specific temperature for a certain duration needs to be estimated at various loading frequencies and temperatures. In other words, $|E^*|$ master curve of aged mixtures should be predicted. Following sections explain the approaches adopted in this study to determine the parameters in kinetic model, and predict the master curve.

3.2 Laboratory Test Method

3.2.1 Materials and Specimen Fabrication

In this research, a lab-mixed lab-compacted HMA, referred to as S4 PG 76-28, is used for laboratory testing. The mixture is composed of a PG 76-28 modified binder, limestone aggregates and fine RAP. All materials were obtained from the designated supplier and quarries in Oklahoma. The aggregate structure was a 12.5 mm Superpave mixture (i.e., nominal maximum aggregate size is 12.5 mm) composed of 37% of 5/8" chips, 36% manufactured sand, 12% sand, and 15% fine RAP. Job mix formula (JMF) and mix design sheet were gained from the bituminous material laboratory at ODOT (Oklahoma Department of Transportation). The optimal binder content was 4.9% by the weight of total mixture. Two representative RAP samples were burned in accordance with the guideline provided by National Center for Asphalt Technology (NCAT) ignition method (ASSHTO T 308) to calculate the percentage of asphalt binder in the RAP. The amount of required virgin binder to produce the mixture was estimated by subtracting the percentage of the recycled asphalt binder from the optimal binder content in

JMF. Aggregates were proportioned and combined according to stockpile percentages, and then mixed with the RAP and virgin asphalt binders at the mixing temperatures of 163˚C.

3.2.2 Laboratory Aging of Asphalt Mixtures

The current standard procedure for long-term aging in the United States is AASHTO R30 protocol. In this procedure, loose asphalt mixture is subjected to short-term aging at 135°C for four hours. Then, it is compacted and a long-term aging simulation is performed at 85°C ± 3°C for 120 ± 0.5 hours to simulate five to ten years of aging in the field. Reed (2010) reported that the AASHTO R30 aging procedure induces micro cracks and distortion (i.e., changes in air void content and geometry) in a compacted specimen. To overcome this problem, NCHRP 9-23 protocol (Houston et al. 2005) recommends wrapping the specimen in a metal wire mesh secured with three clamps to prevent the distortion. Although this approach reduces the distortion, it does not eliminate it completely. Moreover, it has been reported that the AASHTO R30 aging procedure causes oxidation gradient from center to edges of the specimen (Elwardany et al. 2017). The existence of aging gradient is not desirable since it results in an inconsistence dynamic modulus and fatigue performance within the specimen. Elwardany et al. (2017) indicated that long-term aging of loose asphalt mixtures outperform that of the compacted mixtures under same conditions. In order to address the issues related to the long-term aging of compacted asphalt mixtures, and to select the most promising aging method for performance testing, NCHRP 9-54 project (Kim et al. 2018) was defined. Various compacted-specimen aging and loose-mix aging procedures were tried in the project. The integrity of compacted-aged specimen and loose-aged compacted specimen were evaluated by performance testing including dynamic modulus and cyclic direct tension fatigue test. Also, Fourier-Transform Infrared Spectroscopy (FTIR) and Dynamic Shear Rheometer (DSR) testing were conducted for binders

extracted from various locations in aged specimens to evaluate the oxidation gradients. The NCHRP 9-54 recommends loose mix aging in an oven as the most promising aging method in terms of efficiency and integrity. The project showed that aging asphalt mixtures in a loose state expedites oxidation compared to compacted specimen aged under the same conditions. Also, no integrity issue is associated with the loose mix aging, and that compaction effort required to compact long-term aged loose mixes is comparable to that required for short-term aged mixes, with no need to adjust the compaction temperature. Therefore, in this study the loose mix oven aging approach is adopted.

Prior to the long-term aging, loose mixtures were first subjected to the short-term aging (4 hours at 135°C) in a forced draft oven. Then, they were separated into several pans to be placed in the oven for the long-term aging. The total of nine levels of aging were simulated as follows:

- Control. The loose mixture is conditioned at 135˚C for 4 hrs.
- Level 1-65. The loose mixture is conditioned at 135˚C for 4 hrs, then aged at 65˚C for 1 day.
- Level 2-65. The loose mixture is conditioned at 135˚C for 4 hrs, then aged at 65˚C for 3 days.
- Level 3-65. The loose mixture is conditioned at 135˚C for 4 hrs, then aged at 65˚C for 5 days.
- Level 4-65. The loose mixture is conditioned at 135˚C for 4 hrs, then aged at 65˚C for 7 days.
- Level 1-85. The loose mixture is conditioned at 135˚C for 4 hrs, then aged at 85˚C for 1 day.
- Level 2-85. The loose mixture is conditioned at 135˚C for 4 hrs, then aged at 85˚C for 3 days.
- Level 3-85. The loose mixture is conditioned at 135˚C for 4 hrs, then aged at 85˚C for 5 days.
- Level 4-85. The loose mixture is conditioned at 135˚C for 4 hrs, then aged at 85˚C for 7 days.

After aging process was completed, the loose mixtures were remixed to ensure homogeneity, and then they were cooled down to the room temperature. The mixtures were then

reheated to the compaction temperature of 149°C for one hour, and compacted by the Superpave gyratory compactor (SGC) to dimensions of 170 mm in height and 150mm in diameter. Then samples were cored and cut to 100 mm in diameter and 150 mm in height to obtain uniform samples for testing. The air void content of all replicates were between 6.5% and 7%.

3.2.3 Testing Method

Dynamic modulus testing is a standard method for characterizing the stiffness ($|E^*|$), and phase angle (φ). In this study, the dynamic modulus test was performed to determine parameters of the kinetic model and to evaluate the effects of aging on $|E^*|$, and φ. Testing is conducted in accordance with AASHTO TP79-13 protocol by using Asphalt Mixture Performance Tester (AMPT). Three replicates for each aging level were fabricated and tested at frequencies of 25, 10, 5, 1, 0.1, and 0.01 Hz and temperatures of 4˚, 20˚, 40˚, and 50˚C. Peak-to-peak strain levels are set to be within 75 and 95 micro-strain to ensure that no damage occurs during the loading, and that asphalt samples remain in the linear viscoelastic region. AASHTO T 342-11 recommends to adjust the sinusoidal load such that the axial strain between 50 and 150 microstrain is obtained. This range is further evaluated in this study to ensure that asphalt samples remain in the linear viscoelastic region during loading. It was observed when the strain level is in the range of 75-95 microstrain, the magnitude and phase angle of $|E^*|$ remain constant with an increase in the number of loading cycles. This implies that the test is in the nondestructive phase. Time-Temperature Superposition Principle (TTSP) was employed to create the sigmoidal $|E^*|$ master curves at a reference temperature of 20˚C. TTSP is commonly used to determine temperature-dependent mechanical properties of viscoelastic materials from the properties measured at a reference temperature. Dynamic modulus of AC increases with loading rate, but decreases as temperature increases. However, the shape of dynamic modulus

curve as a function of loading rate (or time) does not change when temperature increases; but it only shifts to the left or right. Therefore, a master curve at the reference temperature can be developed to predict the dynamic modulus at different temperatures by using a shift factor. |*E**| master curve can be fitted by a sigmoidal function as shown in Equation (19):

$$\log\left|E^*\right| = a + \frac{b}{1+\frac{1}{e^{c+d\times\log f_R}}} \tag{19}$$

$$f_R = f \times a_T \tag{20}$$

$$\log a_T = \alpha_1 T^2 + \alpha_2 T + \alpha_3 \tag{21}$$

where,

a, b, c and d = fitting parameters;

f_R = reduced frequency, (Hz);

f = testing frequency, (Hz);

a_T = shift factor;

α_1, α_2, α_3 =fitting parameters;

T = testing temperature, (˚C).

3.3 Test Results

Master curves are constructed for the average values of |*E**| measured for two replicates. Figure 6 and Figure 7 present the average |*E**| for specimens conditioned under aging levels at 65˚C and 85˚C, respectively. It is observed that as the level of aging increases, dynamic modulus increases over the entire range of frequency. This trend is more noticeable for mixtures aged at 85˚C. Also, the effect of aging on stiffness is more pronounced at the intermediate and low reduced frequencies. As temperature increases or frequency decreases, the difference between

the modulus of asphalt binder and aggregates becomes higher; thus, an increase in the binder modulus due to aging results in a noticeable effect on the mixture stiffness (Baek et al. 2012).

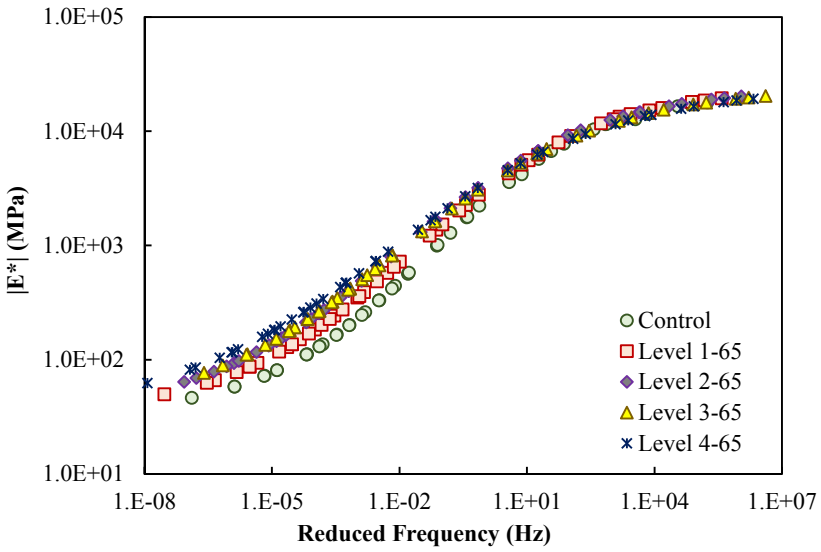

(a)

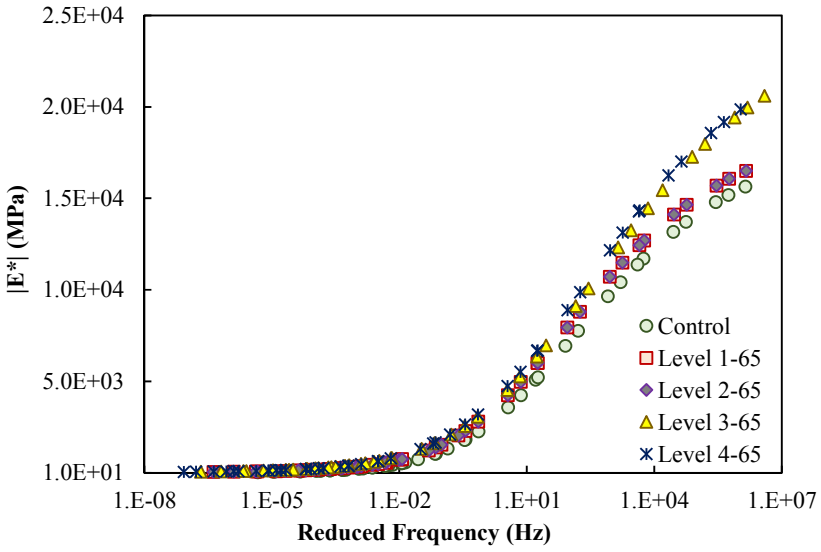

(b)

Figure 6 Dynamic modulus master curve for mixtures aged at 65°C in (a) log-log scale (b) semi-log scale

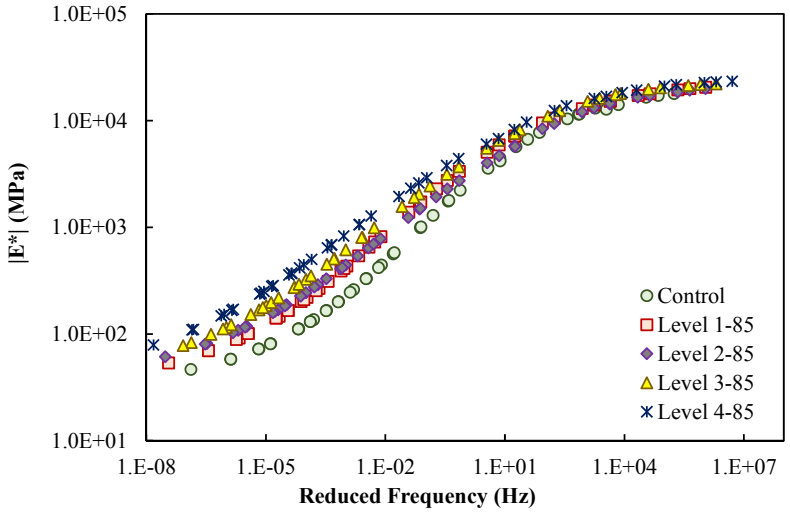

(a)

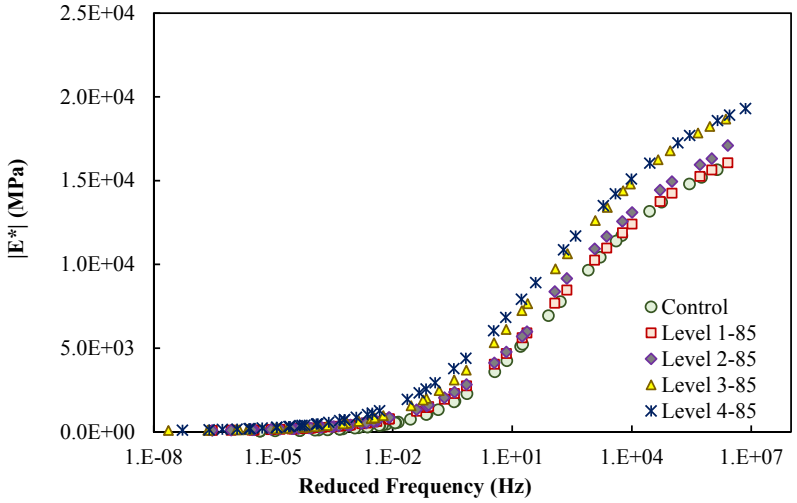

(b)

Figure 7 Dynamic modulus master curve for mixtures aged at 85°C in (a) log-log scale (b) semi-log scale

The master curve of average phase angle for mixtures aged at 85˚C is illustrated in Figure 8. At very low reduced frequency, the behavior of mixture is dominated by the aggregate properties rather than asphalt binder. This implies that phase angle and reduced frequency are

correlated (i.e., as reduced frequency increases phase angle increases as well). However, at high reduced frequency, the mixtures' behavior is mostly dominated by asphalt binder properties. For a viscoelastic material like asphalt binder, reduced frequency and phase angle are negatively correlated. The peak in phase angle master curve corresponds to the transitioning phase, where mixtures' behavior transitions from being dominated by asphalt binder to aggregate (Sias Daniel et al. 2013). With respect to the effect of aging on phase angle, the maximum phase angle slightly shifts to the left with aging time. Such a change is expected because at the intermediate and high reduced frequency, aging causes a decreases in the phase angle, and an increase in the stiffness and elasticity. As a result, asphalt mixture remains in the binder-dominated phase for a longer range of reduced frequency, and transitions to the aggregate-dominated phase at a slower reduced frequency. However, it is observed that at low reduced frequency, aging declines the elasticity of mixtures.

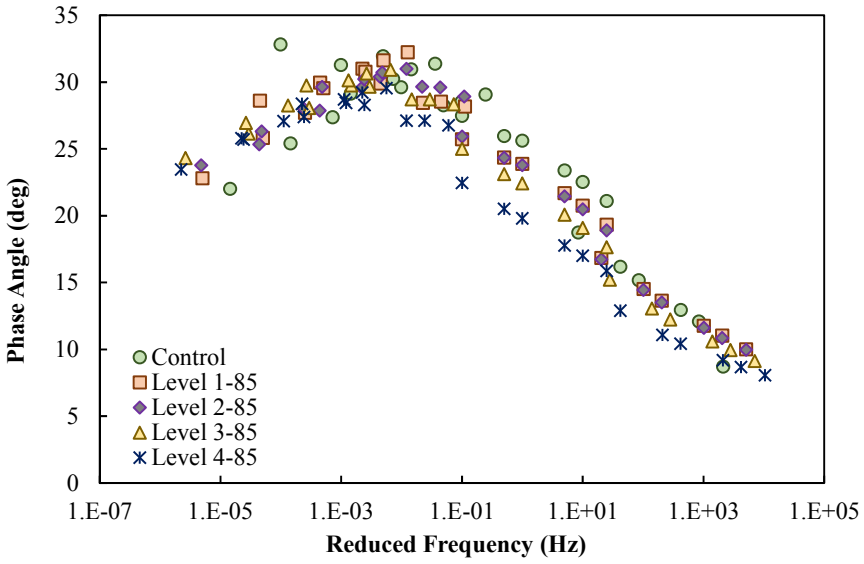

Figure 8 Phase angle master curve for aging conditions at 85˚C

3.4 Development of Aging Function

In this section, the results of $|E^*|$ tests are used to determine the parameters involved in the aging kinetic model (i.e. Equation (16), (17) and (18)). As discussed earlier, the model is able to predict $|E^*|$ only at the aging temperature. In this study, mixtures are conditioned at 65˚C and 85˚C, and so two kinetic equations can be written at these temperatures. Since $|E^*|$ is a function of loading frequency, A_c and $|E^*|_M$ are dependent to the frequency as well. They can be determined at any reduced frequency of interest, which is chosen to be 0.0001 Hz in this study. To estimate the parameters, first, the average $|E^*|$ master curve should be constructed for each mixture aged at the specific aging level explained in Section 3.2.2. Then, for each aging temperature, $|E^*|$ at the reduced frequency 0.0001 Hz needs to be estimated from the master curve and plotted vs. aging time as shown in Figure 9(a). A power law function is then fitted to each curve to calculate $|E^*|$ at every 12 hours as presented in Figure 9(b).

Next step involves the identification of fast and constant-rate aging periods on each curve, which is accomplished by following the approach recommended by Luo X. et al. (2017). In this approach, a linear model is fitted to the constant-rate segment of the curve; the starting point of linear model, which corresponds to the ending point of fast-rate period, is adjusted until the correlation coefficient, R^2, of linear model is 0.99. Dynamic modulus at the starting point of linear model (i.e., intercept of model with vertical axis) is referred to as $|E^*|_M$. Slope of the linear model represents k_c in Equation (16). In order to determine the constant-rate aging activation energy, E_c, and constant-rate pre-exponential factor, A_c, the natural logarithm of k_c for each aging temperature is plotted vs $1/RT$ as shown in Figure 10. The slop and intercept of the fitted line in Figure 10 represents E_c and A_c, respectively. After finding A_c and E_c, the other two parameters (i.e., A_f and E_f) are estimated by substituting the known parameters in Equation (16) and using a

regression analysis. A_f, A_c, E_c, and E_f values vary with mixture types and air void content; these parameters for S4 PG 76-28 mixture with 7% air void are shown in Table 3.

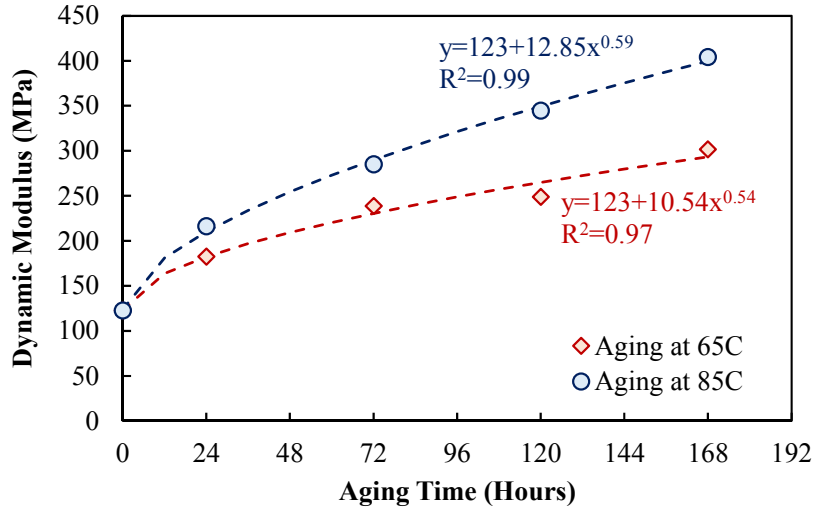

(a)

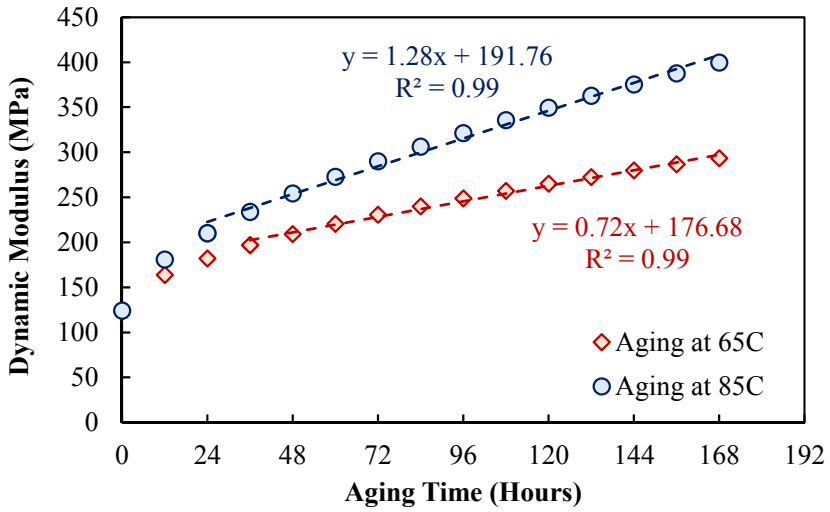

(b)

Figure 9 Dynamic modulus vs. aging time for (a) Fitted |E^*| using master curve, (b) Fitted |E^*| using power low model

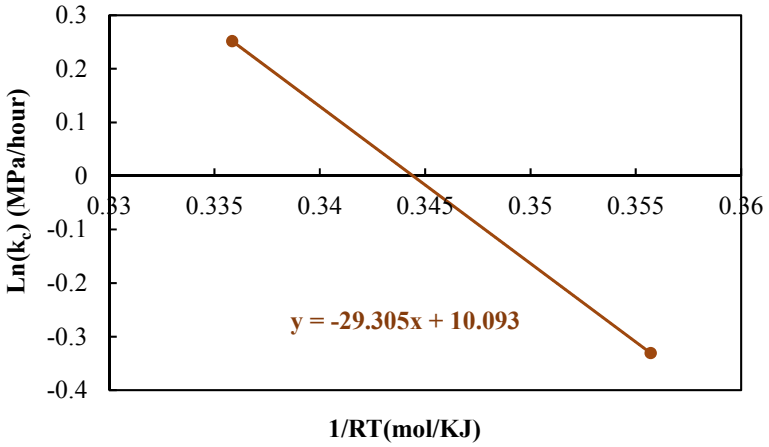

Figure 10 Constant-rate components for S4 PG 76-28 mixture

Table 3 parameters of aging kinetic model for S4 PG 76-28 with 7% air void

E_c (kJ/mol)	A_c (MPa/h)	A_f (1/hours)	E_f (kJ/mol)	E_m (Mpa)
29.31	24173.2	22.16	16.41	200

Note that $|E^*|_i$ (i.e., initial dynamic modulus) in Equation (16) is the dynamic modulus after the short term aging, which refers to the aging condition at the time of production and construction. Glover et al. (2005) found that the early fast-rate period was not passed during hot-mix production and construction. Furthermore, the amount of aging during the fast-rate period after the construction may be significant and sometimes can be equivalent to about four years of the constant-rate aging in a field condition like Texas. Their findings are in agreement with the results of this study. As it can be observed in Figure 9, a part of the fast-rate aging occurs during the long-term aging period.

After finding all the parameters, the kinetic model can be used to predict the $|E^*|$ at any desirable aging temperature and time. Since A_c and $|E^*|_M$ are functions of reduced frequency, the model can predict $|E^*|$ only for the reduced frequency at which the parameters are determined (e.g. 0.0001 in this study). However, for the pavement design purposes, it is more beneficial to predict the dynamic modulus of aged mixtures at every loading temperature and frequency of interest. To overcome this limitation, a method is proposed herein to predict the master curve of the mixtures aged at desired aging conditions. As mentioned earlier, a series of upfront testing is required to compute the parameters in kinetic-model for a certain mixture with a given air void content. An aging function, denoted by λ herein, is developed by rearranging and normalizing the aging kinetic model as shown in Equation (22). The aging function is invariant of the reduced frequency. Therefore, the reduced frequency, at which A_c, $|E^*|_M$ and $|E^*|_i$ are estimated, is not of importance as long as all three parameters are measured at the same reduced frequency. λ characterizes the effect of aging on $|E^*|$ based on the aging properties of a certain mixture (i.e. k_f and k_c) as a function of aging time and temperature. As λ is formulated by normalizing the aging kinetic model, higher value of λ corresponds to stiffer mixtures. Figure 11 shows the change of λ versus aging time for the S4 PG 76-28 HMA with 7% air void aged at 40, 65 and 85°C. The application of λ in the prediction of $|E^*|$ master curve is explained in the next section.

$$\lambda(T,t) = \frac{|E^*| - |E^*|_i}{|E^*|_M - |E^*|_i} = (1 - e^{-k_f t}) + \frac{k_c t}{|E^*|_M - |E^*|_i} \quad (22)$$

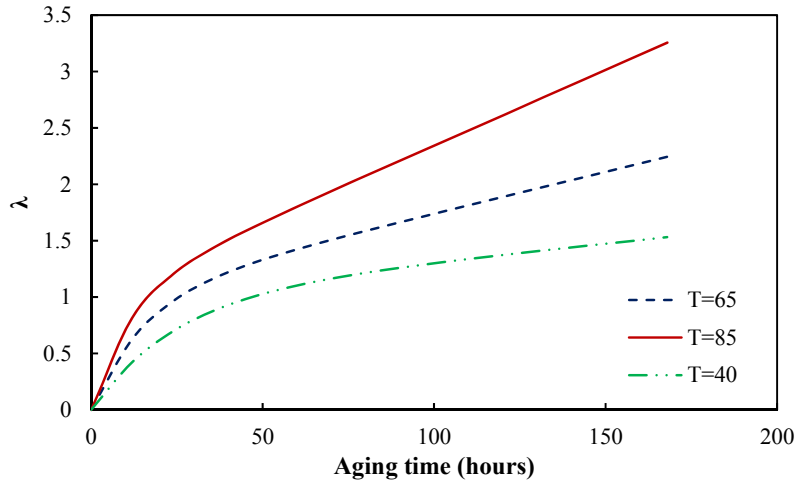

Figure 11 λ versus aging time for S4 PG 76-28 HMA aged at 40, 65 and 85°C

3.5 Prediction of Dynamic Modulus and Phase Angle Master Curve for Aged Mixtures

The sigmoidal function, illustrated in Equation (19), is typically used to develop $|E^*|$ master curve. 10^a and 10^{a+b} are the lower and upper asymptotes of the function, respectively, which are related to the volumetric and aggregate structure of mixtures. The relation of these asymptotes with aggregate structure and volumetric are established in the revised Witczak predictive model (Andrei et al. 1999), which is currently embedded in the Pavement ME. The relation is presented as follows:

$$a = 3.750063 + 0.02932\rho_{200} - 0.001767(\rho_{200})^2 - 0.002841\rho_4 - 0.058097V_a - 0.802208\left[\frac{Vb_{eff}}{Vb_{eff} + V_a}\right] \quad (23)$$

$$b = 3.871977 - 0.0021\rho_4 + 0.003958\rho_{38} - 0.000017\rho_{38}^2 + 0.005470\rho_{34} \quad (24)$$

Where,

ρ_{200} = % passing the No. 200 sieve;

ρ_4 = Cumulative % retained on the No. 4 sieve;

ρ_{38} = Cumulative % retained on the No. 3/8 in sieve;

ρ_{34} = Cumulative % retained on the No. 3/4 in sieve;

V_a = air void content, %;

Vb_{eff} = effective binder content, % by volume.

At very low reduced frequency, binder modulus is extremely small. Therefore, |*E**| mostly depends on the stiffness of aggregates. However, at high reduced frequency, |*E**| is influenced by binder glassy modulus and aggregate structure (Mensching et al. 2017). The mixture volumetric and aggregate structure remain the same during aging, hence, it can be assumed that the values of coefficients *a* and *b* remain relatively the same when aging happens. However, the other two sigmoidal coefficients (i.e., *c* and *d*) are mostly related to the rheological property of asphalt binder and the width of relaxation spectra. These properties are influenced by aging, consequently, the values of coefficients *c* and *d* change as oxidative aging progress within the mixtures. Dependency of the sigmoidal coefficients on aging is examined in this study. |*E**| master curve are developed for all mixtures subjected to nine aging levels. It is observed that the change in values of *a* and *b* with aging is so small such that they can be assumed to remain the constant. As mixture ages and rheological property of binder changes, |*E**| master curve becomes flatter, which corresponds to a smaller value of *d*. The coefficient *d* in the sigmoidal function is related to the width of relaxation spectra (Bhattacharjee et al. 2012), which is defined as the distribution of relaxation time and can be captured by the *R*-value in Christensen-

Anderson (CA) model (Christensen 1992). CA model shown in Equation (25) is a hyperbolic function to fit the master curve of a binder:

$$G^*(\omega) = G_g\left[1+(\frac{\omega_0}{\omega})^{(\log 2)/R}\right]^{-R/(\log 2)} \quad (25)$$

where,

R = rheological index;

$G^*(\omega)$ = the complex shear modulus at frequency ω;

G_g = the glassy modulus;

ω_0, ω = the cross over frequency, and test frequency, respectively.

Therefore, *d* and *R*-values are highly correlated given that both are related to the width of relaxation spectra. Oxidative aging results in widening of the relaxation spectra, which corresponds to a higher *R*-value for binder, and a lower *d*-value for asphalt mixture (Mensching et al. 2017). Also, aging causes inflection point of the master curve, which occurs at the reduced frequency of $10^{-c/d}$, to move towards a slower reduced frequency (i.e., left in the *x* axis). This implies an increase in the *c*-value and a decrease in the *d*-value, which is the indication of more oxidised binder in asphalt mixture. As discussed in the previous section, λ shows the extent of change $|E^*|$ for a certain mixture as the function of time and temperature. Therefore, for each mixture exposed to one of the nine aging levels, a value of λ is calculated by using Equation (22) .The sigmoidal coefficients (i.e., *c* and *d*) and parameters of the shift factor (i.e., α1, α2, α3) are plotted against λ as shown in Figure 12, and a regression analysis is conducted to find the relationship of these coefficient with λ. It is observed that a linear correlation exist between these parameters and λ as illustrated in Figure 12.

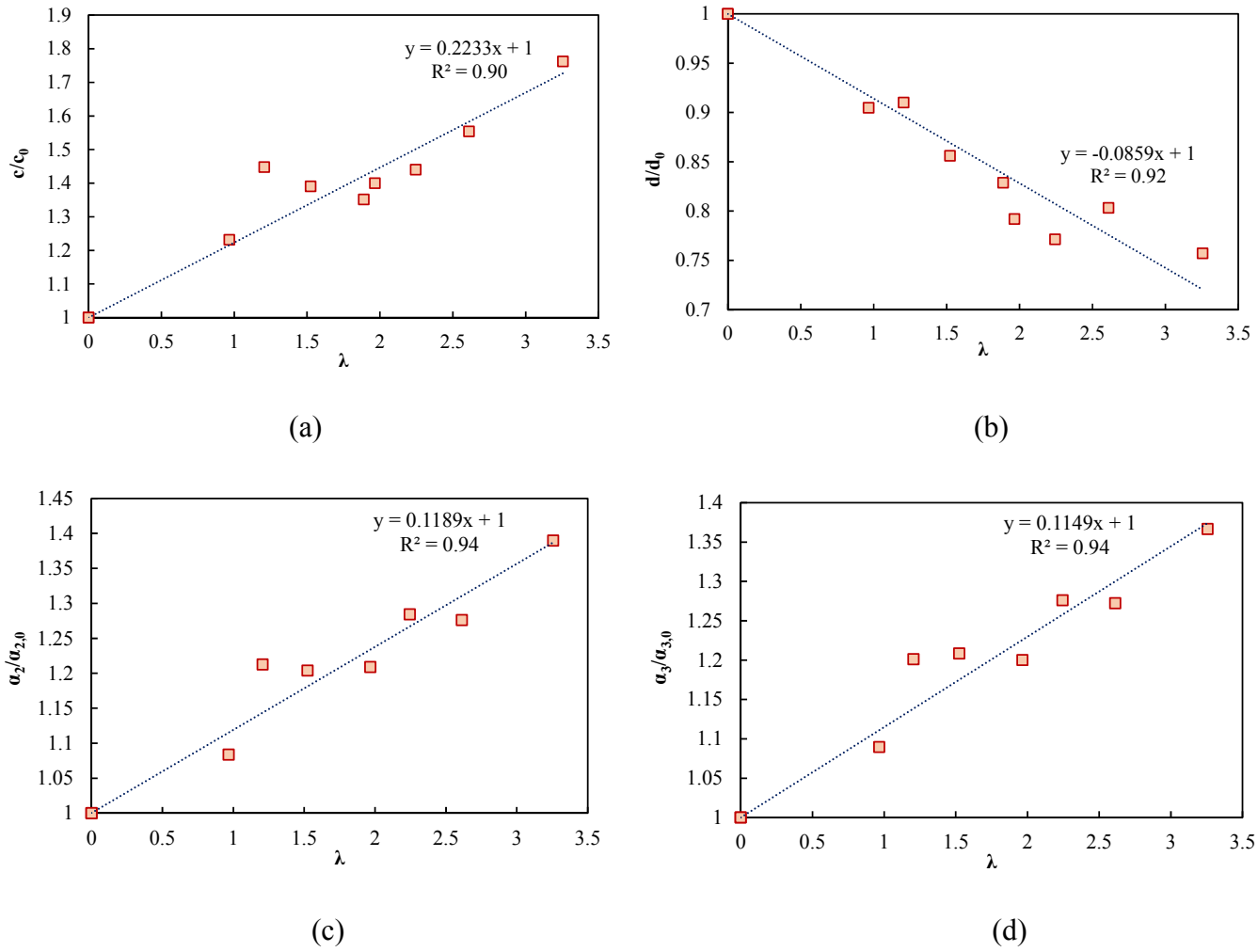

Figure 12 Relationship between sigmoidal coefficients and shift factor parameters with λ for S4 PG 76-28 mixture

According to Equation (21), either of α_1, α_2 and α_3 can be written as a function of the other two. Therefore, if two of them are given based on λ, the third one can be formulated based on λ as well. It should be noted that the linear regression functions shown in Figure 12 are developed for the mixture examined in this study (i.e., S4 PG 76-28). Parameters in the models are controlled by the aggregate structure, volumetric properties, and aging characteristic, and should be determined for each mixture. The actual function types might not be exactly linear.

However, if the value of λ is within the shown range below, which corresponds to the aging temperatures and times commonly used in laboratory-aging procedures, the actual function can be properly approximated by a linear function. In other words, when the domain of interest is close enough to the origin (which is the case in this study), a linear function can be appropriately used in the place of actual function type. However, when the domain of interest is far from the origin, the actual function needs to be considered. In Figure 12, the *y*-axis is the ratio of the coefficients of aged mixtures to those of the unaged ones (i.e., at the control state). This normalization facilitates the generalization of function to predict |*E**| master curve after aging based on λ. Note that λ is a mixture-specific function and needs to be developed for each mixture separately.

In addition, the proposed approach can be employed to predict the phase angle master curve of aged mixtures. A couple of predictive models have been developed by researchers with regard to the phase angle. Christensen Jr et al. (2003) developed the predictive model that relates phase angle to the mixture volumetric and shear modulus of the binder. In another study, Christensen and Anderson (1992) established a model that links phase angle of the asphalt binder to derivative of the logarithm of complex modulus with respect to the logarithm of the reduced frequency. Rowe (2009) investigated the Christen-Anderson phase angle model for a large set of asphalt mixtures, and concluded that the model can be used for mixtures as well. Rowe presented the model by using the sigmoidal coefficients of |*E**| master curve as follows:

$$\varphi = 90 \times \frac{d \log |E^*|}{d \log fr_d} = 90 \times \frac{bd \times e^{-c-d \log fr_d}}{(1+e^{-c-d \log fr_d})^2} \quad (26)$$

Also, in another study conducted by Oshone et al. (2017), the validity of relationship is investigated for a large group of asphalt mixtures. It has been observed that the measured phase

angle and one predicted by Equation (26) have comparable shape and very similar inflection points. If coefficients of the sigmoidal function for the unaged mixture are known, the coefficients of aged mixtures can be estimated from the regression functions in Figure 12. Consequently, the phase angle can be predicted as well as $|E^*|$. The validity of this approach is examined for the S4 PG 76-28 mixture conditioned under Level 1-85 aging process. The results are presented in Figure 13. Three phase angle curves are plotted in this figure. The one labelled as "Level1-85-Measured" indicates the phase angle of the aged mixture measured directly in the lab using AMPT testing machine. The curve labeled as "Level1-85-Predicted from Measured Aged E^*" is constructed by using the sigmoidal coefficients of $|E^*|$ master curve for the aged mixture. The coefficients are plugged in Equation (26) to construct the phase angle master curve. Finally, the last curve labelled as "Level1-85-Predicted by Using λ" is developed by using sigmoidal coefficients of the unaged mixture (i.e., control mixture) and λ. Regression functions in Figure 12 are used to predict the sigmoidal coefficients and shift factor parameters of the aged mixture, and then are plugged in Equation (26) to construct the phase angle master curve.

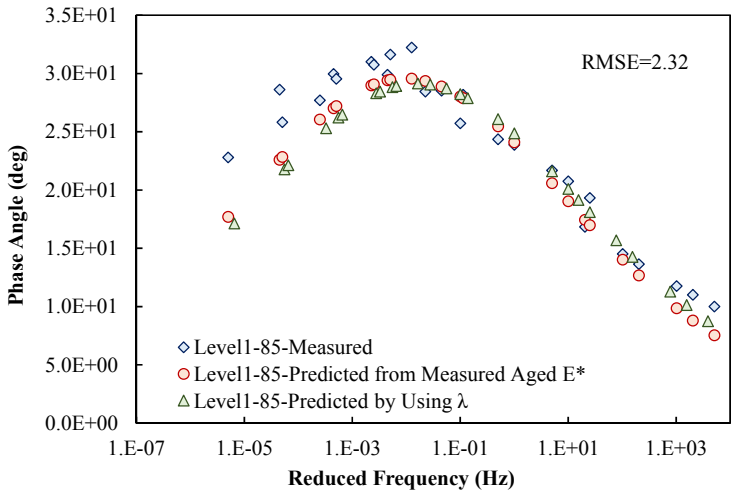

Figure 13 Phase angle master curve for S4 PG 76-28 mixture

In general, the shapes of all three master curves are similar and their maximum values happen almost at the same reduced frequency. It is observed that at high and intermediate reduced frequencies, differences between the three estimates are negligible, but at the low reduced frequency the difference between the measured phase angle and predicted ones is relatively considerable. This difference arises from the existing errors in measuring the phase angles at high temperature or low frequency. The accurate measurement of the phase angle at low frequency and high temperature in the laboratory is challenging, and is prone to error to some extent. At high temperature, deformation waves are noisy, which makes it hard to accurately capture time-lag between load and deformation waves (Oshone et al. 2017). Another source of error in phase angle measurement is related to the calibration of AMPT testing device. AMPT is generally calibrated using a solid fixture indicating a zero-phase angle. However, to precisely calibrate the device for testing asphalt mixture, AMPT should be calibrated by standard materials which have similar stiffness and phase angle to those of asphalt mixture (Oshone et al. 2017). However, these materials are not available, which causes some degree of variability in phase angle measurement at high temperature and low frequency. The comparison between the measured phase angle and predicted ones for S4 PG 64-22 samples subjected to level 1-85 aging are illustrated in Figure 14. Considering the variance of phase angle measurements at high temperatures, both approaches yield to comparable results.

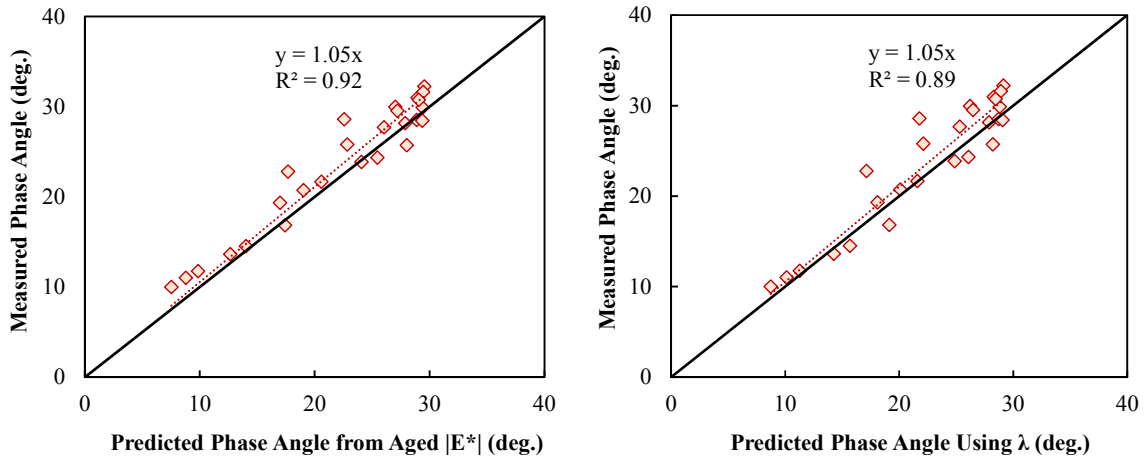

(a) (b)

Figure 14 Comparison of measured phase angle with (a) predicted values using measured aged |E^*| and (b) predicted values using λ

3.6 Validation of Aging Predictive Model

After finding the parameters of aging kinetic model, and formulating the relationship between the sigmoidal coefficients and shift factor parameter with λ, the model can be employed to predict |E^*| and phase angle master curve of mixtures aged in the oven at any aging condition of interest. A comparison was made between the measured |E^*| and φ master curves and predicted ones for a S4 PG 76-28 mixture aged in the force draft oven for 4 days at 85˚C. The results presented in Figure 15 and Figure 16 suggest that the aging model is robust to predict the |E^*| master curve. Considering the variability of phase angle measurements at low reduced frequency, the proposed model can predict the phase angle master curve with acceptable accuracy.

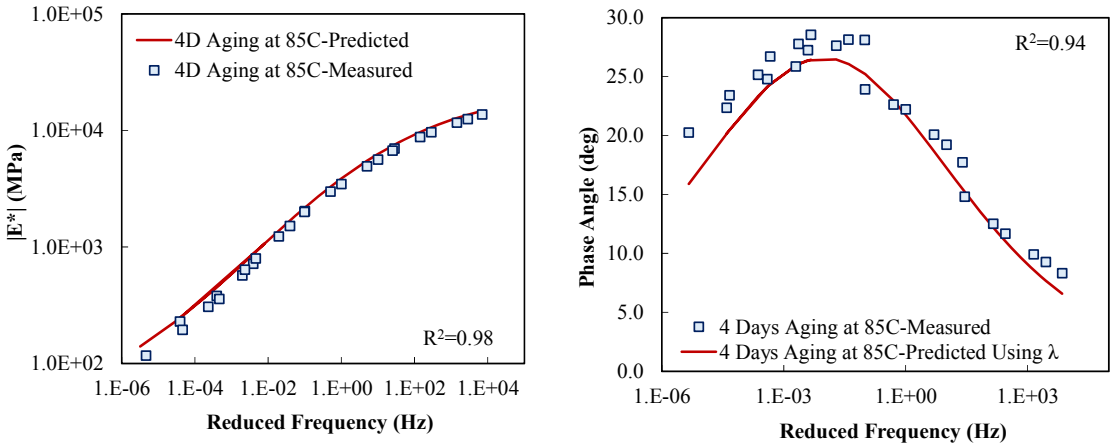

(a) (b)

Figure 15 Predicted and measured (a) |*E|, and (b) phase angle master curves**

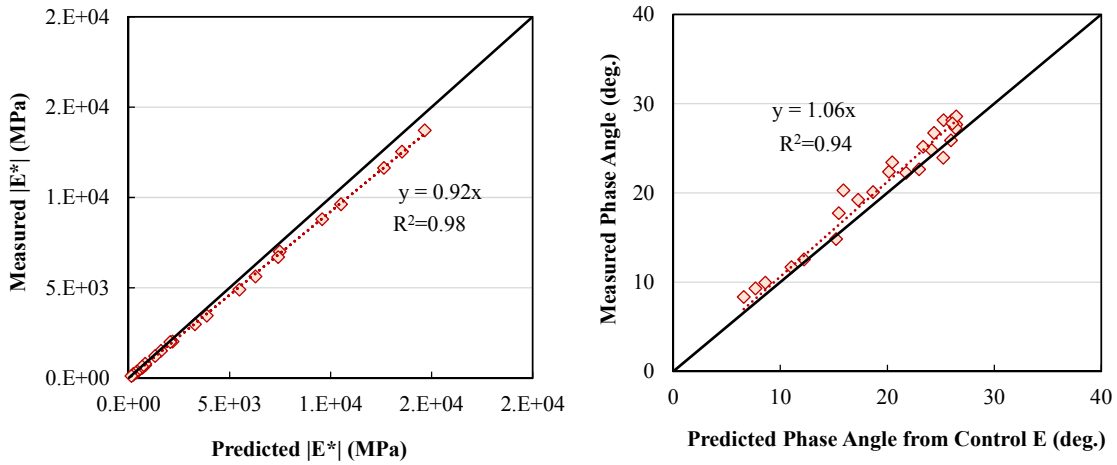

(a) (b)

Figure 16 Predicted and measured (a) |*E| and (b) phase angle master curves**

4. COHESIVE DAMAGE (CD) MODEL

4.1 Model Formulation

Asphalt is a thermoplastic material; it hardens when cooled and softens as heated. Although it is not categorized as a polymer, because of its polymer-type network, it shares common mechanical characteristic with polymers. The main chemical elements in asphalt are carbon and hydrogen, and it also might contain sulfur, nitrogen and oxygen. Asphalt is composed of three chemical groups known as asphaltenes, resins and saturates. The saturates are composed of non-polar chained hydrocarbon and aromatic ring molecules. Asphaltenes consist of polar condensed aromatic rings connected with chain molecules, and they are dispersed in saturates by resin, which contain nonpolar chains and partially polar condensed rings. The bonding force holding together the polar and non-polar molecules is the van der Waals force (Liu 2005). The high molecular weight and long chain causes an entanglement of asphalt molecules as shown in Figure 17. The lack of strong intermolecular bonds eases the mobility of chains, thus, the entangled mobile chains result in viscoelastic properties of the asphalt binders and FAMs.

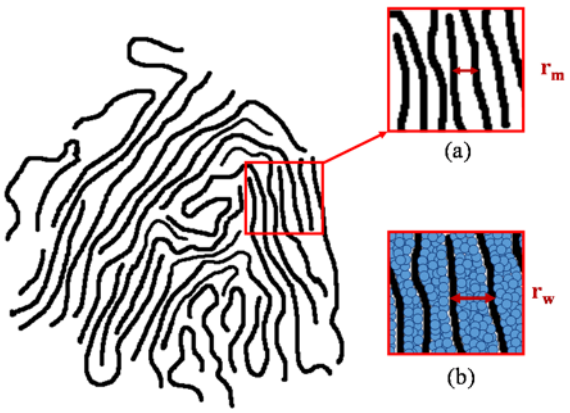

Figure 17 Schematic illustration of high molecular chain of asphalt in (a) dry and (b) wet conditions

According to the Lennard-Jones (LJ) potential shown in Equation (27), and illustrated schematically in Figure 18, the potential energy between molecules varies with the intermolecular distance.

$$V_{LJ} = 4\varepsilon\left[(\frac{\sigma}{r})^{12} - (\frac{\sigma}{r})^{6}\right] = \varepsilon\left[(\frac{r_m}{r})^{12} - 2(\frac{r_m}{r})^{6}\right] \tag{27}$$

$$\sigma \approx 0.89 r_m \tag{28}$$

where,

V_{LJ} = Lennard-Jones Potential;

ε = Depth of the potential well;

σ = The finite distance at which the potential is zero;

r_m = Distance at which the potential reaches its minimum;

r = Distance between the molecules.

The LJ potential is a simple model that describes the interaction between molecules. The r^{-12} term is the repulsive potential describing the repulsion between molecules due to the overlap of electron orbits, and r^{-6} is related to the attraction between molecules. A simplified formulation for LJ potential can be shown as follows:

$$V_{LJ} = \frac{A}{r^{12}} - \frac{B}{r^{6}} \tag{29}$$

where,

$$A = 4\varepsilon\sigma^{12} \tag{30}$$

$$B = 4\varepsilon\sigma^{6} \tag{31}$$

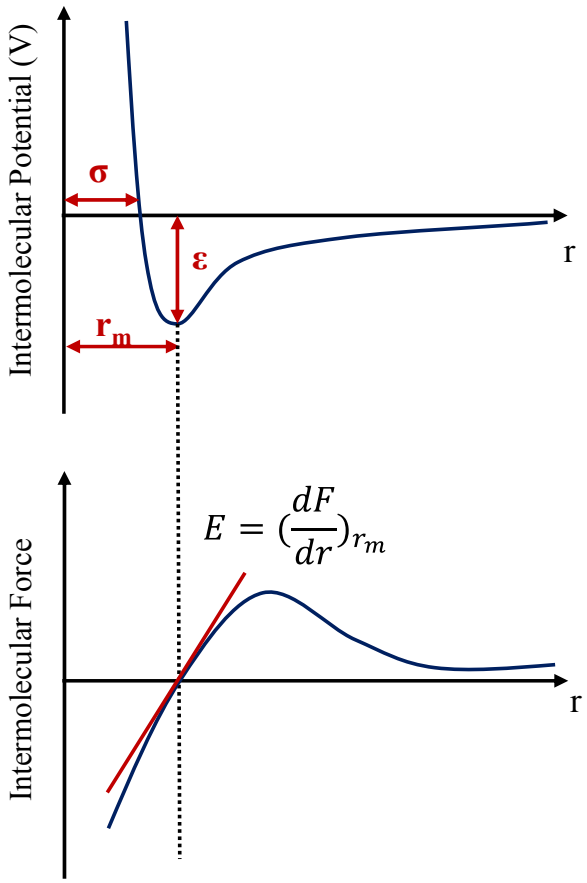

Figure 18 Schematic illustration of Lennard-Jones potential and intermolecular force

The first derivative of the LJ potential with respect to the distance gives an expression for the intermolecular force:

$$F = \frac{dV}{dr} = \frac{-12A}{r^{13}} + \frac{6B}{r^{7}} \tag{32}$$

The modulus of elasticity is a measure of resistance to detachment of the adjacent molecules, and is proportional to the slope of force-distance curve at r_m (Callister and Rethwisch 2011):

$$E \propto \frac{d^2V}{dr^2} = \frac{dF}{dr} = \frac{156A}{r^{14}} - \frac{42B}{r^{8}} \tag{33}$$

As water vapor transports into the asphalt, small molecules of H_2O diffuses between the molecular chains and occupy positions among the molecular chain. Therefore, the molecules are pushed away and the distance between them increases. The separation of chain results in an increase in *r* value in Equations (32) and (33). Consequently, the intermolecular bonding force and modulus of elasticity diminish and the asphalt becomes softer. The schematic picture of this mechanism is presented in Figure 17-b. This change in the molecular structure of asphalt is the main cause of cohesive failure occurring in FAM given the moisture diffusion. Therefore, the CD model, which accounts for the deterioration effect of moisture on modulus of FAM, can be formulated as follows:

$$d_{CD} = 1 - \frac{E_{wet+aged}}{E_{dry+aged}} = 1 - \frac{P \times (E'_{wet+aged}) + (1-P)E'_{dry+aged}}{E'_{dry+aged}} \tag{34}$$

where,

$E'_{wet+aged}$ = the average aged modulus in wet state;

$E'_{dry+aged}$ = the average aged modulus in dry state;

P = the percentage of molecules affected by moisture.

$E'_{wet+aged}$ and $E'_{dry+aged}$ are defined based on Equation (33), assuming that the initial average molecular distance r_m is changed to r_w after water molecules diffuse within chains:

$$E'_{dry+aged} = \frac{156A}{r_m^{14}} - \frac{42B}{r_m^{8}} \tag{35}$$

$$E'_{wet+aged} = \frac{156A}{r_w^{14}} - \frac{42B}{r_w^{8}} \tag{36}$$

Substituting Equations (35) and (36) into Equation (34) gives the following Equation for CD model:

$$d_{CD} = P\left[1-(\frac{r_m}{r_w})^8 \times (\frac{-1+3.7(A/B)\times r_w^{-6}}{-1+3.7(A/B)\times r_m^{-6}})\right] \quad (37)$$

When Equations **Error! Reference source not found.**, (30) and (31) are substituted in Equation (37), the CD model can be rewritten as:

$$d_{CD} = P\left[1+1.17(\frac{r_m}{r_w})^8 - 2.17(\frac{r_m}{r_w})^{14}\right] \quad (38)$$

The next step in the development of CD model involves identifying the functions that properly describes the changes of P and r_w as a function of water content. The more water is absorbed, the more molecules are affected and more separation happens within the molecular chains. Therefore, P and r_w functions should be increasing with respect to the water content. The rate of water diffusion in FAM is fast at the beginning of process, and gradually decreases with time until it becomes close to zero. As diffusion is the main reason for changes in P and r_w, the same trend as diffusion rate should be seen for P and r_w. This further implies that these functions should be concave. In addition, P and r_w functions should have asymptotes so as to illustrate the equilibrium state that happens at the end of diffusion. Three function types satisfying the abovementioned criterion include logarithmic, negative exponential and monomial with the exponent between 0 and 1. All three functions are examined in the study and fitted to the measured data in order to identify the best matching functions. Equations (39) and (40) show the functions that gave the best fit, and so are selected in this study to model P and r_w:

$$P = 1 - \exp(-a'w) \tag{39}$$

$$\frac{r_m}{r_w} = \frac{r_m}{r_m + d' \times w^{c'}} = \frac{r_m}{r_m(1 + \frac{d'}{r_m} \mathrm{w}^{c'})} = \frac{1}{1 + b'w^{c'}} \tag{40}$$

where,

w = gravimetric water content, %;

a', b', c' = fitting parameters.

The ultimate function for CD model is obtained by substituting Equations (39) and (40) into Equation (38) as follows:

$$d_{CD} = [1 - \exp(-\mathrm{a}'\mathrm{w})] \times [1 + \frac{1.17}{(1 + b'w^{c'})^8} - \frac{2.17}{(1 + b'w^{c'})^{14}}] \tag{41}$$

For a viscoelastic material such as FAM, the effect of absorbed water in the degradation is affected by temperature and loading frequency. In general, increasing the temperature and decreasing the frequency result in an aggravation of cohesive deterioration. With respect to the molecular structure, when temperature is raised, the molecular motion of water molecules increases. Therefore, they gain higher energy to force apart macromolecules of FAM, resulting in the more reduction in secondary intermolecular bonding forces. Decreasing the loading rate has the same impact as increasing the temperature. At low frequency, water molecules have more time to push apart macromolecules of FAM and exacerbate the chain separation. This implies that that fitting parameters involved in representing r_w in Equation (40) (i.e., b' and c') are a function of loading frequency and temperature. This conclusion is examined in section 4.4.1. In order to calibrate CD model, a set of laboratory testing is conducted on FAM samples, which is explained in the next sections.

4.2 Materials and Fabrication

The parameters used in CD model are determined by conducting the dynamic modulus test on FAM specimens. FAM specimens are composed of a PG 64-22 asphalt binder and limestone aggregates. They are prepared by using fine portion (i.e. aggregate portions passing No. 16 sieve (1.18 mm)), of a full mixture referred to as S3 PG 64-22 HMA. That is, the gradation of FAM follows the gradation of fine portion in S3 PG 64-22 mixture as illustrated in Figure 19. All materials were obtained from the designated suppliers and quarries in Oklahoma. The S3 PG 64-22 is a 19 mm Superpave mixture (i.e., nominal maximum aggregate size is 19 mm) composed of 30% #67 Rock, 10% 1/2" Chips, 45% Sand, and 15% fine RAP. Job mix formula and mix design sheet are obtained from the bituminous material laboratory at ODOT.

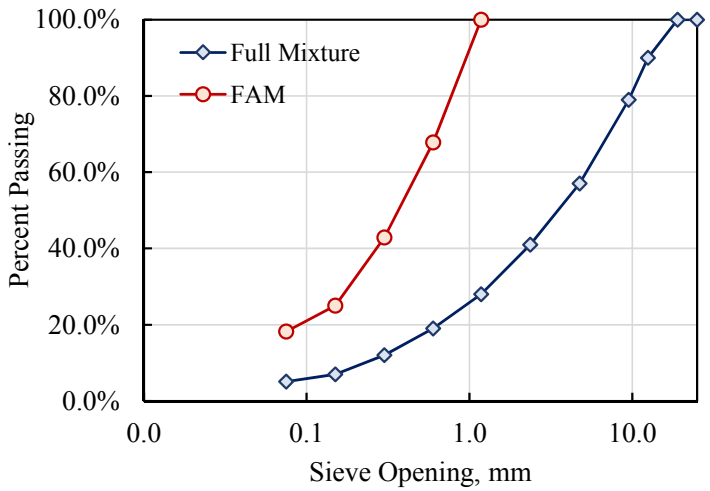

Figure 19 S3 PG 64-22 full mixture and FAM gradation

The binder content of FAM was determined by following the approach developed by Sousa et al. (2013). His approach is based on separating the fine portion of a mixture from the

coarse portion, and burning that in the ignition oven at 427°C. The measured asphalt content for FAM specimens, referred to as S3 PG 64-22 FAM, was measured as 8.5% by weight of the mixture. Loose FAM mixtures were conditioned in the oven at 135°C for two hours to simulate short-term aging, and then compacted by SGC in 150 mm diameter and 120 mm height as shown in Figure 20(a). The required weight of specimens were calculated such that their air void contents were less than 2%. The final cylindrical specimens of 38 mm in diameter and 110 mm in height were cored and cut as illustrated in Figure 20(b), and their volumetric properties are measured following the corresponding AASHTO standards.

(a) (b)

Figure 20 (a) compacted versus (b) cored and cut specimens

4.3 Test Procedure

The number of 34 S3 PG 64-22 FAM specimens were fabricated, and their dry weight were recorded. 18 specimens were placed in the moisture room at 100% relative humidity and 35°C temperature while 16 specimens were put in a chamber at 35°C. 8 conditioning times of 2, 4, 12, 20, 32, 40, 60 and 90 days, were defined for conditioning specimens that were placed in the moisture room. Two replicates were prepared for each conditioning time. When conditioning time

was over, specimens were taken out from the moisture room and prepared for |E^*| testing. Brass buttons were glued to the surface of test specimens using a button gluing jig as shown in Figure 21. Three LVDTs were mounted on the buttons and dynamic modulus was conducted in the strain-control mode by using AMPT. In order to keep the moisture content constant during the test and provide the testing environment close to the environment condition, conditioned specimens were tested at 25, 10, 5, 1, 0.1 Hz frequencies and only one temperature of 35˚C. The objective was to ensure that water vapor concentration resulting from the conditioning in 100% RH is not disturbed during the test. Since the test chamber for |E^*| testing does not provide RH, when conditioned specimens are placed into the chamber, concentration gradients between specimens and surrounding cause the desorption of water from the tested specimens. In order to minimize this desorption, the test is conducted at the conditioning temperature (i.e., 35°C herein). Therefore, specimens can be tested immediately after withdrawing from the moisture room and so water vapor concentration can be assumed to be approximately constant during testing. Peak-to-peak strain level were set to be within 45 and 60 micro-strain to ensure that no damage occurs during the loading, and that FAM samples remain in the linear viscoelastic region.

(a) (b)

Figure 21 (a) brass buttons glued to FAM specimen; (b) dynamic modulus set-up

Dry samples that were placed in the chamber at 35°C were tested after 2, 4, 12, 20, 32, 40, 60 and 90 days of aging time. Two replicates were prepared for each aging time, and |*E**| testing is conducted in the same approach as that adopted for moisture-aged conditioned specimens. The results of dynamic modulus testing are employed in Equation (34) to determine the fitting parameters of CD model.

4.4 Results and Discussion

4.4.1 Calibration of CD Model

Figure 22 presents the measured dynamic modulus for aged samples in 5 aging conditions. As master curves are close to each other, to better see the observed trend 5 conditions are presented out of 8 performed conditions. Also, the dynamic modulus results of moisture-aged conditioned specimens measured at 35°C are illustrated in Figure 23.

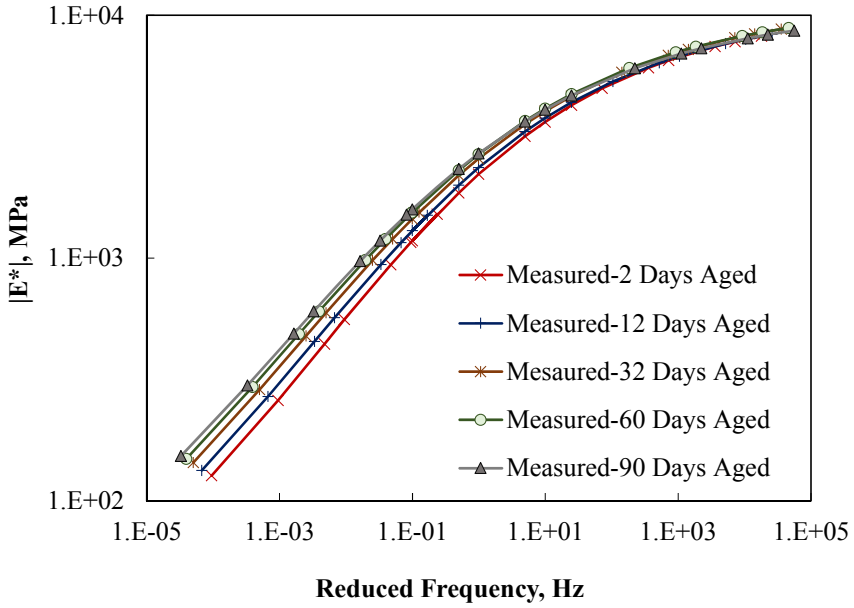

Figure 22 |*E| master curve for aged FAMs in log-log scale**

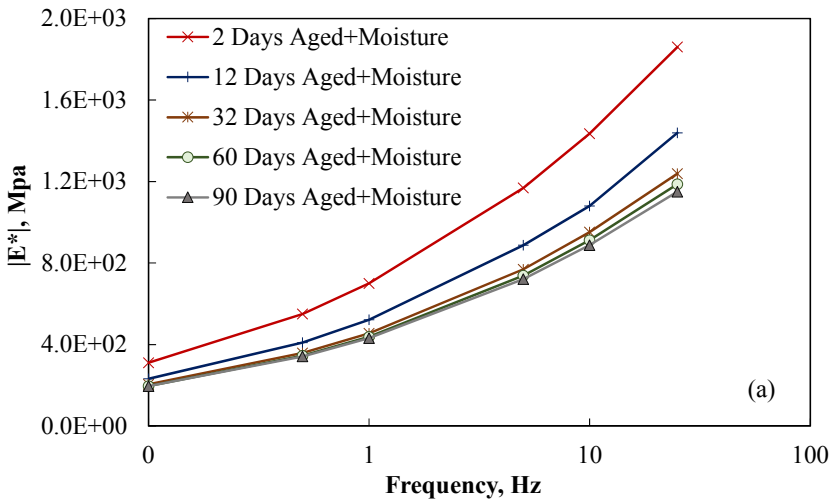

(a)

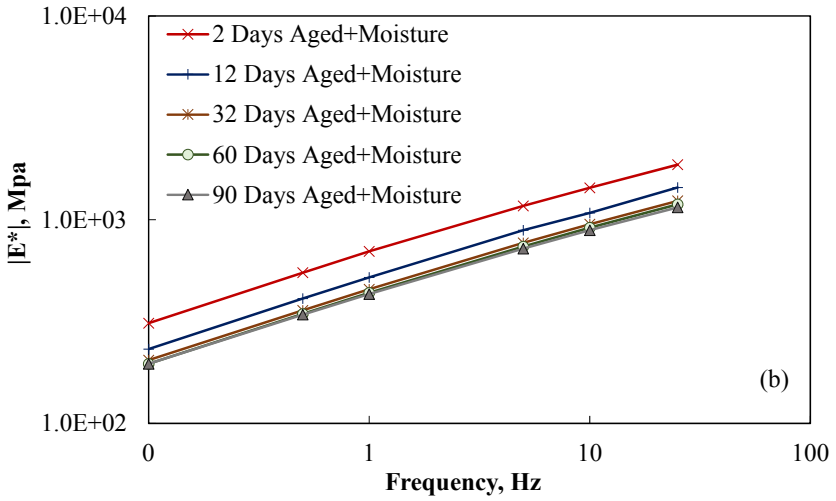

(b)

Figure 23 Measured |*E| at 35°C of conditioned FAMs in (a) semi-log and (b) log-log scales**

The ratio of measured |*E**| values of aged-moisture conditioned specimens to measured |*E**| values of aged specimens is subtracted from one. The remainder indicates the cohesive

damage induced in each conditioned specimen. The gravimetric water content corresponding to each conditioning time is calculated as:

$$w = \frac{m_w}{m} \times 100 \tag{42}$$

where,

m_w = mass of absorbed water in FAM specimen after conditioning time of t, gram;

m = mass of dry FAM specimen, gram.

The measured damage ratio is then plotted versus gravimetric water content in Figure 24. Each data point represents the average cohesive damage introduced into two replicates. The CD model is then fitted to the measured damage ratios to find the fitting parameters of a', b' and c' in Equation (41). Evidently, the cohesive damage aggravates with an increase in the water content. As mentioned in section 4.3, in order to keep the water content constant during testing, $|E^*|$ was conducted only at 35°C but at different loading frequencies. It is observed that the cohesive damage changes with the frequency of loading; at lower frequency the effect of diffused water in reduction of $|E^*|$ is greater than that at higher frequency. Such a trend is expected because as explained previously, at low frequency, water molecules have more time to push apart macromolecules of FAM and exacerbate the chain separation. As shown in Figure 24, the CD model with R^2=98 is robust in predicting the cohesive damage when loading temperature is the same as conditioning temperature.

Dependency of the cohesive damage on frequency is captured by parameters b' and c' while a' accounts for the percentage of molecules affected by absorbed water; Figure 25 shows the relationship between these parameters and loading frequency for S3 PG 64-22 FAM specimens tested here. It is observed that a power law and logarithmic function are capable of

appropriately model b' and c', respectively, as a function of loading frequency. In general, fitting parameters a', b' and c' accounts for the changes happening in the intermolecular bonding force of a FAM subjected to a certain combined aging-moisture conditioning. These parameters change if aging temperature, RH or FAM components alter. P, b' and c' functions are presented in the following equations.

$$P = 1 - \exp(0.25w) \tag{43}$$

$$b' = 0.0205 fr^{-0.181} \tag{44}$$

$$c' = 0.13 \log(fr) + 0.18 \tag{45}$$

Substituting Equation (43),(44) and (45) for a', b' and c' in Equation (41) gives the final form for CD model as follows:

$$d_{CD} = [1 - \exp(-0.25\,\mathrm{w})] \times [1 + \frac{1.17}{(1 + 0.02 fr^{-0.181} w^{0.13 \log fr + 0.18})^{8}} - \frac{2.17}{(1 + 0.02 fr^{-0.181} w^{0.13 \log fr + 0.18})^{14}}] \tag{46}$$

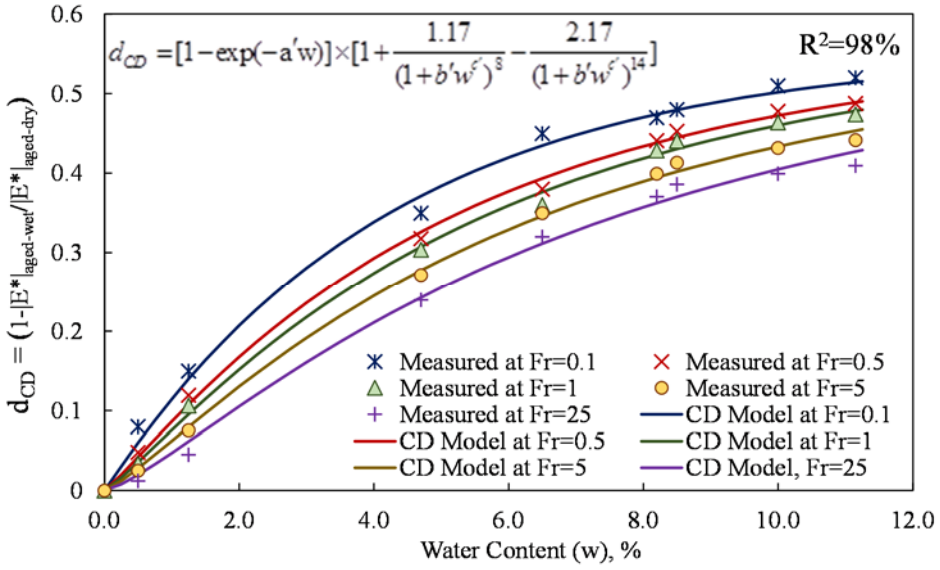

Figure 24 Cohesive damage vs. water content at different frequencies

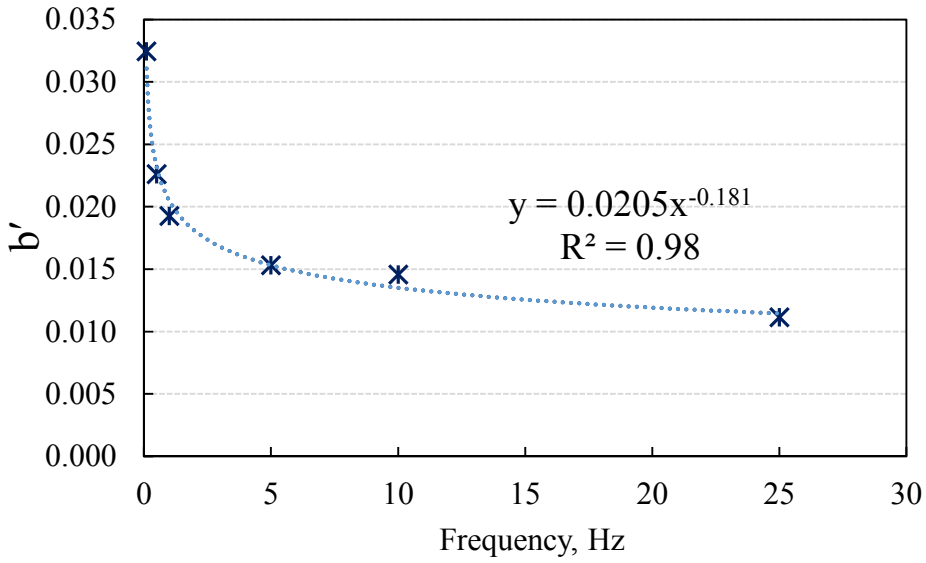

(a)

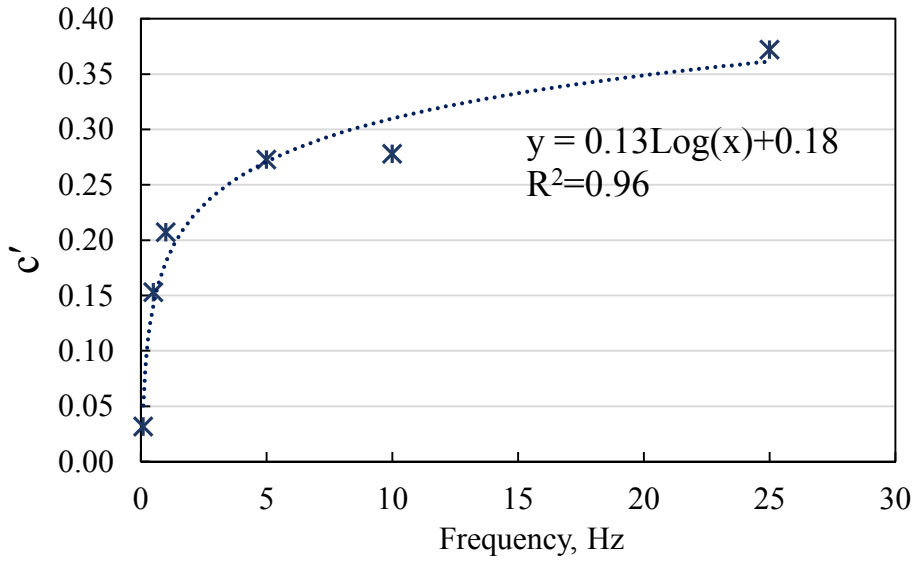

(b)

Figure 25 Fitting parameters (a) *b′* and (b) *c′* versus frequency

4.4.2 Extension of CD Model

As stated in the preceding section, for FAM specimens subjected to the moisture conditioning combined with aging, $|E^*|$ testing is conducted at several frequencies but just one temperature of 35°C to ensure that the water content remains constant during testing. Based on the concept of time-temperature superposition for a viscoelastic material such as FAM, the effect on the material property caused by the frequency changes is similar to that caused by temperature changes. With respect to the effect of diffused water vapor on intermolecular bonding, increasing the temperature causes the same effect on the reduction of intermolecular bond as decreasing the frequency. Therefore, the CD model can be extended to account for the variation in both loading temperature and frequency.

The temperature effects can be simply described by shifting the frequency through a shift factor. Referring to Equations (34) and (41), the $|E^*|$ for an aged-moisture conditioned FAM can be formulated as follows:

$$\left|E^*\right|_{aged+wet} = \left|E^*\right|_{aged} \times (1 - d_{CD}) = \left|E^*\right|_{aged} \times \{1 - [1 - \exp(-a'w)] \times [1 + \frac{1.17}{(1 + b'w^c)^8} - \frac{2.17}{(1 + b'w^{c'})^{14}}]\} \quad (47)$$

Where, b' and c' are formulated as functions of the loading frequency as:

$$b' = 0.02 \times f^{-0.181} \quad (48)$$

$$c' = 0.13 \times Log(f) + 0.18 \quad (49)$$

Since CD model is applied on the aged $|E^*|$, the shift factor of the aged specimens can be used to combine the effect of the temperature and frequency into a single factor, referred to as the reduced frequency:

$$f_R = a_T^{aged} \times f = 10^{(\alpha_1 T^2 + \alpha_2 T + \alpha_3)} \times f \quad (50)$$

where,

f = frequency;

a_T^{aged} = shift factor of the aged FAM specimen;

$\alpha_1, \alpha_2, \alpha_3$ = fitting parameters of the shift factor for the aged specimen.

As Equations (48) and (49) are developed at 35°C, this temperature should be considered as the reference temperature, at which the magnitude of shift factor is 1:

$$a_{T=35^\circ C}^{aged} = \frac{f_R}{f_{T=35^\circ C}} = 1 \tag{51}$$

Substituting Equation (50) into (41) yields the final form of CD model for the tested FAMs as follows:

$$d_{CD} = [1 - \exp(-0.25\,\mathrm{w})] \times [1 + \frac{1.17}{(1 + (0.0205\,\mathrm{f}_R^{-0.181}) w^{(0.13 Log f_R + 0.18)})^8} - \frac{2.17}{(1 + (0.0205\,\mathrm{f}_R^{-0.181}) w^{(0.13 Log f_R + 0.18)})^{14}}] \tag{52}$$

It should be noted that the conditioning temperature in this study is 35°C. However, $|E^*|$ testing can be conducted at a temperature different than conditioning temperature. In order to apply time-temperature superposition to construct the master curve for moisture conditioned specimens, two assumptions should be considered; the first assumption is that water concentration inside the conditioned specimens does not change during testing. Although this assumption might not be completely satisfied in the lab-testing, it is almost valid in the field because as stated in the preceding section, RH in asphalt layer reaches to 100% in a short period of time after construction, and remain constant afterward given that subgrade serves as a reservoir beneath the pavement. Considering the short period of testing compared to the long time period required for desorption of the water from FAM, this assumption can be nearly

satisfied in the lab testing. Therefore, it can be assumed that P function (which represents percentage of molecules affected by the moisture) does not change when $|E^*|$ testing is conducted at different temperatures. The second assumption is that loading temperature during testing does not cause further aging, and that aging mostly happens due to the binder oxidation at the conditioning temperature. This assumption is correct since the change of loading temperature happens at the short period of time during the test, at most two hours, which is not adequate to create significant changes in the oxidation rate. Thus, it can be assumed that the parameters b' and c' do not change significantly when $|E^*|$ testing is conducted at different temperatures. Therefore, CD model presented in Equation (52) can be properly used to quantify the cohesive damage induced in FAM specimen at various loading temperatures and frequencies.

5. ADHESIVE DAMAGE (AD) MODEL

5.1 Model Formulation

The adhesive bond between the aggregate and asphalt binder deteriorates as water enters the interface as shown in Figure 26. The work of adhesion without the presence of water can be determined from Equation (53), which is used to characterize the fracture resistance of asphalt mixtures. ΔG indicates the difference between the final and initial states of energy in a system:

$$\Delta G_{SA}^{AF} = \gamma_S + \gamma_A - \gamma_{SA} = 2(\sqrt{\gamma_A^{LW}\gamma_S^{LW}} + \sqrt{\gamma_A^+\gamma_S^-} + \sqrt{\gamma_A^-\gamma_S^+}) \quad (53)$$

where,

ΔG_{SA}^{AF} = Adhesive bond energy of fracture;

$\gamma_A^{LW}, \gamma_A^+, \gamma_A^-$ = Surface energy components of asphalt binder;

$\gamma_S^{LW}, \gamma_S^+, \gamma_S^-$ = Surface energy components of aggregate;

$\gamma_A, \gamma_S, \gamma_{SA}$ = Surface free energy of asphalt binder, surface free energy of aggregate and interface energy between aggregate and asphalt binder.

When water vapor is present in the interface, water molecules are absorbed by the aggregate. As a result, the surface free energy of aggregate is reduced by the amount of spreading pressure as follows (Zhang and Luo 2017(a)):

$$\gamma_{SV} = \gamma_S - \pi_e \quad (54)$$

where,

γ_{SV} = Surface energy of the aggregate in equilibrium with the saturated water vapor, ergs/cm^2;

π_e = Spreading pressure, ergs/cm^2.

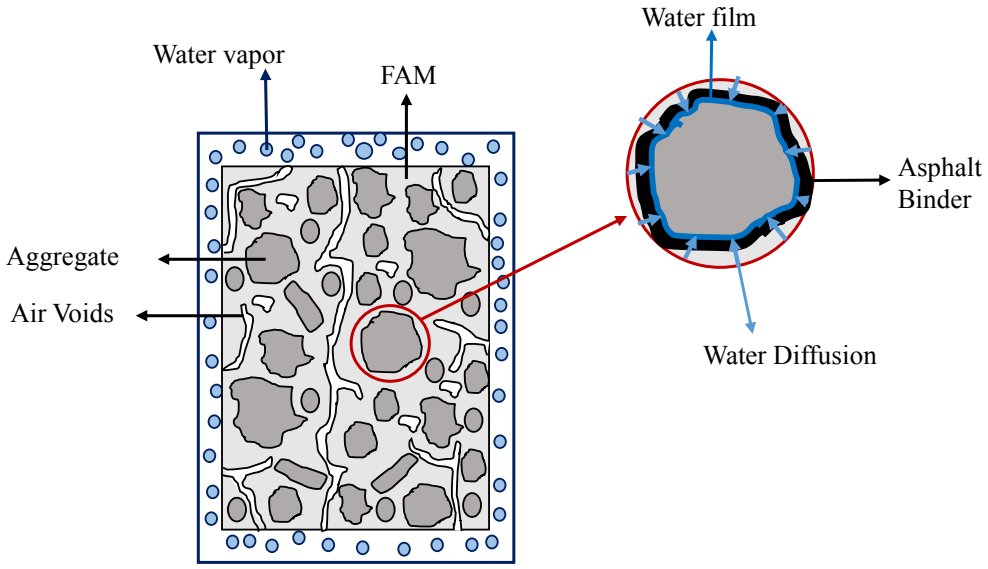

Figure 26 Adhesive bond deterioration mechanism due to water diffusion

π_e is defined as the reduction of surface energy of the aggregate due to the absorption of water vapor, and illustrated as follows (Zhang and Luo 2017(b); Zhang and Luo 2018):

$$\pi_e = \frac{RT}{m_{H_2O} A} \int_0^{P_0} \frac{n}{p} dP \tag{55}$$

where,

R = universal gas constant, 8.314 J/K mol;

T = test temperature, K;

m_{H_2O} = molecular weight of water, 18.015 gr/mol;

A = The specific surface area of aggregate, m^2/gr;

n = amount of vapor absorbed on the aggregate, gr;

P_0 = saturated water pressure at the test temperature, Pa;

P = water vapor pressure, Pa.

Changing the upper limit of integral to a specific water vapor P_1, π_e can be obtained at the corresponding relative humidity, *RH*, as follows:

$$\pi_{e-RH} = \frac{RT}{mA}\int_0^{P_1}\frac{n}{P}dP = \frac{RT}{mA}\int_0^{RH\times P_0}\frac{n}{P}dP \tag{56}$$

The components of Equation (56) are determined by conducting the Universal Sorption Device (USD) test on aggregates. In the presence of water vapor, Equation (53) should be modified to:

$$\Delta G_{SVA}^{AF} = \gamma_{SV} + \gamma_{AV} - \gamma_{SA} \tag{57}$$

Where, ΔG_{SVA}^{AF} is defined as the adhesive bond energy of the fracture process in the presence of water vapor. Since spreading pressure of asphalt binder is negligible, it can be assumed that $\gamma_{AV} = \gamma_A$, implying that surface free energy of asphalt binder is not reduced notably in the presence of water vapor. Combining Equation (54) and (56) with (57), ΔG_{SVA}^{AF} can be estimated at each relative humidity (RH) of interest as follows:

$$\Delta G_{SVA}^{AF} = \Delta G_{SA}^{AF} - \frac{RT}{mA}\int_0^{RH\times P_0}\frac{n}{p}dp \tag{58}$$

It should be noted that P_0 changes as the function of testing temperature. Zhang (2018, personal communication) showed that Equation (58) can be rewritten by an exponential function as shown below to fit the experimental data:

$$\Delta G_{SVA}^{AF} = b - a\exp(RH^c) \tag{59}$$

Where *a*, *b* and *c* are fitting constants specific for an aggregate-asphalt bond. Equation (59) was adopted in this study to characterize the adhesive bond energy with respect to RH for aggregate-asphalt combinations tested.

ΔG_{SA}^{AF} is a thermodynamic property affected by the water vapor presence in the interface. In order to formulate an adhesive damage model (AD), the underlying link between this thermodynamic property and stiffness of AC should be identified. As a composite material, AC stiffness is defined by three constituents including aggregate stiffness, FAM stiffness, and tensile strength of the adhesive bond between aggregate and asphalt. Tensile strength of an adhesive bond shown in Figure 27 can be determined from Equation (60) (Lytton. 2015):

$$\sigma_t = \left[(\frac{8}{3t}) \times (\frac{m}{A} \overline{c}) \times \frac{1}{1+\frac{E_A}{E_S}} \right]^{0.25} (E_A \Delta G_{SA}^{AF})^{0.5} \quad (60)$$

where,

t = binder thickness, m;

m = number of cracks;

A = cross section area of the binder, m^2;

$\overline{c}$ = mean crack size, m;

E_A, E_S = Relaxation modulus and Young modulus of asphalt and aggregate, respectively, Pa;

ΔG_{SA}^{AF} = Adhesive bond energy of fracture between asphalt and aggregate, ergs/m^2.

To account for the deterioration effect of water vapor presence in the adhesive bond, the Adhesive Damage (AD) model is formulated as follows:

$$d_{AD} = 1 - \frac{\sigma_t^{wet+aged}}{\sigma_t^{dry+aged}} \tag{61}$$

Where $\sigma_t^{wet+aged}$ denotes the tensile strength of adhesive bond between an aged binder and aggregate in the presence of water vapor. Replacing dry properties with wet properties $\sigma_t^{wet+aged}$ can be obtained as:

$$\sigma_t^{wet+aged} = \left[(\frac{8}{3t}) \times (\frac{m}{A}\bar{c})^{wet+aged} \times \frac{1}{1 + \frac{E_A^{wet+aged}}{E_S^{wet}}} \right]^{0.25} (E_A^{wet+aged} \Delta G_{SVA-aged}^{AF})^{0.5} \tag{62}$$

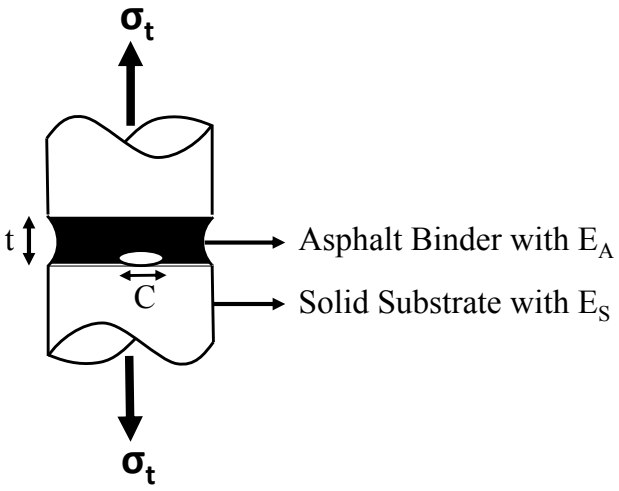

Figure 27 Adhesive failure between asphalt binder and a substrate

Note that "aged" subscript denotes the properties of aged materials, and "wet+aged" subscript indicates property of the materials subjected to the aging coupled with moisture conditioning. Lytton (2015) showed that $\frac{m}{A}\bar{c}$ value is constant for a certain material. This value

represents the amount of cracks developed in the material once tensile stress reaches the maximum value in the stress-strain curve. Thus, $\frac{m}{A}\bar{c}$ value can be assumed to be identical in dry and wet condition given that the same aggregate-asphalt materials are involved in the bond. Substituting Equations (60) and (62) in Equation (61), and canceling out the similar terms from numerator and denominator gives the following expression for AD model:

$$d_{AD} = 1 - \left[\left(\frac{E_S^{wet}}{E_S^{dry}} \times \frac{E_S^{dry} + E_A^{aged}}{E_S^{wet} + E_A^{wet+aged}} \right)^{0.25} \times \left(\frac{E_A^{wet+aged}}{E_A^{aged}} \right)^{0.5} \times \left(\frac{\Delta G_{SVA-aged}^{AF}}{\Delta G_{SA-aged}^{AF}} \right)^{0.5} \right] \tag{63}$$

Young modulus of aggregates are significantly larger than that of asphalt binder even at low temperature and high loading frequency (Allen et al. 2012; Zhou et al. 1995). Also, the effect of absorbed water on changing Young modulus of aggregates is negligible. Aggregates are categorized as the refractory ceramic material. Refractories are often porous and able to absorb water through connected pores. Given the strong interatomic bonding between atoms and molecules in ceramic materials, the absorbed water vapor molecules could not interfere with the intermolecular bonding as opposed to what occurs in polymers. Therefore, Young modulus of wet aggregates are approximately the same as that of dry aggregates. The abovementioned explanation implies the following expressions:

$$\begin{aligned} &E_S^{wet} \simeq E_S^{dry} \\ &E_S^{dry} \gg E_A^{aged} \\ &\frac{E_S^{wet}}{E_S^{dry}} \times \frac{E_S^{dry} + E_A^{aged}}{E_S^{wet} + E_A^{wet+aged}} \simeq 1 \end{aligned} \tag{64}$$

Applying Equations (59) and (64) into (63) yields:

$$d_{AD} = 1 - \left[\left(\frac{E_A^{wet+aged}}{E_A^{aged}} \right)^{0.5} \times \left(\frac{b - a\exp(RH^c)}{b - a} \right)^{0.5} \right] \tag{65}$$

a, *b* and *c* implicitly capture the effect of aging on the adhesive bond if they are determined by conducting the test on aged samples. RH is proportional to the water vapor concentration as demonstrated in Equation (66):

$$RH = \frac{P}{P_0} = \frac{RT}{P_0 m_{H_2O}} C_m \tag{66}$$

Where, C_m is the water vapor concentration at the aggregate-asphalt interface. The value of C_m is controlled by the diffusivity of water vapor in AC and diffusion time. The diffusion coefficient of a certain mixture changes with aging; hence, aging has also an implicit effect on C_m. The final form of AD model is illustrated in Equation (67).

$$d_{AD} = 1 - \left[\left(\frac{E_A^{wet+aged}}{E_A^{aged}} \right)^{0.5} \times \left(\frac{b - a \exp\left(\left\{ \frac{RT}{P_0 m_{H_2O}} C_m \right\}^c \right)}{b - a} \right)^{0.5} \right] \tag{67}$$

5.2 Test Procedure and Material Fabrication

Parameters of AD model are determined by conducting BBS tests on aged-moisture conditioned test specimens in accordance with AASHTO TP 91. As shown in Figure 28, the BBS device is composed of a pressure hose, pneumatic adhesion device, piston, reaction plate and metal pull-out stubs (Moraes et al. 2011). A pull-off force is applied on the test specimen by the metal stubs. When applied stress exceeds the adhesive strength between asphalt and aggregate or cohesive strength within the binder, the failure occurs. The Pull-of Tensile Strength (POTS) is determined from Equation (9) detailed in Section 2.2. Depending on the asphalt thickness, testing temperature, rheology of the asphalt, rate of loading and water presence in the interface, type of failure can be either adhesive, cohesive or combination of both. It has been recognized that the presence of moisture at the interface is one of the main causes for adhesive

failure (Kanitpong and Bahia 2005; Moraes et al. 2011). The AD model is aimed to characterize the bond strength with respect to water vapor concentration. A test set-up was designed to create the concentration gradients at the interface between aggregate and binder with time as illustrated schematically in Figure 29. In order to properly simulate water vapor transport as it happens within the mixture, the substrate surface was prepared by cutting thin slices of 2 cm from S3 PG 64-22 compacted HMA. The top surface and surrounding edges of substrate was covered firmly with cellophane to prevent water vapor from evaporating from the surface, and provide the required boundary condition for solving a one-dimensional diffusion equation.

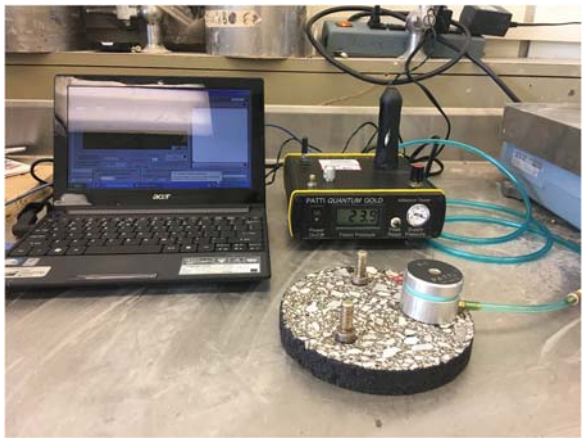

Figure 28 BBS test components

The S3 PG 64-22 HMA is a 19 mm Superpave mixture composed of 30% #67 Rock, 10% 1/2" Chips, 45% Sand, and 15% fine RAP, and its binder content is 4.4% by weight. The procedure detailed in Section 3.2.1 was followed to prepare the compacted mixtures. In total, 33 slices were prepared for BBS test. After cutting, substrates slices were submerged in distilled water at 25°C to remove any surface residue from the cutting process. They were then kept at the

room temperature in front of a fan for two days to remove the absorbed water. Then, acetone was applied on the aggregate surface exposed to air, and metal stubs to remove dust. The metal stub has a diameter of 12.7 mm, and a 0.8 mm thickness surrounding edge. Four cuts exist along the stub edge to allow the flow of excess asphalt binder out as the stub is pressed on the aggregate surface.

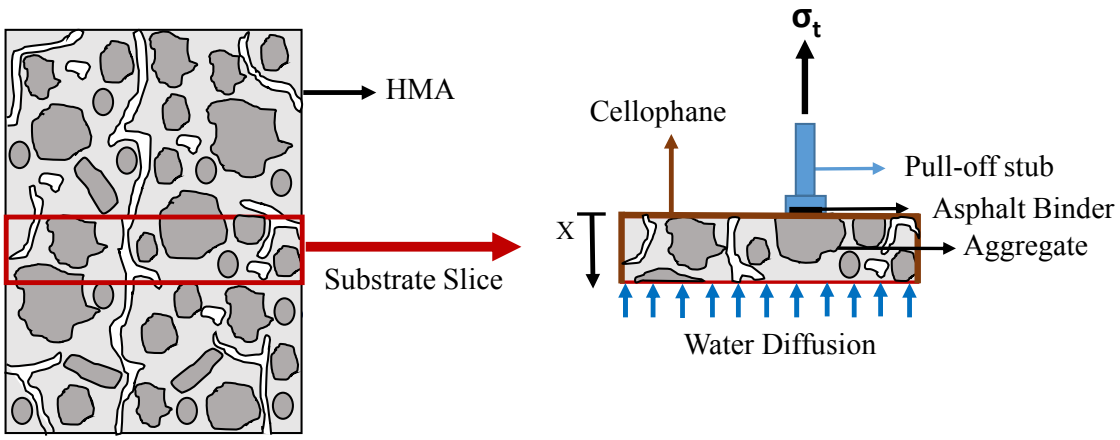

Figure 29 Bitumen Bond Strength Test setup

RFTO-aged PG 64-22 binder was used as an adhesive material to take into account the effect of short-term aging on the bond strength. The substrate slice, stubs and asphalt binder were placed in the oven at 65, 85 and 164°C, respectively, for at least 30 minutes. Asphalt binder was then placed immediately on the surface of stubs, and the stubs containing asphalt were pressed firmly against the aggregate surface without applying the torsion until no excess asphalt binder flows. The excess asphalt was then scrubbed from the aggregate surface to ensure that adhesive measurements solely reflect the aggregate-asphalt bond strength (Figure 30). Four stubs were pressed on each slice, and each slice was subjected to a predefined aging-moisture conditioning

level. Aging-moisture conditioning levels were determined based on the varying time exposure to moisture and aging. 15 test specimens were placed in the moisture room at 100% relative humidity and 35°C temperature; 15 specimens were put in a chamber at 35°C, and one specimen was tested as a control specimen. Two replicates were used for the purpose of finding the diffusion coefficient and maximum water uptake of the test specimen subjected to the predefined conditioning. The saturated surface dry (SSD) weight of these two replicates were measured at various time intervals for one month. The recorded measurements are used to calculate the diffusion coefficient. It was then employed in a close form solution to estimate the water vapor concentration at the interface of aggregate and asphalt binder.

Figure 30 Sample preparation

The samples of pull-out stubs and substrate attached together with asphalt binders were conditioned in either the moisture room or chamber. 15 conditioning times of 1, 3, 12, 24, 32, 48, 72, 96, 120, 144, 216, 312, 384, 432, 500 and 700 hours were considered for conditioning specimens that were placed in the moisture room, and for those put in the chamber. When conditioning time was over, specimens were taken out and cellophane was removed from the top surface and surrounding edges. The BBS test was conducted on conditioned samples at the

loading rate of 0.82 MPa/s (120 psi/s) to measure the POTS. Four POTS measurements were recorded for each conditioning time since four stubs were pressed on each slice.

5.3 Results and Discussion

5.3.1 Diffusion Model

AD model is the function of water vapor concentration and so the first step toward the calibration of model is to find the water vapor concentration at the top surface as the function of time. The diffusion process that occurs through the test specimens when placed in moisture room is described by Fick's second law of diffusion in one-dimension (Callister and Rethwisch 2011):

$$\frac{\partial C}{\partial t} = D\frac{\partial^2 C}{\partial x^2} \tag{68}$$

where,

C = water vapor concentration, gr/mm^3;

t = time, s;

D = diffusion coefficient, mm^2/s;

x = position, mm.

For the specific test configuration shown in Figure 29, the following boundary conditions were applied to Equation (68):

$$X = L \rightarrow C = C_0 \qquad t \geq 0 \tag{69}$$

$$X = 0 \rightarrow \frac{\partial C}{\partial X} = 0 \qquad t \geq 0 \tag{70}$$

$$0 \leq X \leq L \rightarrow C = 0 \qquad t = 0 \tag{71}$$

where,

C_0 = constant water vapor concentration on the bottom surface of the specimen, gr/mm^3;

L = Specimen thickness, 20mm; and

X = Diffusion distance, mm.

For the specific conditioning selected for this test (i.e., 100% RH and T=35°C) C_0 is determined as follows:

$$C_0 = \frac{RH \times P_0 \times m_{H_2O}}{RT} = 39.37 \times 10^{-9}\, g/mm^3 \tag{72}$$

The diffusion process for the test configuration is the case of an absorption by a membrane where the initial concentration in the region $0 \le X \le L$ is zero, and bottom surface is kept at a constant concentration. The solution for the absorption in the form of a trigonometrical series is presented as follows (Crank 1979):

$$C = C_0 \times \left[1 - \frac{4}{\pi} \sum_{n=0}^{\infty} \frac{(-1)^n}{2n+1} \exp\left\{ -D(2n+1)^2 \pi^2 t / 4L^2 \right\} \cos \frac{(2n+1)\pi x}{2L} \right] \tag{73}$$

Where D is the diffusivity of the membrane. The amount of absorbed water entered the membrane at time t is determined by integrating C over the entire volume:

$$M_t = M_\infty \left[1 - \sum_{n=0}^{\infty} \frac{8}{(2\mathrm{n}+1)^2 \pi^2} \exp\left\{ -D(2\mathrm{n}+1)^2 \pi^2 t / 4L^2 \right\} \right] \tag{74}$$

Where M_∞ denotes the maximum water uptake after infinite time.

Equation (74) is used to fit the measured water uptake and back calculate the diffusion coefficient. Then, Equation (73) is employed to estimate C at X=0, which is denoted by C_m in Equation (67). The fitting procedure and C_m calculation was implemented in MATLAB. Figure 31 and Figure 32 indicate M_t and C_m versus diffusion time.

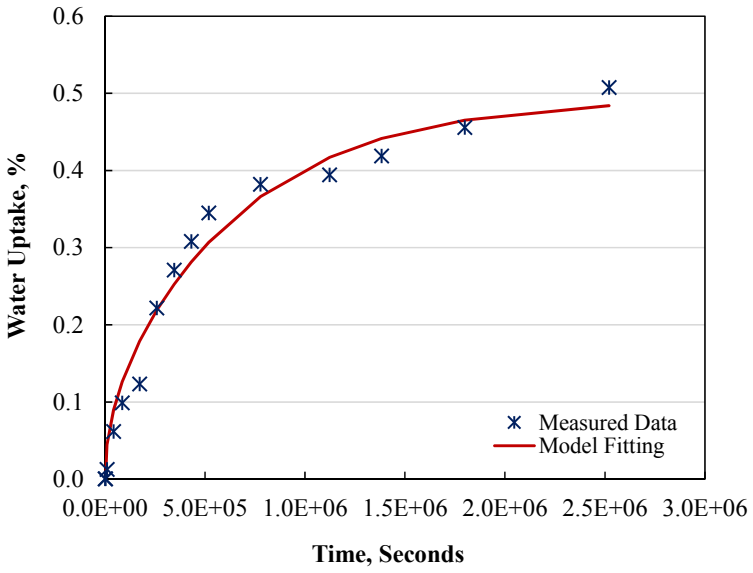

Figure 31 Moisture uptake versus time for S3 64-22 HMA slice at 35°C

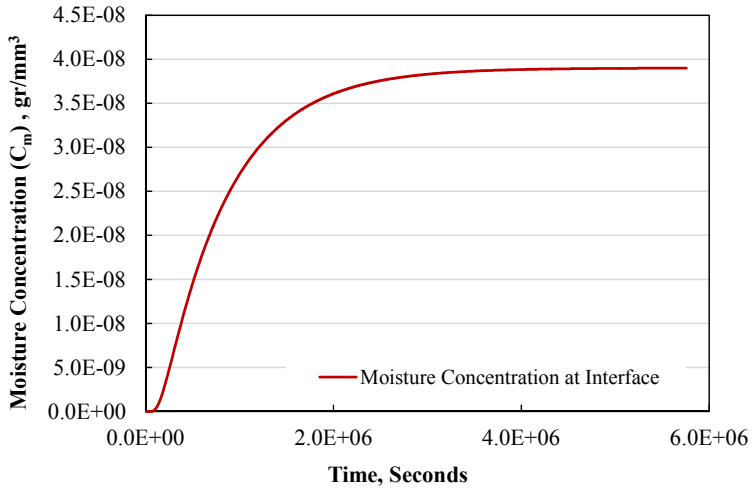

Figure 32 Water vapor concentration at interface

5.3.2 Calibration of AD Model

The results of BBS test on aged as well as aged-moisture conditioned specimens are presented in Figure 33 . It is observed that as conditioning time increases, the reduction in POTS

increases as well, which is obviously caused by the increased amount of accumulated water vapor concentration at the interface with time. Another possible explanation for the damage growth can be related to the potential of aging to worsen the moisture damage as discussed in Section 2.2. Figure 34 shows the images of failure on the surface recorded at various conditioning times. The first image on the left indicates the failure surface for the dry specimen; as moving to the right, conditioning time increases and so a greater amount of water vapor are diffused into the substrate, resulting in the growth of moisture damage.

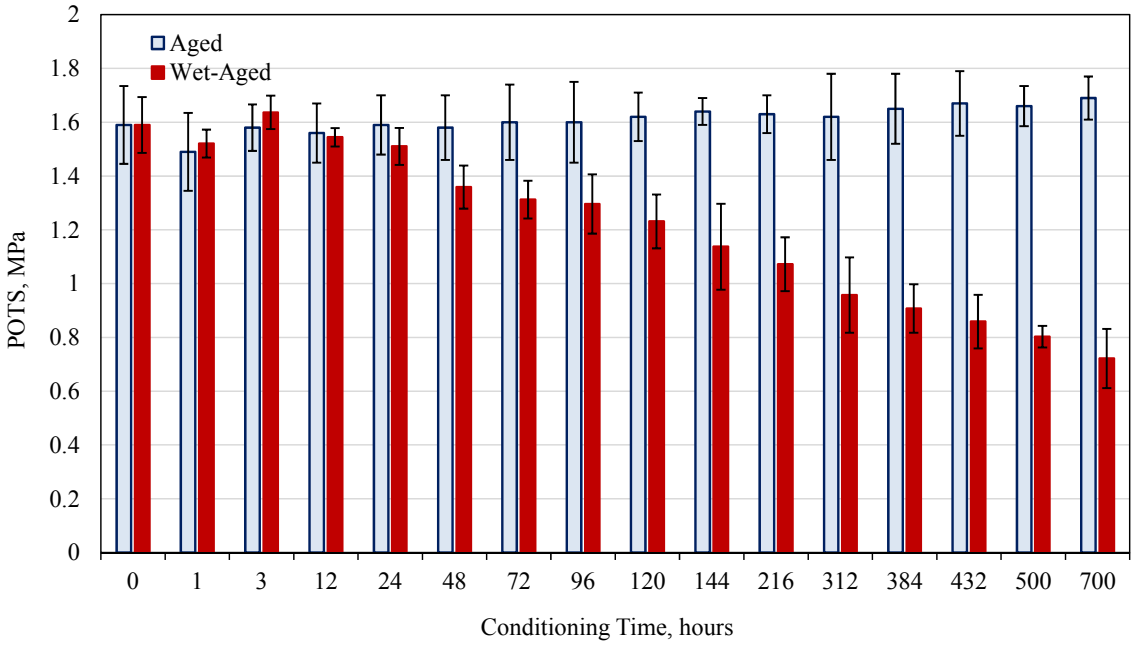

Figure 33 Measured POTS for aged and aged-moisture conditioned specimens

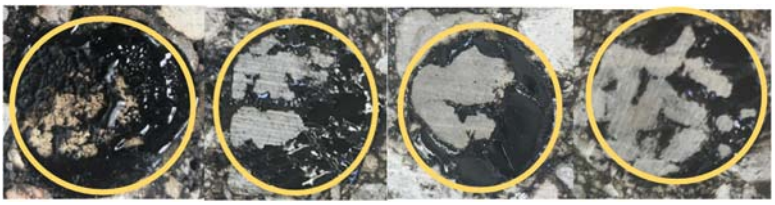

Figure 34 Moisture damage growth with conditioning time, increasing from left to right

The ratio of the POTS for aged-moisture conditioned specimens to POTS for aged specimens are determined. This ratio is then subtracted from one; the remainder indicates the measured adhesive damage induced at the interface. Adhesive damage is plotted versus conditioning time as shown in Figure 35. Each data point indicates the average adhesive damage introduced into four tested bonds. The C_m corresponding to each conditioning time is extracted from Figure 32, and then adhesive damage is plotted vs C_m in Figure 36. The AD model is then fitted to the measured damage to find the fitting parameters described in Equation (67). C_m can be converted to *RH* using Equation (66) to plot the damage against *RH* as presented in Figure 37.

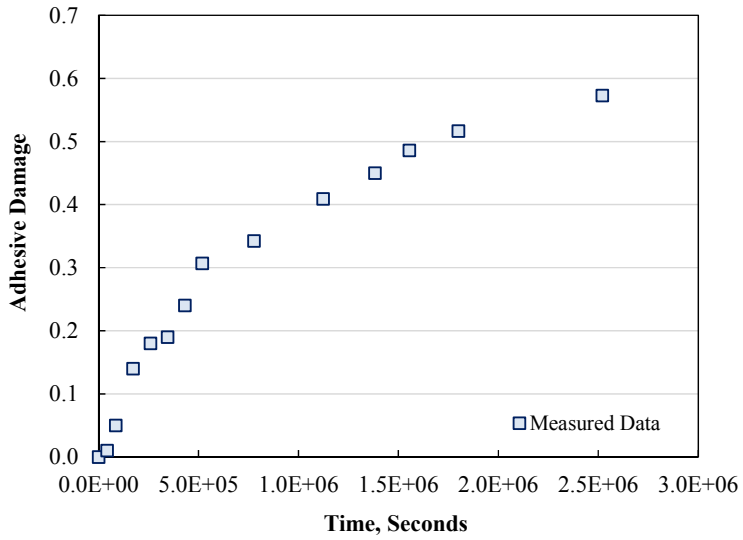

Figure 35 Adhesive damage versus time

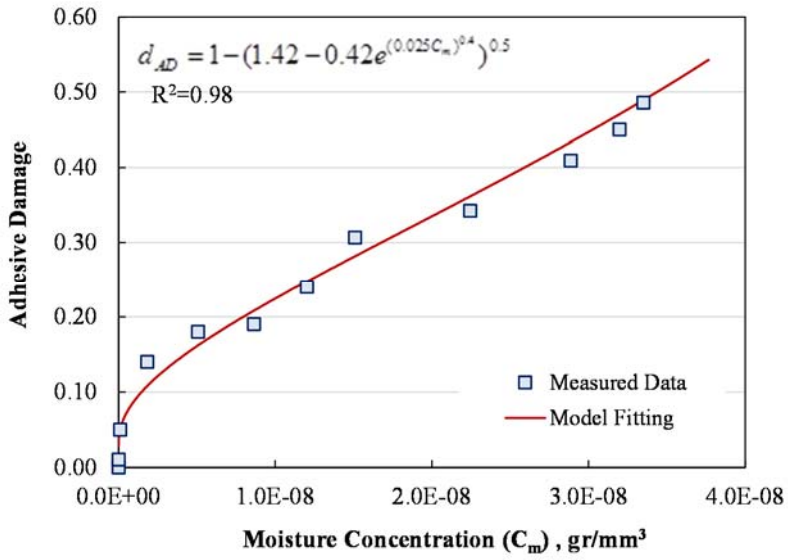

Figure 36 Adhesive damage vs C_m

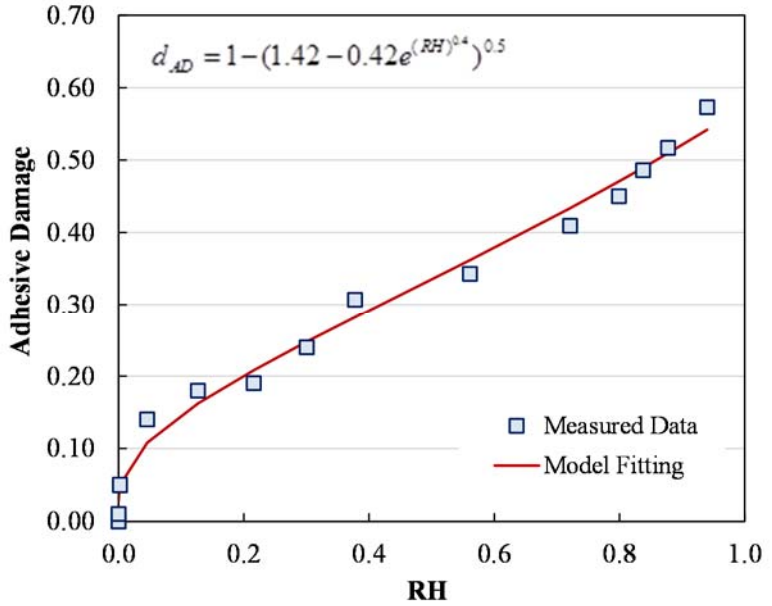

Figure 37 Adhesive Damage vs *RH*

Equation (75) and (76) present the final form of AD model for the tested materials. For the specific material tested in this study, *a*, *b* and *c* are found to be 97.57 ergs/cm^2, 304.85 ergs/cm^2 and 0.4, respectively. These parameters account for the coupling effect of aging and moisture. For the test configuration selected in this study, one month of conditioning at 100% *RH* and 35°C is needed to change *RH* at the interface from 0 to 1. When *RH* at interface reaches 1, diffusion process gradually stops given that concentration gradient along the specimen, which is the driving force for the diffusion, approaches zero. Time frame over which bond deterioration happens, depends on specimen dimensions, aggregate and asphalt source, moisture concentration available in the environment and temperature. Considering the actual dimensions of the pavement in field, the maximum damage generating in the bond occurs at much longer time than calculated value here.

$$d_{AD} = 1 - (1.42 - 0.42e^{(0.025C_m)^{0.4}})^{0.5} \tag{75}$$

$$d_{AD} = 1 - (1.42 - 0.42e^{(RH)^{0.4}})^{0.5} \tag{76}$$

The $\frac{E_A^{wet+aged}}{E_A^{aged}}$ term in AD model was obtained by conducting the regression analysis, and plotted versus *RH* in Figure 38. It is observed that this ratio decreases almost linearly with RH from 1 to near 0.88. Such a trend is expected because water vapor molecules diffuse into the asphalt binder after they reach the interface. However, since the diffusivity of asphalt binder is smaller than that of asphalt mixture (Arambula et al. 2009), and also time frame examined in this study is short, the induced damage in asphalt binder is not significant. To simplify the AD model, the averaged ratio, which is 0.96, is used in the model. It should be noted that the asphalt film thickness around the aggregates in AC pavements in the field is significantly smaller than

that in BBS test configuration. When asphalt film is very thin, a steady state diffusion process occurs rather than non-steady steady, thus, water vapor passes through the film rather instead of being accumulated. Consequently, the asphalt-aggregate bond deterioration precedes the modulus reduction of asphalt. Therefore, average ratio of 0.96 can reasonably represent the modulus reduction of asphalt film involved in adhesive bond for in-service pavements.

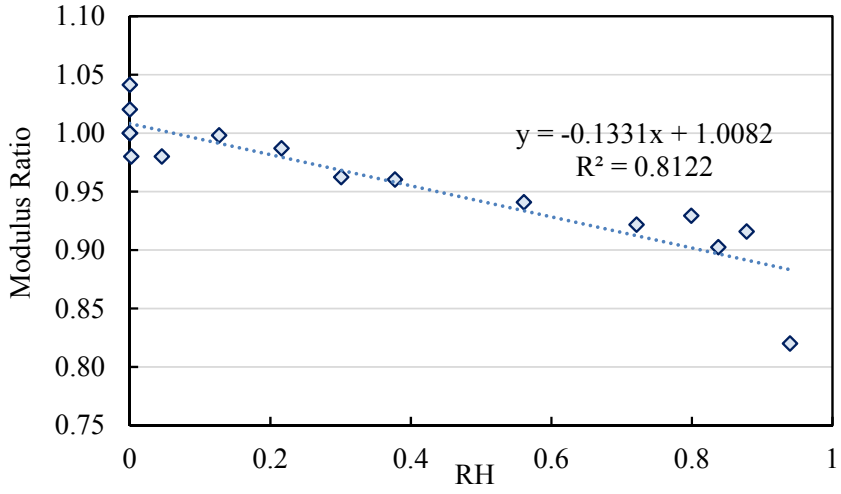

Figure 38 Ratio of wet+aged modulus to the aged modulus versus *RH*

5.3.3 Extension of AD Model

As stated in the preceding sections, test specimens were conditioned and tested at 35°C, and AD model was calibrated only at this temperature. Adhesive bond energy components described in Equations (53) and (59) change with the temperature. It has been recognized that surface tension of asphalt binders decreases linearly with temperature (Pauli 2014). As the adhesive and cohesive bond energies pertain directly to the surface tension of asphalt binder, it is assumed that the adhesive bond energy declines linearly with temperature as well. This

assumption is used in this study to extend the AD model so as to account for the variation in temperature.

Using *a*, *b* and *c* parameters that are backcalculated from BBS test, adhesive bond energy for the tested material (i.e., limestone aggregate and PG 64-22 asphalt binder) at 35°C can be determined from Equation (59) and plotted versus corresponding RH, shown in Figure 39. In order to formulate a linear model that takes into account the temperature variation, another set of bond energy data for similar materials at temperatures different than 35°C is needed. The required data is explored from the study conducted by Zhang (2018, personal communication) on approximately similar materials to those tested in this study but at different temperature, which is 20°C. Zhang used a direct approach combing the vapor adsorption and Wilhelmy plate method to determine the adhesive bond energy at 20°C. The result is shown in Figure 39. It is observed that the curve of bond energy at 35°C lies below the one at 20°C for most values of *RH*, which is an expected trend due to negative effect of increasing temperature on the bond energy. However, the slopes of curves, which describes the rate of bond energy reduction with *RH*, are different. One possible explanation is related to the different approaches used to estimate the *RH*. In Zhang' study, *RH* is changed by applying various vapor pressures in vapor adsorption device. However, in this study, water vapor diffusion is the main cause of change in moisture concentration at the interface, resulting in the change of *RH*. Also, it should be noted that materials tested in the studies were not exactly the same, which can be another reason to explain having various slopes.

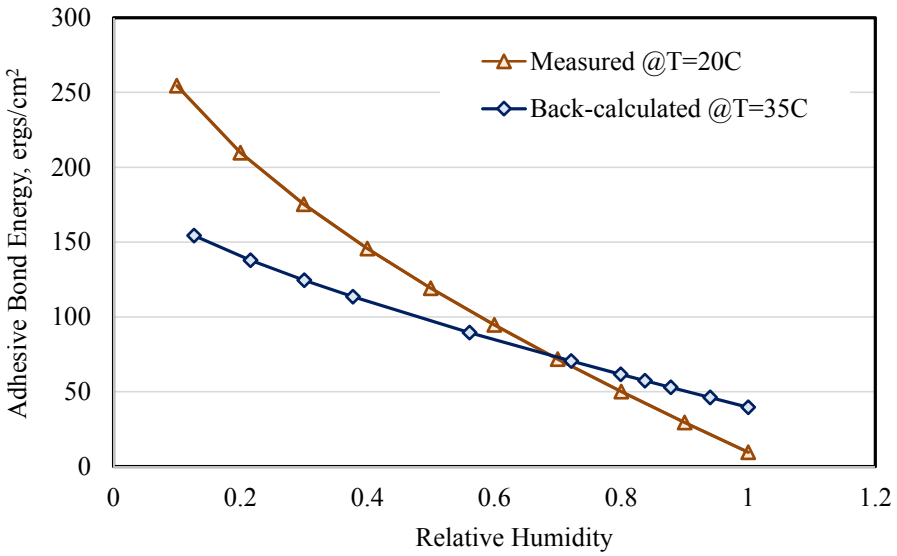

Figure 39 Adhesive bond energies at two different temperatures

In order to determine the value of bond energy when *RH* is zero, curves can be extrapolated to intersect with the vertical axis. Such values are defined as bond energy at the specific temperature for the aggregate-asphalt system without the presence of water vapor. Assuming the linear reduction of bond energy with temperature, the following linear function can be written to link ΔG_{SA}^{AF} to the temperature:

$$\Delta G_{SA}^{AF-T} = \frac{\Delta G_{SA}^{AF-T_2} - \Delta G_{SA}^{AF-T_1}}{T_2 - T_1} \times (\mathrm{T} - \mathrm{T}_1) + \Delta \mathrm{G}_{SA}^{AF-T_1} \qquad (77)$$

where,

T_1, T_2 = Two temperatures at which bond energy values are available (herein 35 and 20°C), °C;

$\Delta G_{SA}^{AF-T_1}, \Delta G_{SA}^{AF-T_2}$ = Values of adhesive bond energy at the given temperatures, ergs/cm^2.

Equation (77) gives the bond energy values at the desired temperatures when water vapor is not present; the function is illustrated in Figure 40.

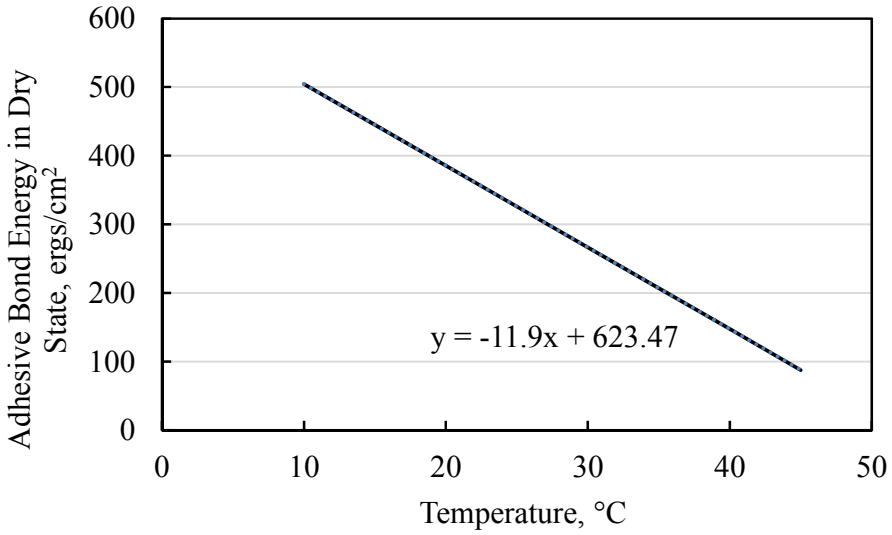

Figure 40 Adhesive bond energy in dry state versus temperature

A generalizes bond energy model should account for the effect of both temperature and *RH*. In order to develop this model, one of the curves in Figure 39 was selected as the reference curve. The one determined from backcalculation of BBS is selected as the reference one since it most accurately represents the bond properties of the tested materials. The existing curve indicates the susceptibility of the adhesive bond energy with respect to RH at temperature 35°C. The curve needs to be adjusted to take into account variation in the temperature as well. The changes in temperature affect the adhesive bond energy in two ways; first, the intrinsic bond energy decreases with the temperature. Second, the moisture sensitivity of the bond energy alters with the temperature. In other word, the rate of bond energy reduction with *RH* is the function of temperature. The water vapor concentration in a chamber with 100% *RH* and temperature of 35°C is almost twice the amount of water vapor concentration in a chamber with 100% *RH* and 20°C temperature. Furthermore, the former more severe conditioning is able to cause more damage in the bond energy. The slope of bond energy curve versus *RH* represents the

susceptibility of the bond to moisture. In addition, the impact of *RH* on decreasing the bond energy is stronger at high temperature. These two concepts are employed here to generate the bond energy vs *RH* curve at different temperatures by shifting the reference curve. The starting point of this curve (i.e., at *RH*=0) is generated by shifting the starting point of reference curve along the vertical axis based on the deviation from $\Delta G_{SA}^{AF-T_{ref}}$. In fact, the vertical shift factor is the function of temperature and is defined as follows:

$$\alpha_T = \Delta G_{SA}^{AF-T} - \Delta G_{SA}^{AF-T_{ref}} \tag{78}$$

where,

$\Delta G_{SA}^{AF-T_{ref}}$ = the adhesive bond energy at the reference temperature (i.e., 35°C herein); and

ΔG_{SA}^{AF-T} = the adhesive bond energy at the desired temperature determined from Equation (77).

The shape of reference curve is then defined by the parameters *a*, *b* and *c* in Equation (59), which can be rewritten here again:

$$\Delta G_{SVA}^{AF} = b - a\exp(\mathrm{RH}^c)$$

$a_{ref}, b_{ref}, c_{ref}$ denote these parameters for the reference curve as follows:

$$\Delta G_{SVA}^{AF-T_{ref}} = b_{ref} - a_{ref}\exp(\mathrm{RH}^{c_{ref}}) \tag{79}$$

When RH is zero, the value of bond energy is controlled by b_{ref}, a_{ref}:

$$\Delta G_{SA}^{AF-T_{ref}} = b_{ref} - a_{ref} \tag{80}$$

Adhesive bond energy at the desired temperature can be also written as a function of RH:

$$\Delta G_{SVA}^{AF-T} = b_T - a_T\exp(\mathrm{RH}^{c_T}) \tag{81}$$

Consequently, when RH is zero the following Equation gives the value of bond energy:

$$\Delta G_{SA}^{AF-T} = b_T - a_T \tag{82}$$

Substituting Equations (80) and (82) into (78) yields the following relationship between $a_T, b_T, a_{ref}, b_{ref}$:

$$(\mathrm{b}_T - \mathrm{a}_T) - (\mathrm{b}_{ref} - \mathrm{a}_{ref}) = \alpha_T \tag{83}$$

To account for the impact of temperature on moisture sensitivity, it can be assumed that the slope of secant line passing through the start and end points of the bond energy curve vs *RH* is proportional to the maximum water vapor concentration (i.e., C_m) at 100% *RH* and the desired temperature. Note that C_m is determined using Equation (66). It should be noted that the start point corresponds to the intersection of curve with vertical axis, and the end point corresponds to 100% *RH*. The following Equation can be written to link the slope to C_m:

$$\frac{\Delta G_{SVA}^{AF-T} - \Delta G_{SA}^{AF-T}}{\Delta G_{SVA}^{AF-T_{ref}} - \Delta G_{SA}^{AF-T_{ref}}} = \frac{C_m^T}{C_m^{T_{ref}}} \tag{84}$$

ΔG_{SVA}^{AF-T} and $\Delta G_{SVA}^{AF-T_{ref}}$ are related to the bond energy at *RH* of 100%, and determined by plugging *RH* = 1 into Equation (79) and (81), respectively. Applying Equation (79) (80), (81) and (82) into (84) gives:

$$\frac{a_T}{a_{ref}} = \frac{C_m^T}{C_m^{T_{ref}}} \tag{85}$$

Finally, combining Equations (83) and (85) yield:

$$b_T = \alpha_T + b_{ref} + a_{ref}\left(\frac{C_m^T}{C_m^{T_{ref}}} - 1\right) \tag{86}$$

In the simplest form, it can be postulated that the parameter *a* captures the moisture susceptibility of bond with temperature. Hence, the parameter *c* can remain constant:

$$c_T = c_{ref} \tag{87}$$

Using Equations (85), (86) and (87), a_T, b_T, c_T corresponding to every C_m are determined. By substituting a_T, b_T, c_T into (81), the bond energy can be estimated at each temperature and *RH* of interest:

$$\Delta G_{SVA}^{AF-T} = \alpha_T + b_{ref} - a_{ref}\left[1 - k(1 - \exp(\mathrm{RH})^{c_{ref}})\right] \tag{88}$$

where, $k = \dfrac{C_m^T}{C_m^{T_{ref}}}$.

Following the abovementioned approach, the shifted bond energy curve at 25°C is determined and shown along with the reference curve in Figure 41 .

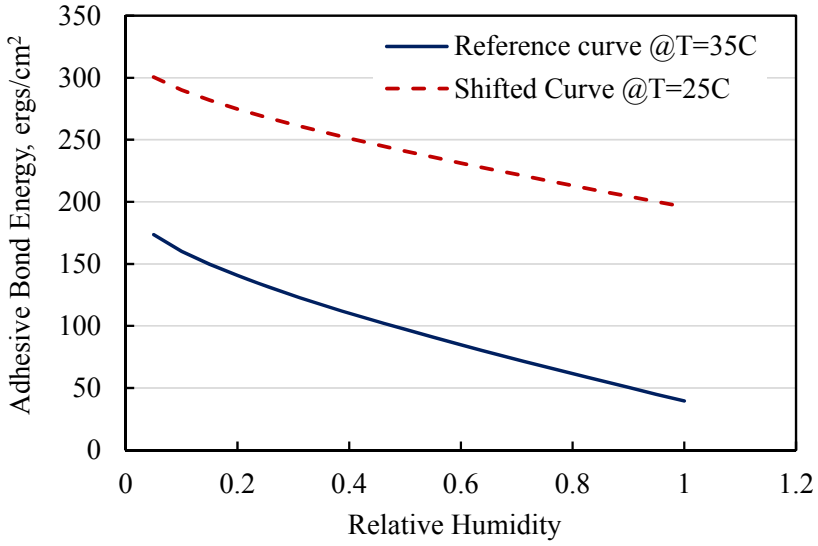

Figure 41 Variation of the bond energy with temperature and RH

Applying Equation (88) into (65) yields the final form of AD model, which accounts for the variation of both temperature and *RH*:

$$d_{AD} = 1 - \left[\left(\frac{E_A^{wet+aged}}{E_A^{aged}} \right)^{0.5} \times \left\{ \frac{\alpha_T + b_{ref} - a_{ref}\left[1 - k(1 - \exp(\mathrm{RH})^{c_{ref}})\right]}{b_{ref} + \alpha_T - a_{ref}} \right)^{0.5} \right] \quad (89)$$

With regard to $\frac{E_A^{wet+aged}}{E_A^{aged}}$ in AD model, it can be assumed that as temperature increases, both numerator and denominator increase with almost the same rate such that this ratio does not change significantly. As stated earlier, for a case of very thin asphalt film coating the aggregate, water vapor passes through the film rather than being accumulated during the diffusion process. Therefore, as far as the bond deterioration is concerned, which is the case in AD model, it can be postulated that passing water vapor through thin film does not cause significant reduction in modulus. On the other hand, it is mentioned in Section 2.1.1 that the presence of water at the ambient pressure has no significant impact on the aging rate. Hence, 0.96 average ratio for $\frac{E_A^{wet-aged}}{E_A^{aged}}$, determined in the preceding section, can be extended for the use in AD model when various temperatures are applied. Note that 0.96 average value is specific for the asphalt binder tested in this study, and in case of using different binder, this value might change. Equation (89) is employed to predict the adhesive damage at 25°C as shown in Figure 42.

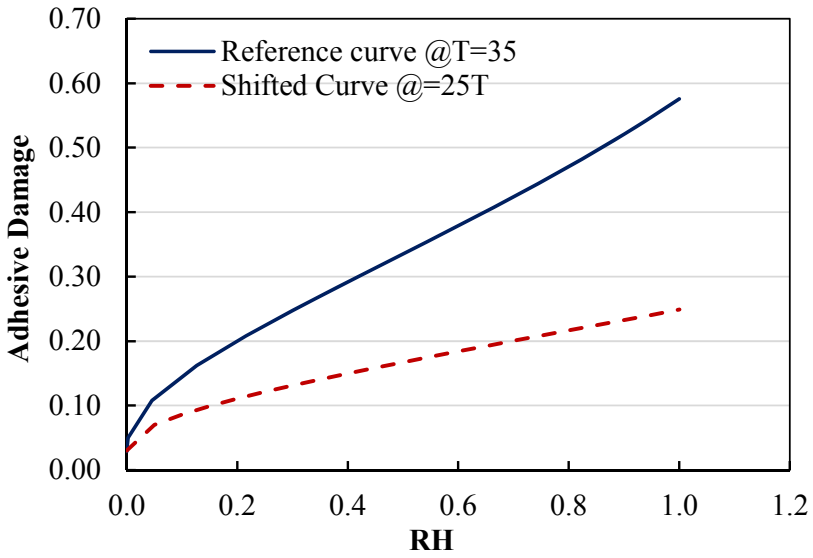

Figure 42 Adhesive damage in limestone-PG 64-22 bond vs. RH at two different temperatures

6. INTEGRATED AGING-MOISTURE PREDICTIVE (IAMP) MODEL

The concept of IAMP model is detailed in Section 2.3. AC is a composite material consisting of aggregates, FAM and air void. The mechanical characteristics of AC depends on not only the properties of FAM and aggregates but also on the interfacial bond between the aggregates and asphalt. The interfacial bond is responsible to transmit the load from FAM, which acts as a matrix phase, to aggregate particles. In other words, the degree to which a load is transferred from FAM to aggregate is controlled by the strength of interfacial bond. The presence of moisture in AC deteriorates FAM cohesiveness as well as the strength of interfacial bond, resulting in the reduction of stiffness. The deterioration effect of moisture on dynamic modulus of a full mixture is quantified by integrating d_{AD} and d_{CD} factors into a single moisture damage factor, denoted by d_{MD}, through a linear map:

$$d_{MD} = \alpha \times d_{AD} + \beta \times d_{CD} \tag{90}$$

Where α and β are the parameters representing the contribution of adhesive and cohesive damage to the total moisture damage. The value of these parameters are determined by fitting the model to data obtained directly from dynamic modulus test. The IAMP model modifies the aging model by incorporating the MD factor:

$$\left|E^*\right|_{Aging+Moisture} = \left|E^*(\mathrm{t},\mathrm{T})\right|_{aging} \times (1 - d_{MD}(T, f, C_m(\mathrm{t}), w(t))) \tag{91}$$

Combining Equations (90) and (91) with (41) and (41) provide the final equation to predict the $|E^*|$ for aged-moisture conditioned samples:

$$\left|E^*\right|_{Aging+Moisture} = \left|E^*(t,T)\right|_{aging} \times (1-\alpha+\alpha\times\{(\frac{E_A^{wet-aged}}{E_A^{aged}})^{0.5}\times(\frac{b-a\exp(\{\frac{RT}{P_0 m_{H_2O}}C_m\}^c)}{b-a})^{0.5}\} \quad (92)$$
$$-\beta\times[1-\exp(-a'w)]\times[1+\frac{1.17}{(1+b'w^{c'})^8}-\frac{2.17}{(1+b'w^{c'})^{14}}])$$

For S3 PG 64-22 mixture tested in this study, fitting parameters a, b, c , a′, b′, c′ are determined in Section 4 and 5. Substituting these parameters in Equation (92) gives IAMP model for S3 PG 64-22 HMA:

$$\left|E^*\right|_{Aging+Moisture} = \left|E^*(t,T)\right|_{aging} \times [1-\alpha+\alpha(1.42-0.42\,e^{(0.025C_m)^{0.4}})^{0.5}]$$
$$-\beta\times[1-\exp(-0.25\,w)]\times[1+\frac{1.17}{(1+(0.02\,fr^{-0.18})w^{(0.13Logfr+0.18)})^8}-\frac{2.17}{(1+(0.02\,fr^{0.18})w^{(0.13Logfr+0.18)})^{14}}] \quad (93)$$

MD model is a function of moisture concentration at the interface, and water content in FAM. Hence, to use these models for a mixture, the values of moisture concentration and water content at each conditioning level are required. These values can be determined using the diffusion model as described in the following subsection.

In this section, IAMP model is calibrated and validated for S3 PG 64-22 HMA. The next section provides the aging model to predict |*E**| for aged S3 PG 64-22 HMA. The subsequent sections detail the diffusion model used to determine the water vapor concentration through the AC samples and mass of absorbed water in FAM. Generalization of AD and CD model for AC are discussed next. Parameters of α and β are estimated in Section 6.5 by fitting IAMP model to |*E**| data measured directly in the lab for aged-moisture conditioned specimens. IAMP model is also validated in Section 6.5.

6.1 Aging Model

The procedure for developing the aging model is detailed in Section 3 for S4 PG 76-28 mixture. In this section, aging model is developed for S3 PG 64-22 mixture. To do so, a series of upfront testing is conducted to compute the kinetic parameters involved in Equations (16), (17) and (18). Sections 3 details required steps to determine the parameters by conducting a series of dynamic modulus tests on loose-mix-aged specimens as recommended by NCHRP 9-54 project (Kim et al. 2018). However, in this section, the parameters are determined by performing dynamic modulus tests on compacted-aged S3 PG 64-22 specimens in accordance to AASHTO R30 protocol. The reason is that the aging model developed in this section will be used to predict the aged modulus for compacted samples conditioned at 100% RH and 35°C for varying times. In other words, specimens are compacted during the aging process and so parameters of the aging model should account for a compacted-aged state and not a loose-mix-aged state. After finding the parameters, they are plugged in aging function model (i.e., λ), presented in Equation (22).

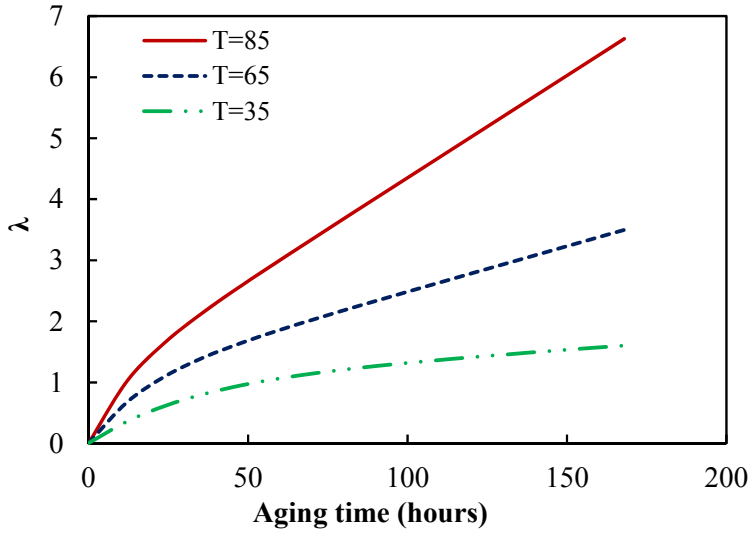

Figure 43 λ versus aging time for S6 PG 64-22 mixtures

Figure 43 indicates λ versus aging time for S3 PG 64-22 mixture aged at 35, 65 and 85°C. Parameter λ characterizes the effect of aging on |*E**| based on the aging properties of S3 PG 64-22 mixture (i.e. k_f and k_c) as a function of aging time and temperature.

Next, the relation between normalized sigmoidal coefficients and λ are formulated using regression analysis as shown in Equation (94) and Figure 44. For S3 PG 64-22 mixture, power law functions provide a better fit to the measured data compared to the linear functions introduced in Section 3.5. It should be noted that the type of functions and values of their fitting parameters vary depending on the aging susceptibility of mixtures. As shown in Figure 44, the rates of changes in sigmoidal coefficients and shift factor parameters with aging decreases gradually as λ exceeds the specific value, which is found to be 3.5 for S3 PG 64-22 mixture. One possible explanation is that the diffusivity of oxygen in AC diminishes as the amount of oxidation products increases. In other words, vacancies between molecular chains are slowly occupied by the oxidation products, resulting in a diffusion resistance within the mixture. The impact of oxidative aging is manifested through the changes of sigmoidal coefficients with λ. Therefore, the reduction in the rate of these changes implies a growth of diffusion resistance with time.

$$\begin{aligned}
\frac{c}{c_0} &= 1.05\lambda^{0.06} \\
\frac{d}{d_0} &= 0.98\lambda^{-0.035} \\
\frac{\alpha_2}{\alpha_{2_0}} &= 1.25\lambda^{0.065} \\
\frac{\alpha_3}{\alpha_{3_0}} &= 1.15\lambda^{0.07}
\end{aligned} \tag{94}$$

Assuming $a = a_0$ and $b = b_0$, by plugging c, d, α_2, α_3 in Equations (19) and (21), $|E^*|$ master curve can be predicted for the aging level of interest. Figure 45 shows the predicted master curves for S3 PG 64-22 mixture aged at 35°C for 60 and 90 days.

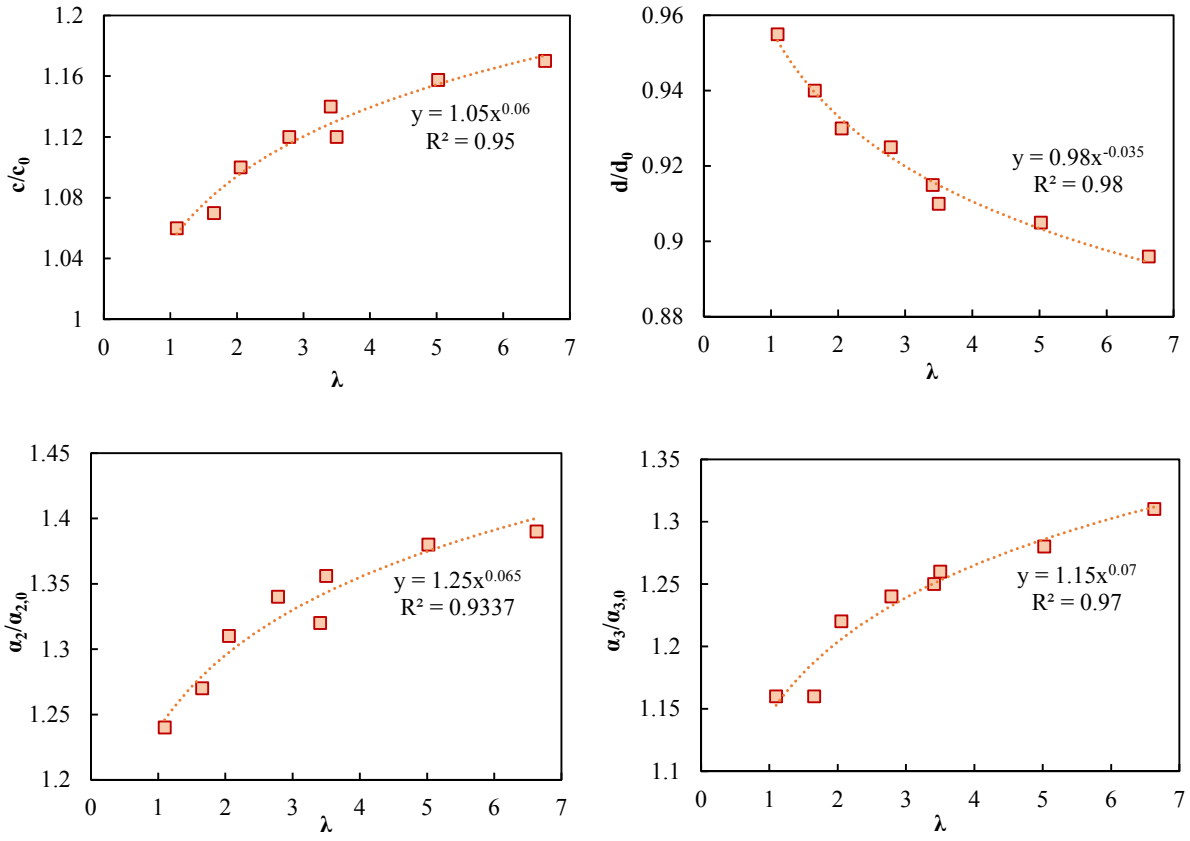

Figure 44 Relationship between sigmoidal coefficients and shift factor parameters with λ for S3 PG 64-22 mixture

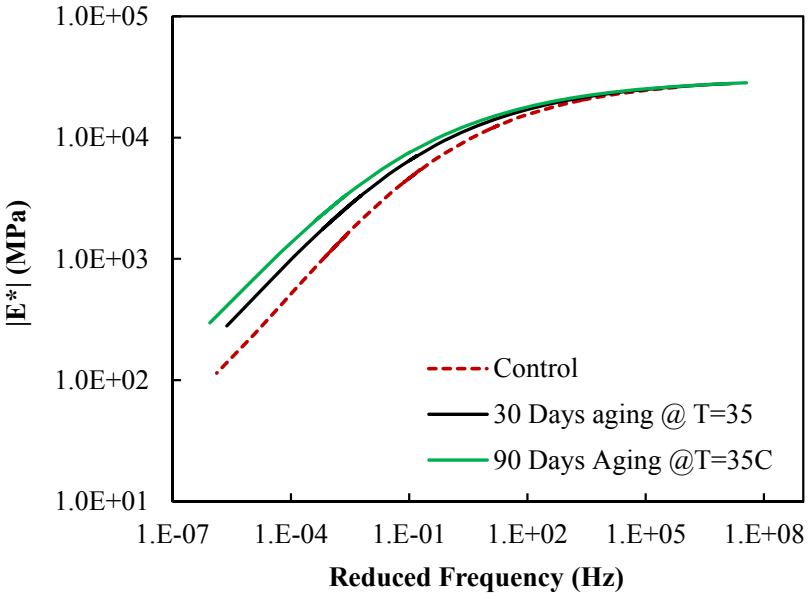

(a)

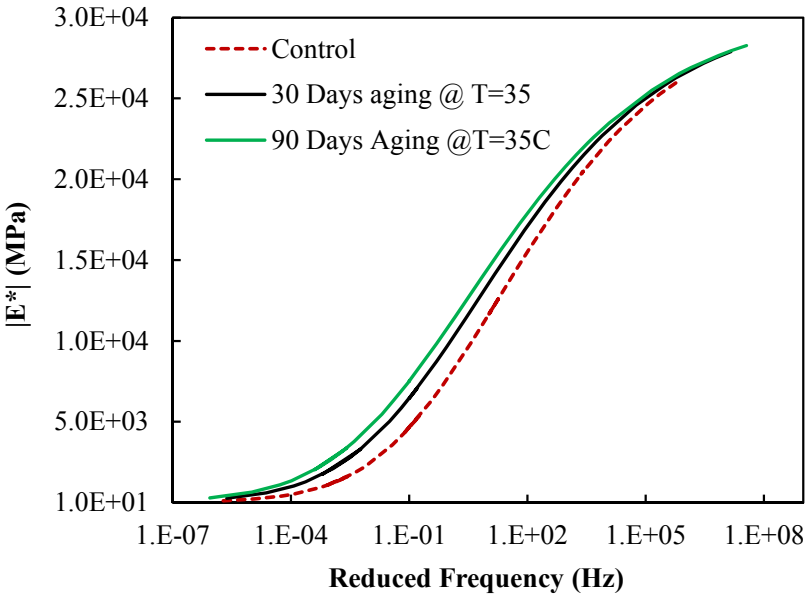

(b)

Figure 45 Predicted master curve for the aged S3 PG 64-22 mixture in (a) semi-log, and (b) log-log scales

6.2 Diffusion Model

Moisture diffusivity through AC and the capacity of AC to absorb water are two important factors that should be considered in characterizing the moisture susceptibility of asphalt mixtures and developing the moisture damage models. The newly fabricated AC specimens have *RH* of almost 0 when they first are placed in the moisture room. Then, water vapor accumulates within the specimens through a non-steady state diffusion process driven by the water vapor concentration gradients between AC specimens and surrounding air. The diffusion of water vapor can be described by Fick's second law as follows:

$$\frac{\partial C}{\partial t} = D\frac{\partial^2 C}{\partial x^2} \tag{95}$$

Where

C = water vapor concentration, gr/mm^3;

t = time, s;

D = diffusion coefficient, mm^2/s;

x = position, mm.

The close form solution for Equation (95) is determined based on the initial and boundary conditions and geometry of specimens. A solution to Equation (95) has one of the two standard forms. One form consists of a series of error functions, which converge suitably at small time; the other form comprised of a trigonometrical series which converge most satisfactorily for large values of time (Crank 1979). If the diffusion direction is considered to be radial, trigonometric solution is replaced by a series of Bessel functions (Vasconcelos et al. 2010). Luo and Huang (2018) developed a three-dimensional diffusion model to characterize the diffusivity of water

vapor through AC in a cylindrical coordinate. Considering the water vapor diffusion in a cylindrical coordinate, Fick's second law is rewritten as follows:

$$\frac{\partial C(r,y,t)}{\partial t} = \frac{D}{r}\frac{\partial}{\partial r}\left[r\frac{\partial C(\mathrm{r,z,t})}{\partial r}\right] + \frac{1}{r}\frac{\partial^2 C(r,z,t)}{\partial \theta^2} + r\frac{\partial^2 C(r,z,t)}{\partial z^2} \tag{96}$$

where,

$C(r,z,t)$ = total water vapor concentration, g/mm^2;

D = diffusion coefficient of water vapor in the specimen, mm^2/s;

r = diffusion radius, mm;

z = diffusion distance along the axial direction, mm;

θ = angular coordinate in the xy plane;

t = diffusion time, s.

For the AC configuration and diffusion procedure adopted in this study (shown in Figure 46) the following boundary conditions should be applied to Equation (96):

$$C(r,0,t) = C_0 \qquad 0 \le r \le R,\ t \ge 0 \tag{97}$$

$$C(\mathrm{r,H},t) = C_0 \qquad 0 \le r \le R,\ t \ge 0 \tag{98}$$

$$C(r,\mathrm{z},t) = C_0 \qquad 0 \le z \le H\ ,\ t \ge 0 \tag{99}$$

$$C(r,z,0) = 0 \qquad \begin{matrix} 0 \le r \le R \\ 0 \le z \le H \end{matrix} \tag{100}$$

where,

C_0 = constant water vapor concentration on the surface of the A specimen;

H = height of the specimen;

R = radius of the specimen.

Luo and Huang (2018) determined the final solution of C to the diffusion equation as:

$$C(r,z,t) = C_0 - \frac{8C_0}{\pi}\sum_{k=1}^{\infty}\sum_{m=1}^{\infty}\frac{J_0(\frac{x_m^0}{R}r)}{(2k-1)x_m^0 J_1(x_m^0)}\cdot e^{-\{\frac{(x_m^0)^2}{R^2}+\frac{(2k-1)^2\pi^2}{H^2}\}D_r t}\sin\left[\frac{(2k-1)\pi}{H}z\right] \quad (101)$$

where,

J_0 = Bessel's function of the first kind of zero order;

J_1 = Bessel's function of the first order;

x_m^0 = roots of $J_0(r)=0$ m = 1, 2, …., ∞ (102)

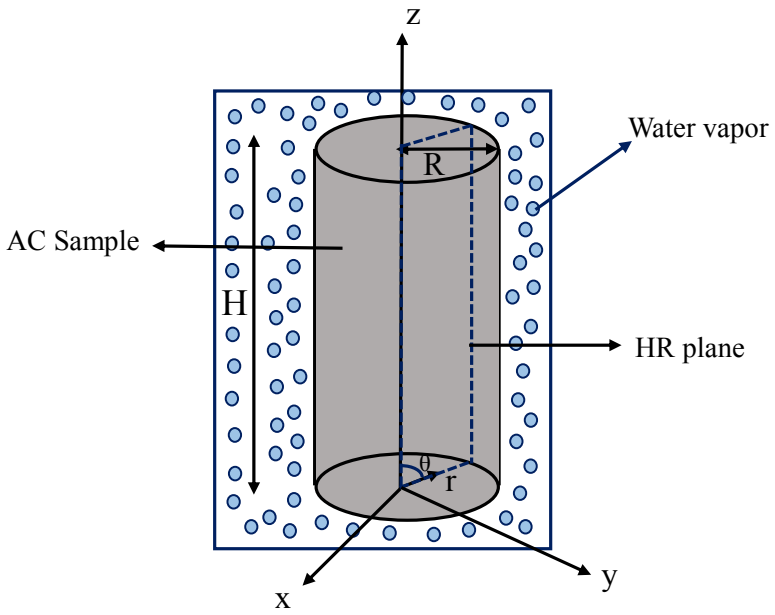

Figure 46 AC configuration in diffusion process

The total weight of diffused water vapor can be obtained by integrating water vapor concentration, *C*, over the total volume of specimen:

$$M = \int_0^H \int_0^{2\pi} \int_0^R C_r(r, z, t) r dr d\theta dz \quad (103)$$

Integrating C over the volume provides the formulation for the total mass of absorbed as a function of diffusion time t (Luo and Huang (2018)):

$$M(t) = M^{\infty}\left[1 - \frac{32}{\pi^2}\sum_{k=1}^{\infty}\sum_{m=1}^{\infty}\frac{1}{(2k-1)^2 (x_m^0)^2} e^{-\left\{\frac{(x_m^0)^2}{R^2} + \frac{(2k-1)^2\pi^2}{H^2}\right\}Dt}\right] \quad (104)$$

where,

M^{∞} = maximum water mass absorbed in the specimen

Equation (104) is adopted in this study to backcalculate the diffusion coefficient, and maximum water mass diffused in AC specimens. Also, Equation (101) will be used in the following section to determine the water vapor concentration in HMA mixtures. To do so, two AC samples in 100 mm diameter and 150 mm height were prepared from S3 PG 64-22 mixtures, and placed in the moisture room with 100% *RH* and 35°C temperature. The weight of samples were recorded twice a day for 75 days to estimate the amount of water uptake, then, Equation (104) was fitted to the measured mass of absorbed water. The diffusivity of water vapor at 35°C in S3 PG 64-22 AC specimen is determined to be $2.19E^{-5}$ mm^2/s. Diffusion coefficients of water vapor in AC found through the literature are summarized in Table 4. The molecules of water vapor are smaller than molecules of liquid water; thus, it is expected for diffusivity of water vapor to be greater than that of liquid water. Also, temperature has an important effect on the diffusivity such that rising the temperature increases the diffusion coefficient of the most non-aging materials. However, for aging materials such as HMA and asphalt binder, an increase in

the diffusivity due to raising the temperature might be counterbalanced to some extent by age hardening which is the result of formation of polar components. In general, comparing the estimated coefficient in this study with the diffusion coefficients reported in the literature (Shown in Table 4) suggests that the one calculated here is acceptable.

Table 4 Diffusion coefficients for AC in the literature

Reference	Diffusion Coefficient (mm^2/s)	Experimental Condition
Huang and Luo (2018)	5×10^{-6}-1×10^{-5}	Water Vapor at 40°C
Tong (2013)	2×10^{-5}-3×10^{-5}	Water vapor 100 RH at 20°C
Kringos et al. (2008)	1×10^{-7}-3×10^{-6}	Water vapor 100 RH at 25°C
Arambula et al. (2009)	1×10^{-4}- 2.5×10^{-4}	Water vapor 100 RH at 35°C

Figure 47 illustrates the typical water uptake data for the conditioned AC specimen. Also, the total water uptake at the end of diffusion process which is estimated from Equation (104) is shown in Figure 48.

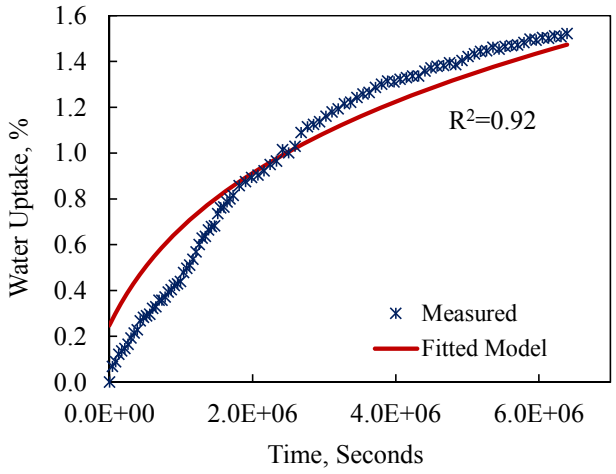

Figure 47 Moisture uptake versus time for the S3 64-22 AC specimen at 35°C

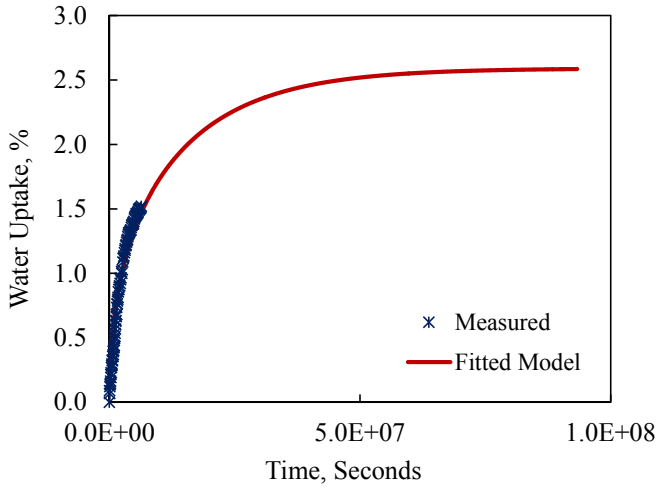

Figure 48 Predicted water uptake as the function of time using three-dimensional diffusion model

6.3 Calculation of Effective Adhesive Damage Factor

The AD model developed in Section 5 characterizes the adhesive bond energy between one aggregate and asphalt binder with respect to the water vapor concentration at the interface, C_m. Evidently, C_m changes through the AC sample. In this section, the calculation of effective adhesive damage factor, which represents the adhesive damage factor for a representative volume element (RVE) of AC, is presented. For $|E^*|$ measurements, RVE is defined as the volume of a cylindrical specimen of 100 mm in diameter and 150 mm in height. To this end, AC is assumed as a homogenous material in which aggregates, asphalt binder and air void are distributed uniformly.

As detailed in Section 6.2, a three-dimensional diffusion model can be used to characterize the water vapor diffusion in cylindrical test specimens. The diffusion coefficient determined in the preceding section is plugged in Equation (101) to find the distribution of water vapor concentration through the sample (i.e. C_m). Note that the value of C_0 at RH=100% and

35°C is 39.37E-9 gr/mm^2. Figure 49(a) and (b) show a three dimensional distribution of C_m through the cylindrical AC sample after 20 and 110 days of conditioning calculated using Equation (101) for S3 PG 64-22 specimens.

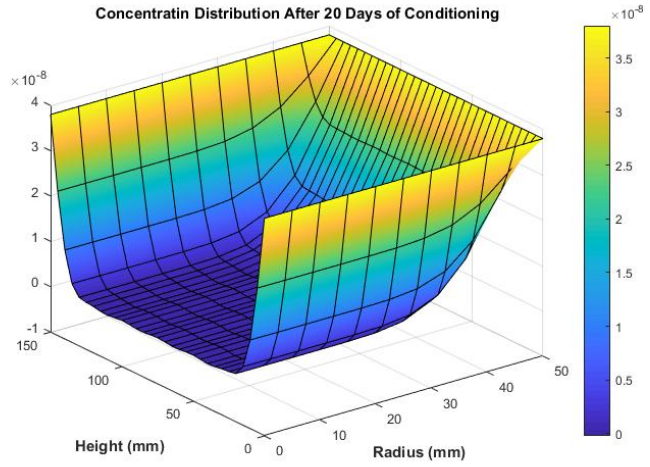

(a)

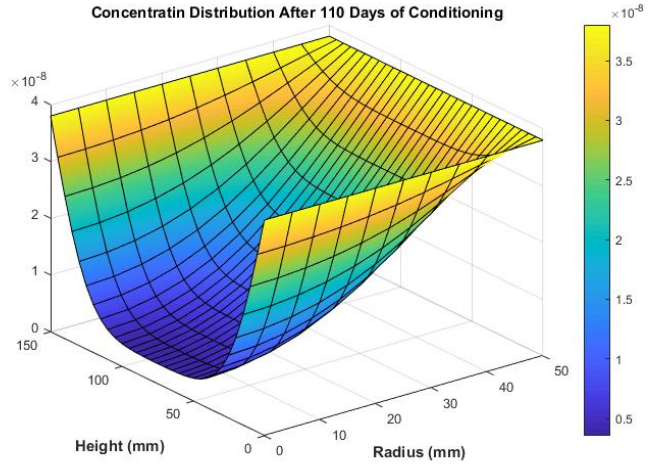

(b)

Figure 49 C_m distribution through the AC sample after (a) 20, and (b) 110 days conditioning

It can be observed that the maximum C_m happens on the outer shells close to the surface of the specimens, and as diffusion time increases, the C_m increases in inner shells as well. Figure 50(a) and (b) illustrate a two-dimensional distribution in z and r directions, respectively after 110 days of conditioning.

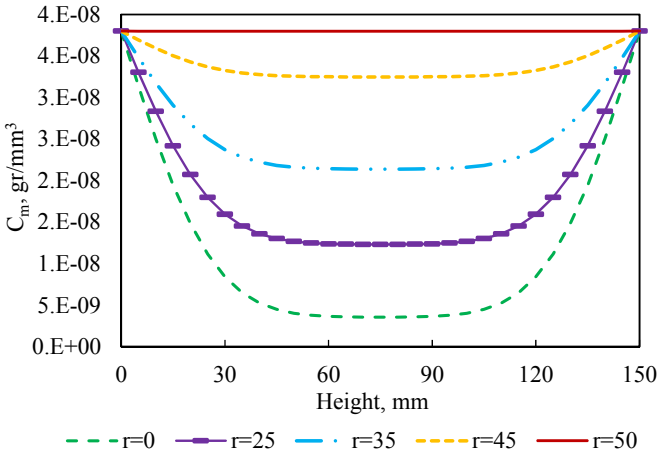

(a)

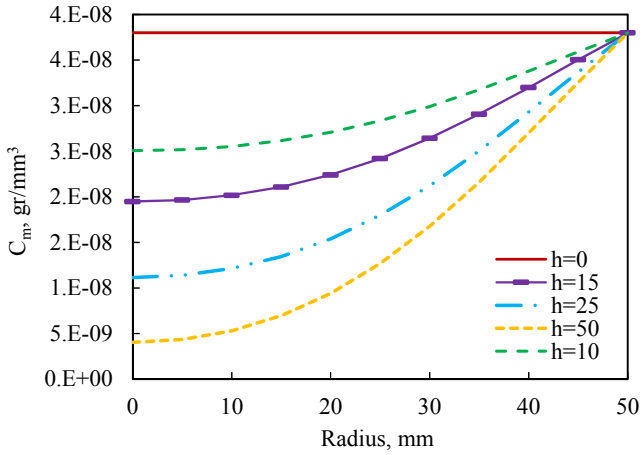

(b)

Figure 50 C_m distribution through the AC sample after 110 days conditioning in (a) z, and (b) r directions

The calibrated AD factor developed in Section 5.3.2 is the function of C_m; the factor is presented here again:

$$d_{AD} = 1 - (1.42 - 0.42e^{(0.025C_m)^{0.4}})^{0.5} \tag{105}$$

Substituting C_m from Equation (101) into **Error! Reference source not found.** yields:

$$d_{AD} = 1 - (1.42 - 0.42e^{(0.025\{C_0 - \frac{8C_0}{\pi}\sum_{k=1}^{\infty}\sum_{m=1}^{\infty}\frac{J_0(\frac{x_m^0}{R}r)}{(2k-1)x_m^0 J_1(x_m^0)}\cdot e^{-\{\frac{(x_m^0)^2}{R^2}+\frac{(2k-1)^2\pi^2}{H^2}\}D_f t}\sin\left[\frac{(2k-1)\pi}{H}z\right]\})^{0.4}})^{0.5} \tag{106}$$

Since C_m changes through the sample, the Effective Adhesive Damage (d_{EAD}) factor should be calculated for the whole sample using the following equation:

$$d_{EAD} = \frac{\int_0^R \int_0^H \mathrm{d}_{AD}(C_m(r,z))drdz}{\int_0^R \int_0^H drdz} \tag{107}$$

Evidently, calculating d_{EAD} is not possible analytically. Thus, it should be discretized and computed numerically. The adhesive damage introduced within the AC samples can be represented by a *damage matrix* such that each entry (i.e., d_{zr}) indicates *AD* factor at the height of *z* and radius of *r*. The adhesive damage developed in the sample of 50 mm in radius and 150 mm in height after 20 and 110 days of conditioning at 100% *RH* and 35°C is presented as two examples of damage matrixes in Equations (108) and (109). Damage factors are calculated at 10 mm increments on the HR plane shown in Figure 46. For 20 and 110 days of conditioning, the EAD factors are calculated to be 0.15 and 0.27, respectively.

$$d_{AD(t=20days)} = \begin{bmatrix} 0.451 & 0.451 & 0.451 & 0.451 & 0.451 & 0.451 \\ 0.175 & 0.174 & 0.175 & 0.183 & 0.253 & 0.450 \\ 0.047 & 0.046 & 0.047 & 0.071 & 0.190 & 0.450 \\ 0.029 & 0.026 & 0.029 & 0.061 & 0.187 & 0.450 \\ 0 & 0 & 0 & 0.051 & 0.184 & 0.450 \\ 0.027 & 0.025 & 0.027 & 0.061 & 0.187 & 0.450 \\ 0 & 0 & 0 & 0.053 & 0.185 & 0.450 \\ 0.017 & 0.012 & 0.017 & 0.057 & 0.186 & 0.450 \\ 0.017 & 0.012 & 0.017 & 0.057 & 0.186 & 0.450 \\ 0 & 0 & 0 & 0.053 & 0.185 & 0.450 \\ 0.027 & 0.025 & 0.027 & 0.061 & 0.187 & 0.450 \\ 0 & 0 & 0 & 0.051 & 0.184 & 0.450 \\ 0.029 & 0.026 & 0.029 & 0.061 & 0.187 & 0.450 \\ 0.047 & 0.046 & 0.047 & 0.071 & 0.190 & 0.450 \\ 0.175 & 0.174 & 0.175 & 0.183 & 0.253 & 0.450 \\ 0.451 & 0.451 & 0.451 & 0.451 & 0.451 & 0.451 \end{bmatrix} \quad (108)$$

$$d_{AD(t=110days)} = \begin{bmatrix} 0.451 & 0.451 & 0.451 & 0.451 & 0.451 & 0.451 \\ 0.323 & 0.328 & 0.343 & 0.369 & 0.408 & 0.451 \\ 0.227 & 0.235 & 0.261 & 0.309 & 0.375 & 0.451 \\ 0.162 & 0.174 & 0.210 & 0.271 & 0.355 & 0.451 \\ 0 & 0 & 0 & 0.253 & 0.345 & 0.451 \\ 0.109 & 0.125 & 0.172 & 0.245 & 0.341 & 0.450 \\ 0 & 0 & 0 & 0.243 & 0.340 & 0.450 \\ 0.102 & 0.119 & 0.168 & 0.243 & 0.340 & 0.450 \\ 0.102 & 0.119 & 0.168 & 0.243 & 0.340 & 0.450 \\ 0 & 0 & 0 & 0.243 & 0.340 & 0.450 \\ 0.109 & 0.125 & 0.172 & 0.245 & 0.341 & 0.450 \\ 0 & 0 & 0 & 0.253 & 0.345 & 0.451 \\ 0.162 & 0.174 & 0.210 & 0.271 & 0.355 & 0.451 \\ 0.227 & 0.235 & 0.261 & 0.309 & 0.375 & 0.451 \\ 0.323 & 0.328 & 0.343 & 0.369 & 0.408 & 0.451 \\ 0.451 & 0.451 & 0.451 & 0.451 & 0.451 & 0.451 \end{bmatrix} \quad (109)$$

6.4 Calculation of Effective Cohesive Damage Factor

The CD model developed in Section 4 is a function of gravimetric water content absorbed in the FAM. Hence, in order to apply the model to whole AC sample, the water mass absorbed in the FAM portion of an AC sample needs to be determined. The water vapor concentration through the sample is calculated using Equation (101), and defined as the mass of absorbed water per volume at any location within the sample. The water mass absorbed in the FAM portion of differential volume shown in Figure 51 is calculated by multiplying $C(r,\mathrm{z},t)$ by the differential volume of FAM:

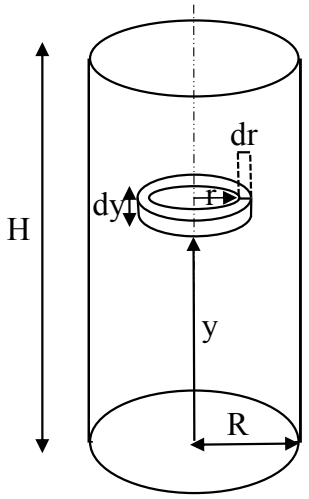

Figure 51 Configuration of differential element

$$dW_f = c(r,\mathrm{z},t)\times dV_f \tag{110}$$

where,

dW_f = differential mass of water absorbed in FAM;

dV_f = differential volume of FAM.

Assuming FAM is distributed uniformly in the mixture, dV_f is calculated as follows:

$$dV_f = \nu_f \times dV_T = \nu_f \times 2\pi r dr dy \tag{111}$$

where,

ν_f = volumetric distribution of FAM in the whole AC sample, defined as:

$$\nu_f = \frac{V_f}{V_T} \tag{112}$$

V_f is the total FAM volume and V_T is the total volume of AC sample. Substituting Equations (101) and (111) into (110) gives:

$$dW_f(t) = 2\pi r \nu_f \times c(r,z,t) \times dr dy = 2\pi r \nu_f \times \left\{ C_0 - \frac{8C_0}{\pi} \sum_{k=1}^{\infty} \sum_{m=1}^{\infty} \frac{J_0(\frac{x_m^0}{R} r)}{(2k-1) x_m^0 J_1(\mathrm{x}_m^0)} \cdot e^{-\{\frac{(x_m^0)^2}{R^2} + \frac{(2k-1)^2 \pi^2}{H^2}\} D_r t} \sin\left[\frac{(2k-1)\pi}{H} z \right] \right\} dr dy \tag{113}$$

The total water mass absorbed in FAM is determined by integrating dW_f over the entire volume of AC sample:

$$W_f(t) = \int_0^H \int_0^R 2\pi r \nu_f \times \left\{ C_0 - \frac{8C_0}{\pi} \sum_{k=1}^{\infty} \sum_{m=1}^{\infty} \frac{J_0(\frac{x_m^0}{R} r)}{(2k-1) x_m^0 J_1(\mathrm{x}_m^0)} \cdot e^{-\{\frac{(x_m^0)^2}{R^2} + \frac{(2k-1)^2 \pi^2}{H^2}\} D_r t} \sin\left[\frac{(2k-1)\pi}{H} z \right] \right\} dr dy \tag{114}$$

Considering Equations (103) and (104), Equation (114) can be rewritten as:

$$W_f(t) = \nu_f \times M^{\infty} \left[1 - \frac{32}{\pi^2} \sum_{k=1}^{\infty} \sum_{m=1}^{\infty} \frac{1}{(2k-1)^2 (\mathrm{x}_m^0)^2} e^{-\left\{ \frac{(x_m^0)^2}{R^2} + \frac{(2k-1)^2 \pi^2}{H^2} \right\} D t} \right] \tag{115}$$

M^{∞} is the maximum water mass absorbed in the entire AC sample. Gravimetric water content in FAM portion is then calculated as:

$$w_f(t) = \frac{W_f(t)}{M_f} = \frac{v_f}{M_f} \times M^{\infty} \left[1 - \frac{32}{\pi^2} \sum_{k=1}^{\infty} \sum_{m=1}^{\infty} \frac{1}{(2k-1)^2 (\mathrm{x}_m^0)^2} e^{-\left\{ \frac{(x_m^0)^2}{R^2} + \frac{(2k-1)^2 \pi^2}{H^2} \right\} Dt} \right] \quad (116)$$

Where, M_f is the dry mass of FAM in AC sample. Applying Equation (112), $\frac{v_f}{M_f}$ can be written as:

$$\frac{v_f}{M_f} = \frac{V_f}{V_T M_f} = \frac{1}{V_T \gamma_{mm}^f} = \frac{1}{V_T G_{mm}^f \rho_w} \quad (117)$$

where,

G_{mm}^f = maximum specific gravity of FAM;

ρ_w = water density, gr/cm^3.

Combining Equations (117) and (116) gives the ultimate function to calculate the gravimetric water content in FAM:

$$w_f(t) = \frac{1}{V_T G_{mm}^f \rho_w} \times M^{\infty} \left[1 - \frac{32}{\pi^2} \sum_{k=1}^{\infty} \sum_{m=1}^{\infty} \frac{1}{(2k-1)^2 (\mathrm{x}_m^0)^2} e^{-\left\{ \frac{(x_m^0)^2}{R^2} + \frac{(2k-1)^2 \pi^2}{H^2} \right\} Dt} \right] \quad (118)$$

where,

V_T = Total volume of AC sample, cm^3;

D = Diffusion coefficient of water vapor in AC sample, mm^2/s;

R = Radius of AC sample, mm;

H = Height of AC sample, mm;

t = Diffusion time, s.

Plugging the measured properties and dimensions of the AC sample tested in this study into Equation (118) yields to the following $w_f(t)$ as a function of t:

$$w_f(t) = 3\times(1-\frac{32}{\pi^2}\sum_{k=1}^{\infty}\sum_{m=1}^{\infty}\frac{1}{(2k-1)^2(\mathrm{x}_m^0)^2}e^{-\left\{\frac{(x_m^0)^2}{R^2}+\frac{(2k-1)^2\pi^2}{H^2}\right\}2.19\times10^{-5}t}) \quad (119)$$

Where $w_f(t)$ is the percentage of gravimetric water content in the FAM. Figure 52 shows the change of $w_f(t)$ against diffusion time when *k* and *m* are selected to be 6.

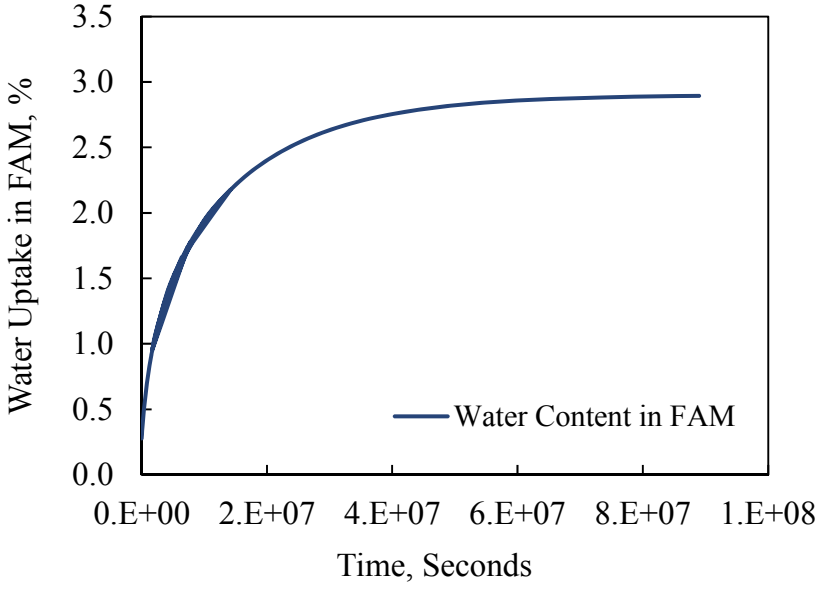

Figure 52 Water content in FAM versus diffusion time

The cohesive damage induced in FAM after conditioning time *t* is estimated by plugging $w_f(t)$ in CD model, which is rewritten here again:

$$d_{ECD} = [1-\exp(-0.25\,\mathrm{w})]\times[1+\frac{1.17}{(1+(0.0205\,\mathrm{f}_R^{-0.181})w^{(0.13L\mathrm{ogf}_R+0.18)})^8}-\frac{2.17}{(1+(0.0205\,\mathrm{f}_R^{-0.181})w^{(0.13L\mathrm{ogf}_R+0.18)})^{14}}] \quad (120)$$

For instance, 20 days of conditioning AC at 100% *RH* and 35°C creates 1.02 % water content in FAM which results in the cohesive damage shown in Figure 53. It should be noted that as discussed in Section 4.4.1, d_{CD} changes with the loading frequency.

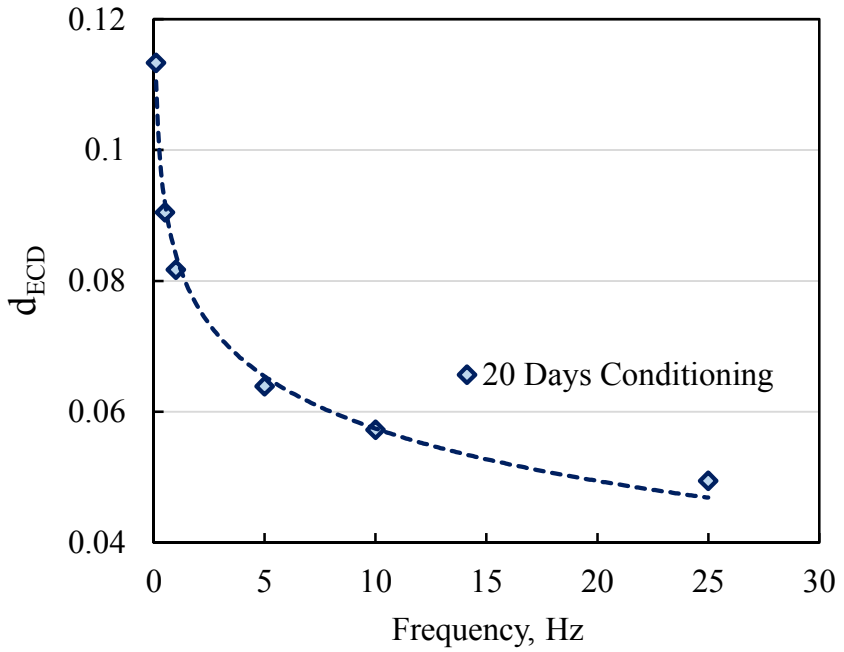

Figure 53 Effective cohesive damage induced in FAM after 20 days of conditioning AC sample at 100% RH and 35° C

6.5 IAMP Model Calibration and Validation

In this section, parameters α and β in Equation (93) are determined by fitting the IAMP model to $|E^*|$ data obtained directly from conducting dynamic modulus test on aged-moisture conditioned HMA samples. AD and CD models are integrated linearly into a single MD model. As mentioned previously, α and β present the contribution of adhesive and cohesive damages to deterioration of $|E^*|$. Evidently, d_{AD} and d_{CD} both affect $|E^*|$, but whether or not they have the

same influence is recognized by fitting the IAMP model to the measured data. IAMP model is presented here again:

$$|E^*|_{Aging+Moisture} = |E^*(t,T)|_{aging} \times [1-\alpha+\alpha(1.42-0.42e^{(0.025C_m)^{0.4}})^{0.5}]$$
$$-\beta \times [1-\exp(-0.25w)] \times [1+\frac{1.17}{(1+(0.0205f_R^{-0.181})w^{(0.13Logf_R+0.18)})^8} - \frac{2.17}{(1+(0.0205f_R^{-0.181})w^{(0.13Logf_R+0.18)})^{14}}] \quad (121)$$

$|E^*(t,T)|_{aging}$, C_m and w are predicted using the aging and diffusion model detailed in subsection 6.1 and 6.2, respectively. $|E^*|_{Aging+Moisture}$ is measured in the lab by conducting the dynamic modulus test on S3 PG 64-22 AC specimens conditioned for 20, 40, 62, 74 and 85 days at 100% *RH* and 35°C. Two replicates with diameter of 100 mm and height of 150 mm were prepared for each conditioning time. Dynamic modulus test was conducted on samples after their corresponding conditioning times were completed. The test was conducted at 6 different frequencies, 0.1, 0.5, 1, 5, 10 and 25, and only one temperature 35°C. Temperature 35°C was selected as the temperature during loading time to provide a testing environment close to the conditioning environment and minimize the evaporation of absorbed water. Figure 54 shows the average |*E**| values for the conditioned samples in the semi-log and log-log scale, respectively.

Leave-one-out cross-validation technique is used to train and validate the IAMP model simultaneously. The purpose of training is to determine α and β in Equation (93). In this technique, the data set is divided into 5 subsets, and the model is trained and tested 5 separate times. Each time, one subset is used as the test set, and the other 4 subsets are employed for training. Then, the average α and β across all 5 trials are computed. Figure 55-Figure 59 illustrate the cross validation results for training and testing data set. α and β estimated for each trial using the corresponding training set are also shown in the figures. In each figure, training set is composed of the conditioning data that are not included in the testing set. For instance, Figure 55

illustrates the leave-one-out cross validation results for (a) training set composed of 20, 40, 62 and 74 day-conditioning data and (b) testing set composed of 85-day-conditioning data. The validation results suggest that the IAMP model is robust to predict the |*E**| for aged-moisture-conditioned samples.

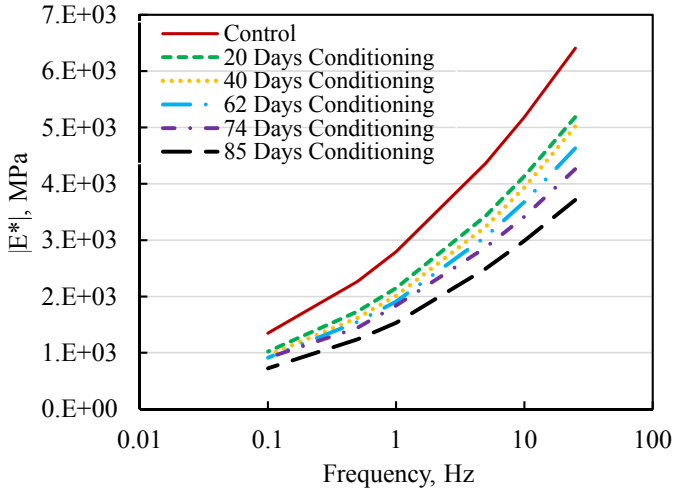

(a)

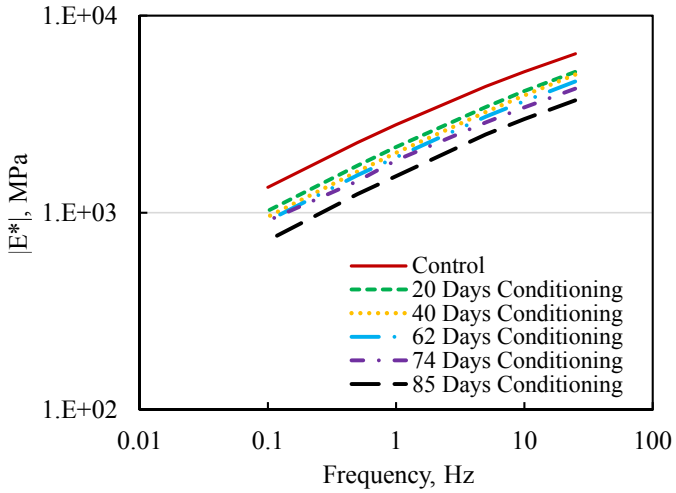

Figure 54 Average |*E| values for the conditioned samples in (a) semi-log scale, and (b) log-log scale**

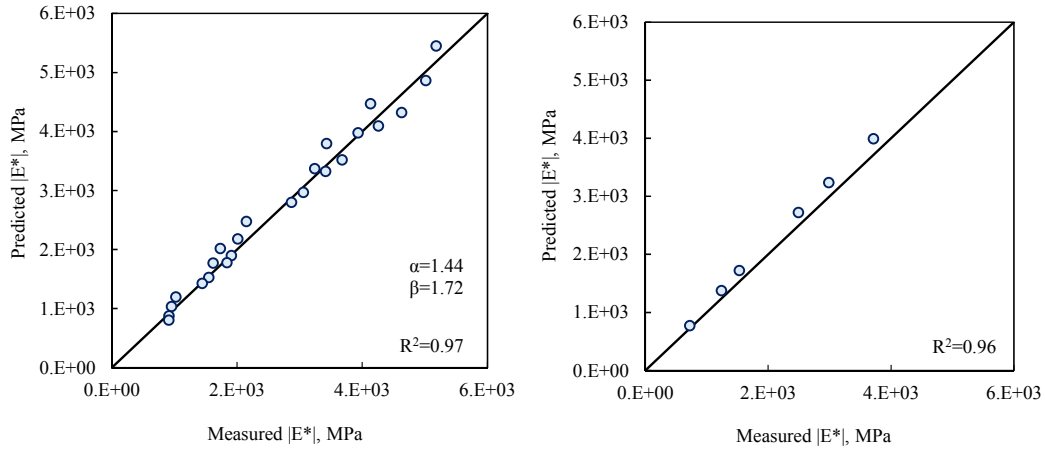

(a) (b)

Figure 55 Illustration of cross validation results for (a) training set (b) testing set composed of 85-day conditioning data

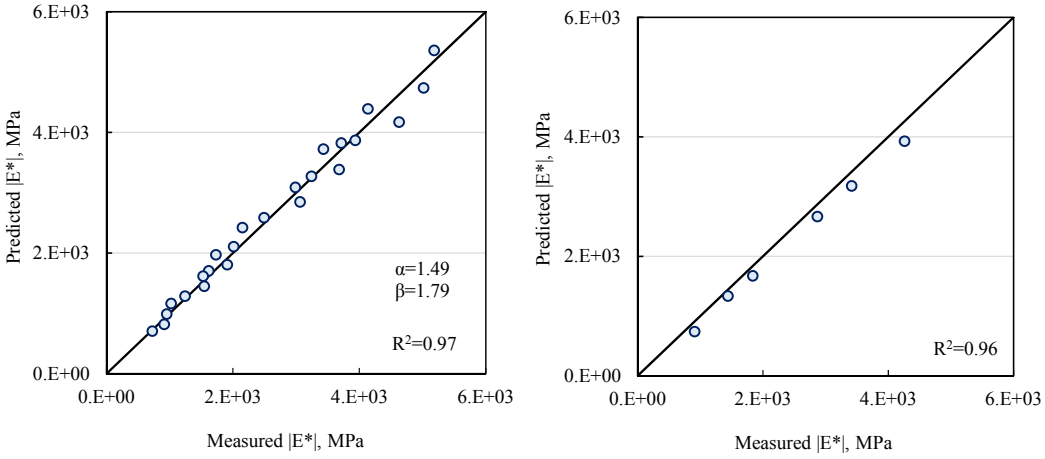

(a) (b)

Figure 56 Illustration of cross validation results for (a) training set (b) testing set composed of 74-day conditioning data

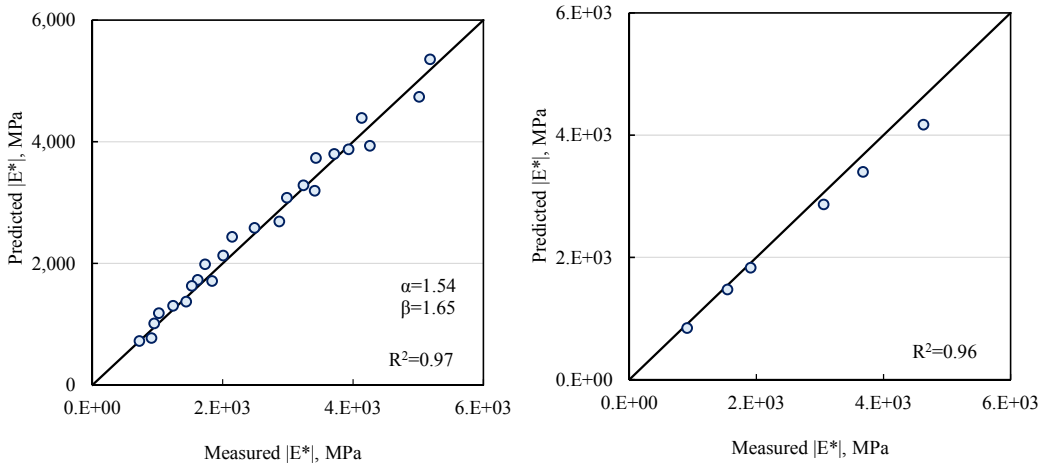

(a) (b)

Figure 57 Illustration of cross validation results for (a) training set, and (b) testing set composed of 62-day conditioning data

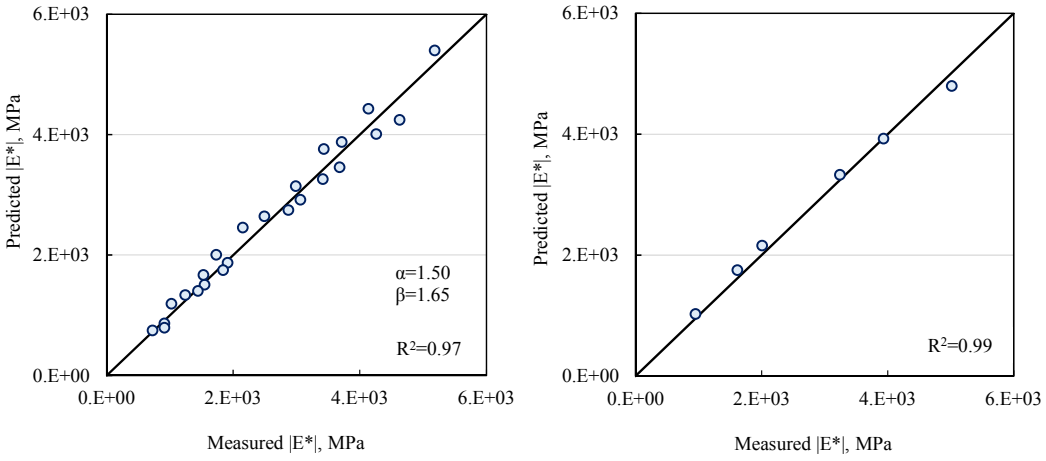

(a) (b)

Figure 58 Illustration of cross validation results for (a) training set, and (b) testing set composed of 40-day conditioning data

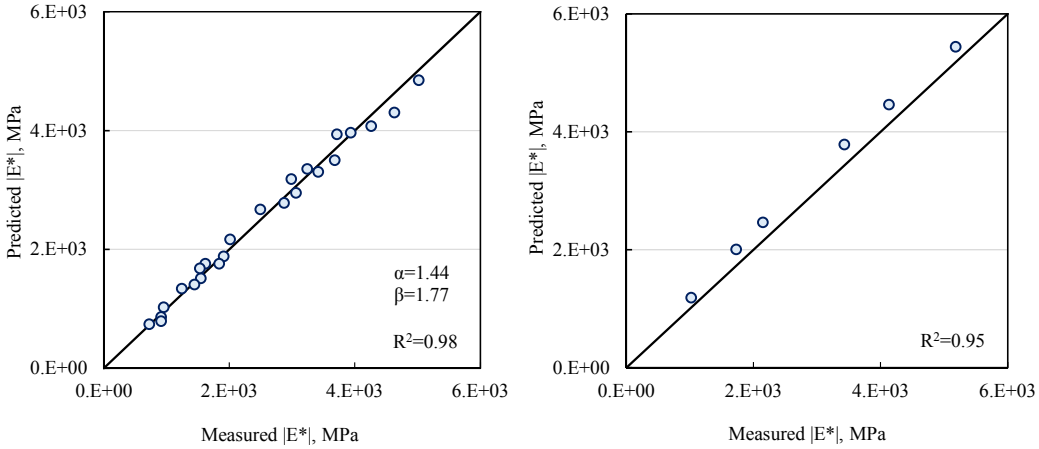

(a) (b)

Figure 59 Illustration of cross validation results for (a) training set, and (b) testing set composed of 20-day conditioning data

The averaged value of α and β are determined to be 1.48 and 1.71, respectively. Finally, these values are plugged in Equation (121) to finalize the development of IAMP model. Note that α has a greater value than β, implying that the contribution of cohesive damage in the reduction of dynamic modulus might be stronger than that of adhesive damage. Figure 60-Figure 64 illustrate the effects of aging (red line) and moisture (dark blue line) on $|E^*|$ for conditioned samples according to the IAMP model. In these figures, markers show the measured data.

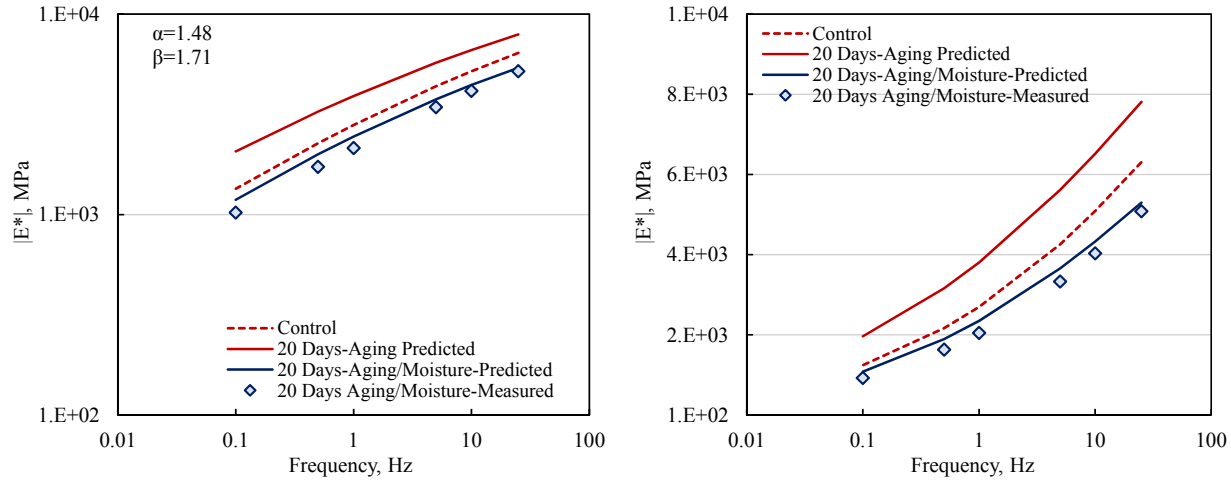

Figure 60 Predicted/measured values of |*E| after 20 days conditioning in (a) log-log, and (b) semi-log scales**

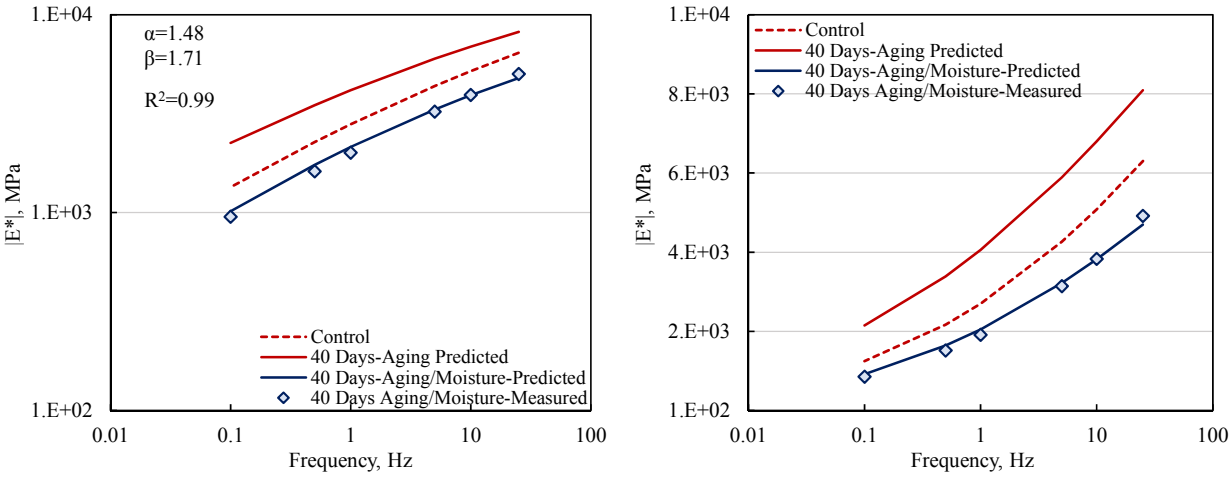

Figure 61 Predicted/measured values of |*E| after 40 days conditioning in (a) log-log, and (b) semi-log scales**

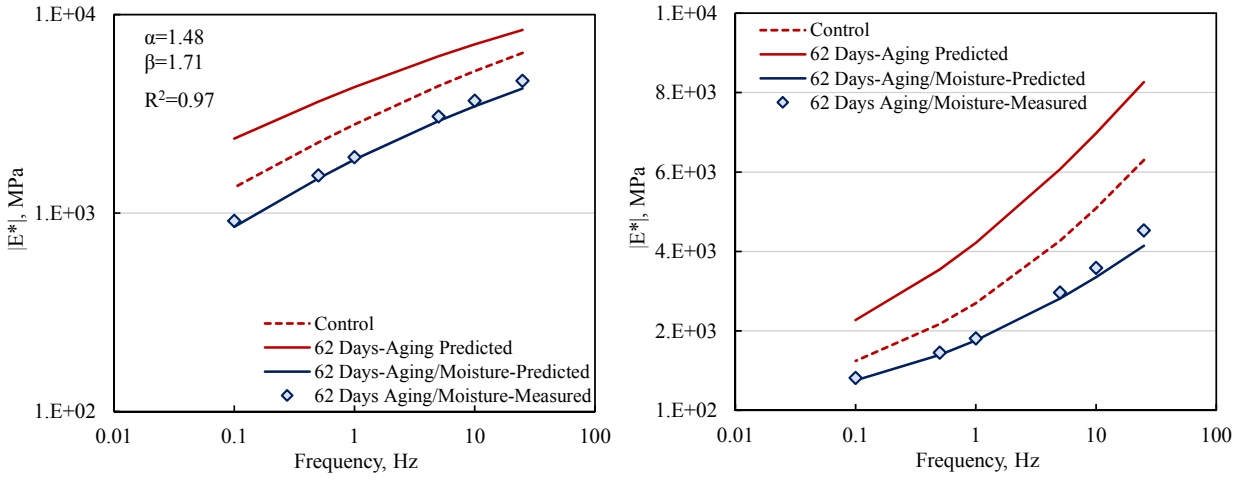

Figure 62 Predicted/measured values of |*E| after 62 days conditioning in (a) log-log, and (b) semi-log scales**

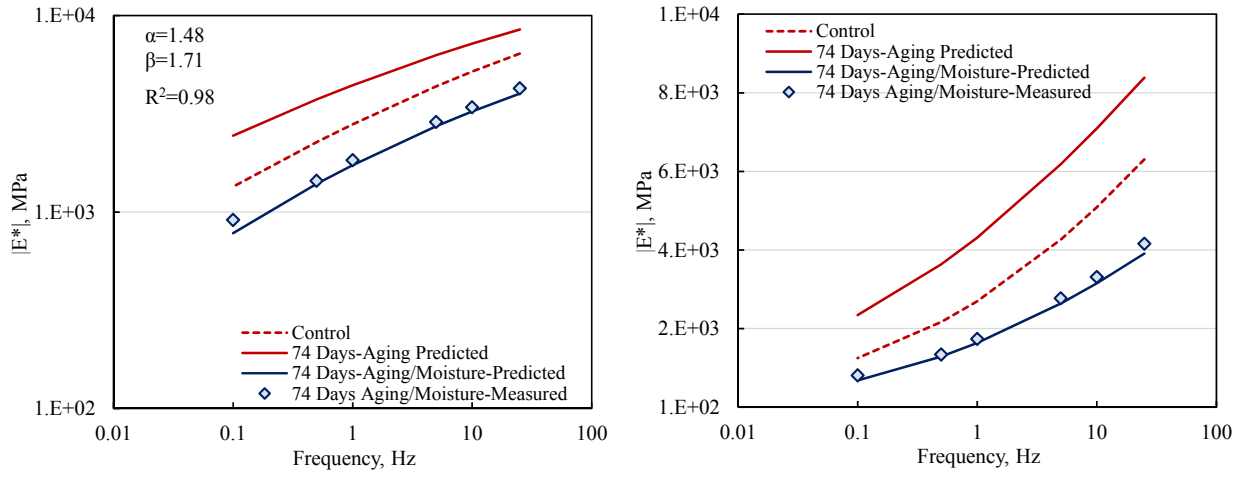

Figure 63 Predicted/measured values of |*E| after 74 days conditioning in (a) log-log, and (b) semi-log scales**

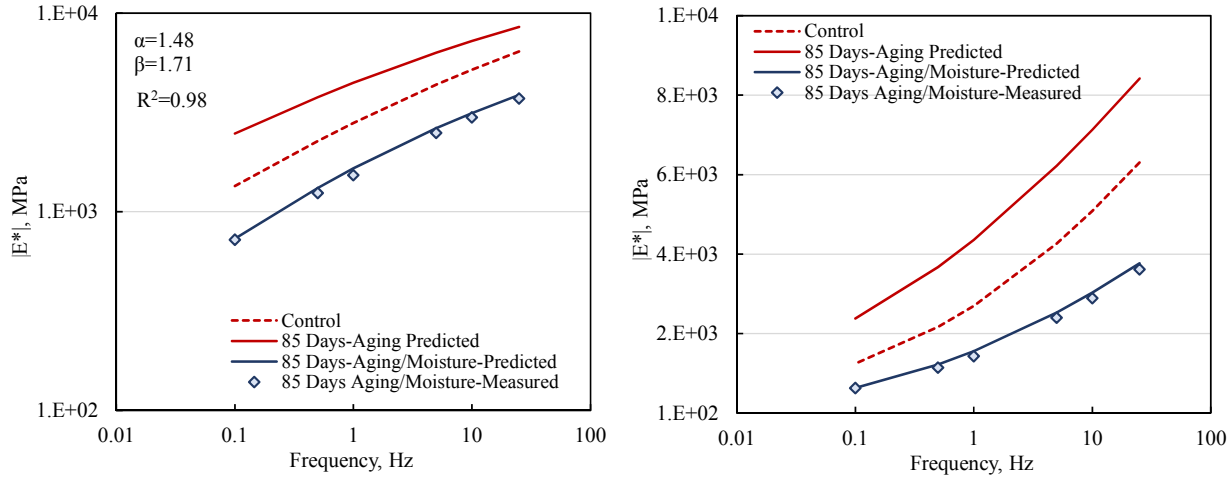

Figure 64 Predicted/measured values of |*E| after 85 days conditioning in (a) log-log, and (b) semi-log scales**

The moisture damage factors corresponding to each conditioning time are presented in Figure 65; the adhesive and cohesive damage factors (i.e. d_{AD} and d_{CD}) associated with each moisture damage factor (i.e. d_{MD}) are presented in Table 5.

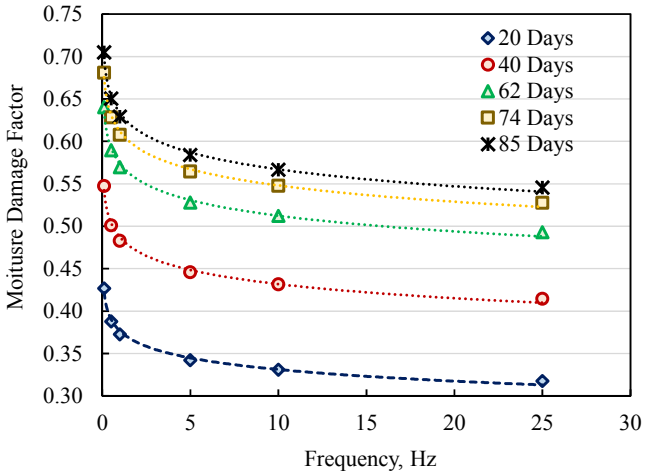

Figure 65 Moisture damage factor corresponding to different durations of conditioning

Table 5 Calculated Adhesive and Cohesive Damage Factors

Conditioning Days	Frequency (Hz)	d_{AD}	d_{CD}
20	25	0.157	0.049
	10	0.157	0.057
	5	0.157	0.064
	1	0.157	0.082
	0.5	0.157	0.090
	0.1	0.157	0.113
40	25	0.198	0.070
	10	0.198	0.080
	5	0.198	0.088
	1	0.198	0.110
	0.5	0.198	0.121
	0.1	0.198	0.148
62	25	0.233	0.086
	10	0.233	0.097
	5	0.233	0.107
	1	0.233	0.131
	0.5	0.233	0.142
	0.1	0.233	0.172
74	25	0.248	0.093
	10	0.248	0.105
	5	0.248	0.114
	1	0.248	0.140
	0.5	0.248	0.152
	0.1	0.248	0.182
85	25	0.252	0.101
	10	0.252	0.113
	5	0.252	0.123
	1	0.252	0.149
	0.5	0.252	0.162
	0.1	0.252	0.194

It is observed that the rate of increase in d_{MD} decreases with time, which is an expected trend given the intrinsic nature of the diffusion process in AC. IAMP model first predict the

effect of aging on |*E**|, then the corresponding d_{MD} is multiplied by |*E**| to account for the effect of moisture coupled with aging. Figure 66 compares predicted/measured values of |*E**| for the samples subjected to 20 and 85 days of conditioning.

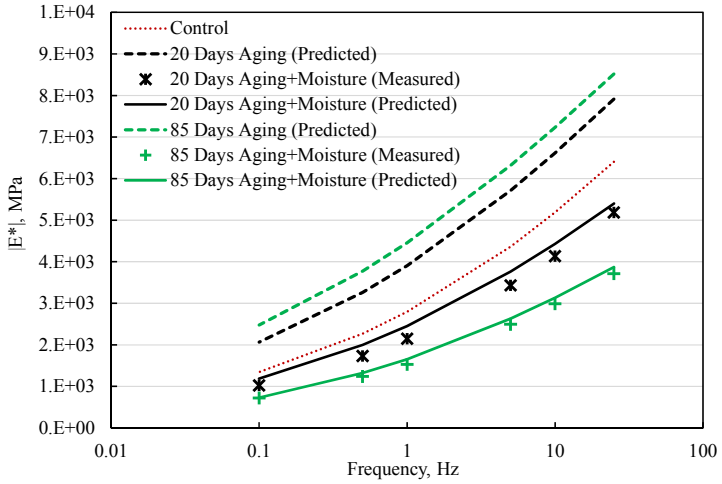

(a)

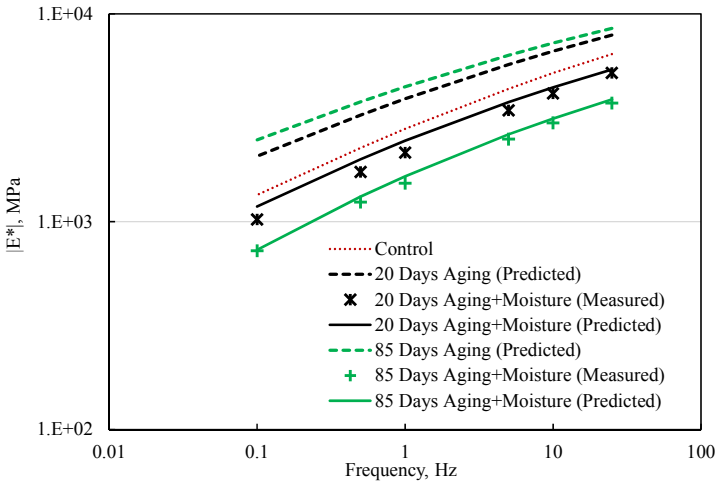

4

(b)

Figure 66 Predicted/measured values of |*E| for the samples subjected to 20 and 85 conditioning days in (a) semi-log, and (b) log-log scales**

6.6 Extension of IAMP Model

In the previous sections, the IAMP model was trained and validated to predict |*E**| for AC samples conditioned at 100% RH and 35°C. The dynamic modulus test was conducted at 35°C to maintain the loading environment close to the conditioning environment, and minimize the desorption of the water. If assuming that water content remains constant during conducting the test at various temperatures, the extension of CD model detailed in Section 4.4.2 can be employed to construct the |*E**| master curve. It should be noted that the cohesive damage continues to be formed during loading given that the deterioration effect of absorbed water on the reduction of dynamic modulus changes with the loading frequency and temperature. However, the adhesive damage mostly occurs during the conditioning period as the absorbed water vapor deteriorates the interfacial bond before loading when AC is being conditioned. Therefore, to construct the master curve, MD model is formulated by combing the AD model and extended CD model as follows:

$$d_{MD} = 1.48\times[1-(1.42-0.42e^{C_m^{0.4}})^{0.5}]+1.71\times[1-\exp(-0.25\,\mathrm{w})]\times \\ [1+\frac{1.17}{(1+(0.0205\,\mathrm{f}_R^{-0.181})w^{(0.13L\mathrm{ogf}_R+0.18)})^8}-\frac{2.17}{(1+(0.0205\,\mathrm{f}_R^{-0.181})w^{(0.13L\mathrm{ogf}_R+0.18)})^{14}}] \quad (122)$$

f_R is calculated using Equations (50) and (51), and C_m and w are computed as detailed in Sections 6.3 and 6.4. Figure 67 and Figure 68 illustrate the predicted |*E**| master curve for the samples subjected to 20 and 62 conditioning days according to the extended IAMP model. The regression models developed in Section 6.1 are employed to construct the |*E**| for aged samples, then, d_{MD}, presented in Figure 69, are applied to account for the moisture damage.

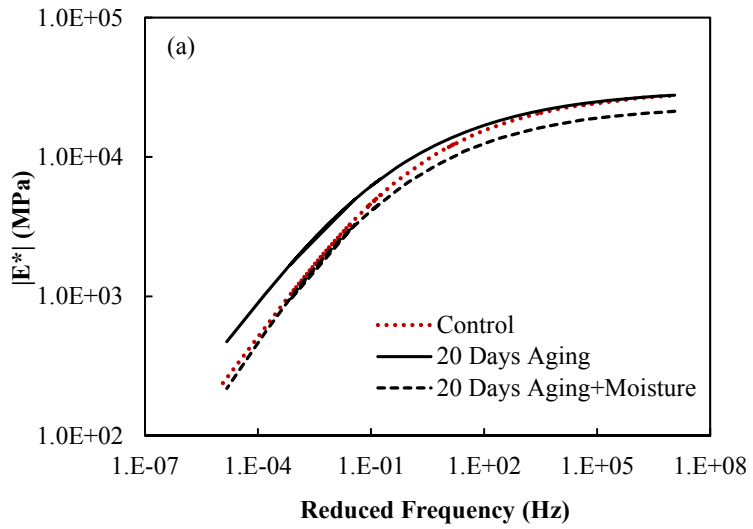

(a)

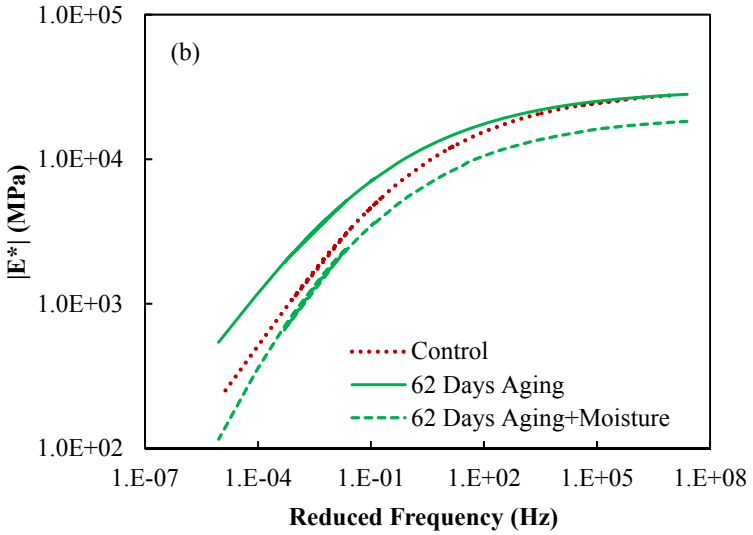

(b)

Figure 67 Predicted values of |*E| after (a) 20 and (b) 62 days of conditioning in log-log scale**

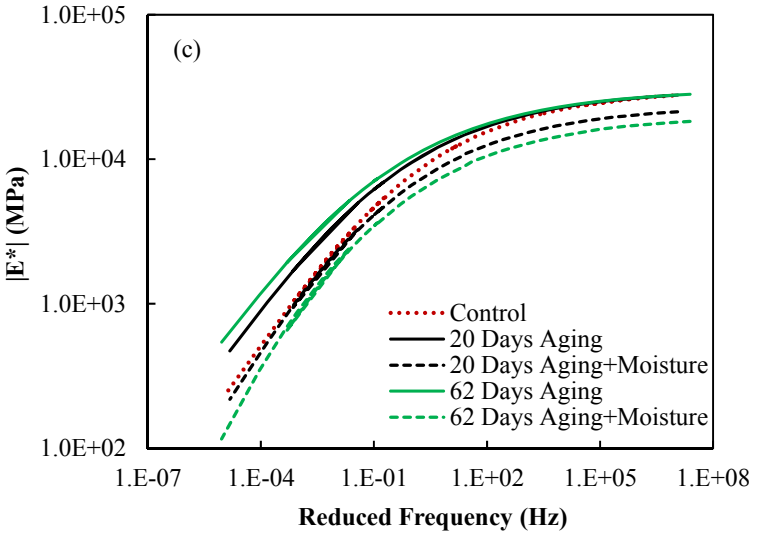

Figure 68 Predicted values of |*E| after 20 and 62 days of conditioning in log-log scale**

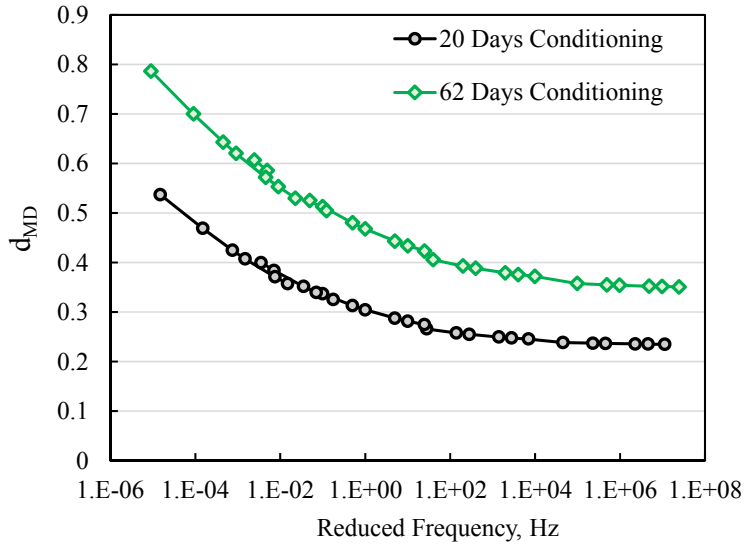

Figure 69 Moisture damage factor corresponding to 20 and 62 days of conditioning in semi-log scale

The assumption that water content remains constant in AC samples during the dynamic modulus test at various temperatures might underestimate |*E**| master curve. The reason is that

|E^*| testing is conducted at 0% RH chamber, resulting in a gradual desorption of water from AC, specifically when testing lasts for a couple of hours. Therefore, the actual induced cohesive damage might be less than the one predicted by Equation (122). Evaluating the accuracy of extended model to predict the master curve needs more work, which necessitates performing |E^*| test on the conditioned samples at different temperatures. However, in the field, temperature at which loading is applied, is the same as conditioning temperature. Thus, the actual in-service performance of AC pavements can be simulated by the IAMP model instead of extended IAMP. In other words, instead of predicting the master curve, it would be more beneficial to calibrate and validate the IAMP model at various temperatures. The validity of the model at the conditioning defined in this study is explicitly shown for S3 PG 64-22 mixture. As the model is mounted on the fundamental mechanical and physical properties of the materials, it is expected for the IAMP model to be capable of predicting |E^*| at other conditionings as well. The key is to conduct a series of upfront tests to determine the values of its parameters. As a continuation of this study, more validation and calibration work are required to confirm the accuracy of the model.

7. CONCLUSION AND RECOMMENDATION

This dissertation studies the coupling effect of aging and moisture damage on the dynamic modulus of asphalt concrete. Dynamic modulus is recognized as one of the most important properties of asphalt concrete for pavement design. Hence, characterizing the degradation of this property due to the combination of aging and moisture helps in the design of long-lasting pavements and preventing a premature failure. Diffusion of subsurface water vapor through pavement is one of the major moisture transport modes, resulting in the evolution of early moisture-related distresses in the pavements located in regions with desert climate. Therefore, water vapor diffusion is considered in this dissertation as the main contributor to moisture induced damage.

A comprehensive literature review was conducted to identify the effects of moisture presence on aging process, and the impact of age-hardening on the evolution of moisture damage. It is recognized that moisture does not have significant effects on the progress of aging at atmospheric pressure. However, at high pressures, water participates in the oxidative reaction and leads to the formation of more oxidized products. Since aging and moisture damage occur at the atmospheric pressure in the field, this implies that the presence of water does not influence the aging process. However, with regard to the impact of aging on moisture damage mechanism, aging has significant effects on the progress of moisture induced damage via changing asphalt binders' surface free energy and moisture diffusion coefficient. Therefore, this interaction should be considered when developing predictive models to characterize the coupled aging-moisture degradation.

In this dissertation an integrated aging-moisture predictive model was developed to characterize the simultaneous effects of aging and moisture on the dynamic modulus of asphalt concrete which is a primary material property in the design of a pavement. The integrated model consists of a predictive kinetic-based aging model and a moisture damage model. The models are developed by identifying underlying causes of degradation, and considering the interactions among chemical and physical properties influenced by aging and moisture. They are calibrated by conducting corresponding tests on conditioned specimens. Diffusion of water vapor through asphalt concrete is simulated by conditioning asphalt mixture specimens in moisture room at 100% relative humidity. Also, to combine the moisture induced damage with aging, the specimens are subjected to an aging temperature of 35°C. This temperature is selected as it can reasonably represent the average pavement temperature for a long period of time during a year. The following sections summarize the main findings obtained in this study.

7.1 Predictive Aging Model

The effect of aging on $|E^*|$ and phase angle was investigated by conducting the dynamic modulus testing on HMA specimens subjected to nine aging levels in laboratory. The results showed that:

- $|E^*|$ increases with the aging temperature and time over the entire range of reduced frequencies. However, phase angle decreases with the aging at intermediate and high reduced frequencies, while it increases when the reduced frequency is low.
- The kinetic-based aging model is able to predict $|E^*|$ of mixtures conditioned in oven at high temperatures well. Long-term oven aging of asphalt mixtures is composed of a fast-rate period followed by a constant-rate period.

- The fast-rate period is not passed during the short-term aging process, and a part of that occurs during the long-term aging.

In addition, this dissertation proposes a model to predict $|E^*|$ and φ master curves of aged mixtures. The model is developed based on the relation of sigmoidal coefficients for the master curves and the shift factor parameters with a function value. This function, denoted by λ, characterizes the effects of aging on $|E^*|$ based on the aging properties of a certain mixture aged in the oven at a temperature T for the time duration of t. Parameters of λ account for the aging characteristics of a mixture, such as aging activation energy and pre-exponential factor. The proposed model was validated for a mixture aged under an aging condition of interest. Validation results suggest that the model is able to predict $|E^*|$ and φ with acceptable accuracy.

7.2 Cohesive Damage Model

Cohesive damage model proposed in this study accounts for the softening FAM (Fine Aggregate Matrix) due to the diffused water vapor. The model was formulated using the Lennard-Jones potential, and relating its components to the diffused water content. The calibration of developed model was completed by conducting the dynamic modulus test on FAM specimens conditioned at 100% *RH* and 35°C so that the parameters used in model can capture the impact of aging on the cohesive damage. It was observed that the cohesive damage changes with the frequency of loading; at lower frequencies, the effect of diffused water in reduction of $|E^*|$ is greater than that at higher frequencies. A goodness of fit of R^2=98% for the cohesive damage model suggests the capability of this model in quantification of the impact of diffused water vapor on the stiffness degradation of FAM. The cohesive damage was extended based on the concept of time-temperature superposition to predict the cohesive moisture damage at various frequencies and temperatures.

7.3 Adhesive Damage Model

Adhesive damage model accounts for the deterioration of adhesive bond between aggregate and binder as water vapor reaches the interface. The model is formulated by linking a thermodynamic property (i.e., adhesive bond energy) to a mechanical property (i.e., tensile strength of the interfacial bond) of asphalt mixture. Adhesive bond energy is characterized based on the water vapor concentration at the interface and relative humidity. A diffusion model is employed to estimate the water vapor concentration at the interfacial bond. Parameters of the adhesive model are determined by conducting the Bitumen Bond Strength test on aged-moisture conditioned test samples. It was observed that as conditioning time increases, reduction in tensile bond strength increases as a result of increased amount of accumulated water vapor concentration at the interface, and potential of aging to worsen the moisture damage. The validation results show that the adhesive damage model performs well in modeling the effect of water vapor concentration on the bond strength deterioration.

7.4 Integrated Aging-Moisture Predictive Model

Three aforementioned models, i.e., aging, cohesive moisture damage, and adhesive moisture damage models, were integrated to predict the dynamic modulus of aged-moisture conditioned specimens. The deterioration effects of water vapor on dynamic modulus was quantified by combining the adhesive damage model with cohesive damage model into a single moisture damage model through a linear map. The integrated model modifies the aging model by incorporating the moisture damage model. The corresponding coefficients of the adhesive and cohesive damage model in the linear moisture damage model are obtained by fitting the integrated model to dynamic modulus data measured for aged-moisture conditioned asphalt concrete specimens. These coefficients account for the contribution of adhesive and cohesive

damages to deterioration of dynamic modulus. The performance of developed model was evaluated through cross-validation. It was observed that the cohesive damage has a greater contribution in the reduction of dynamic modulus than the adhesive damage. The validation results suggest that the integrated model is robust to predict the dynamic modulus for aged-moisture conditioned samples when loading temperature is the same as conditioning temperature.

7.5 Future Research Work

The proposed integrated model is developed based on thermodynamic, chemical, physical and mechanical processes involved in the age-hardening and moisture damage of asphalt concrete. The validity of developed model was examined at a certain conditioning circumstances for a Superpave mixture. In order to generalize the use of this model for pavement design, the parameters used in moisture damage model should be determined under various conditioning circumstances. Conditioning temperatures can be selected such that each represents the dominant average aging temperature during different seasons. The integrated model can be embedded in pavement design programs. The variables used in the new model include diffused water content in FAM, water vapor concentration at the interface and aging temperature and time. Aging model predicts the master curve at a given aging temperature and time; a series of upfront tests are required to obtain the aging properties involved in the aging model. Numerical solution or analytical models can be used to solve the diffusion problems and estimate the water content and water concentration within the asphalt concrete pavements.

Some future work related to this dissertation are mentioned as follows:

- More calibration and validation works are needed to confirm the accuracy of the extended adhesive damage model to quantify the effect of RH at various temperatures on the adhesive bond strength.

- AASHTO R30 recommends aging asphalt mixtures in the oven at 85°C to simulate the long-term aging equivalent to 8-10 years of the pavement service life. This standard is followed in this research to prepare aged mixtures for dynamic modulus testing. The predictive aging model is developed based on the results of dynamic modulus test on lab-aged specimens. As a future work, one can examine the validity of aging model for field aged samples.
- This study was focused on water vapor diffusion. As a continuation of this research, one may examine the effect of two other water transport modes, which are capillary rise and permeability, on moisture damage as well.
- The integrated model is proposed for a hot mix asphalt mixture. Some modification might be needed to apply the model for warm mix asphalt too. Warm mix asphalt mixtures are more susceptible to moisture damage as water is added in the production process. Therefore, in addition to the adhesive and cohesive damage induced gradually due to water vapor diffusion, an additional moisture damage factor can be considered to account for the added water.
- Validity of the model is shown for a Superpave mixture. More FAM and HMA mixtures are recommended to be studied to further examine the effectiveness of the model.
- The results of this study should be compared with field data to see if further adjustments are needed.

REFERENCES

AASHTO PP1, Standard practice for accelerated aging of asphalt binder using a pressurized aging vessel (PAV). Washington, DC.

AASHTO R 30, Standard Practice for Mixture Conditioning of Hot Mix Asphalt (HMA). AASHTO, Washington, D.C.

AASHTO T 240, Standard Method of Test for Effect of Heat and Air on a Moving Film of Asphalt binder (Rolling Thin-Film Oven Test), Washington, DC.

AASHTO T 283, Standard Method of Test for resistance of compacted asphalt mixtues to moisture-induced damage, Washington, DC.

AASHTO T 308, Determining the Asphalt Binder Content of Hot Mix Asphalt (HMA) by the Ignition Method. AASHTO, Washington, D.C.

AASHTO T 342-11, Standard Method of Test for Determining Dynamic Modulus of Hot-Mix Asphalt Concrete Mixtures. AASHTO, Washington, D.C.

AASHTO TP 79-13, Determining the Dynamic Modulus and Flow Number for Asphalt Mixtures Using the Asphalt Mixture Performance Tester (AMPT). AASHTO, Washington, D.C.

AASHTO TP 91, Standard Method of Test for Determining asphalt Binder Bond Strength by Means of the Binder Bond Strength (BBS) Test, AASHTO, Washington, D.C.

Aguiar-Moya, J. P., Salazar-Delgado, J., Baldi-Sevilla, A., Leiva-Villacorta, F., and Loria-Salazar, L. (2015). "Effect of aging on adhesion properties of asphalt mixtures with the use of

bitumen bond strength and surface energy measurement tests." Transportation Research Record: Journal of the Transportation Research Board(2505), 57-65.

Allen, R. G., Little, D. N., Bhasin, A., and Lytton, R. L. (2012). "Identification of the composite relaxation modulus of asphalt binder using AFM nanoindentation." Journal of Materials in Civil Engineering, 25(4), 530-539.

Andrei, D., Witczak, M., and Mirza, M. (1999). "Development of a revised predictive model for the dynamic (complex) modulus of asphalt mixtures." Development of the 2002 Guide for the Design of New and Rehabilitated Pavement Structures, NCHRP.

Arambula, E., Masad, E., and Martin, A. E. (2007). "The influence of air void distribution on the moisture susceptibility of asphalt mixes." Journal of Materials in Civil Engineering (ASCE), 19(8), 655-664.

Arambula, E., Caro, S., and Masad, E. (2009). "Experimental measurement and numerical simulation of water vapor diffusion through asphalt pavement materials." Journal of Materials in Civil Engineering, 22(6), 588-598.

Baek, C., Underwood, B., and Kim, Y. (2012). "Effects of oxidative aging on asphalt mixture properties." Transportation Research Record: Journal of the Transportation Research Board(2296), 77-85.

Barbour, F.A., Barbour, R.V., Peterson, J.C. (1974). "A study of asphalt-aggregate interactions using inverse gas-liquid chromatography." Journal of Applied Chemistry and Biotechnology 24(11), 645-654.

Bell, C. A., D. Sosnovske. (1994). "SHRP-A-384: Aging: Binder Validation. " TRB, National Research Council, Washington, D.C.

Bhattacharjee, S., Swamy, A. K., and Daniel, J. S. (2012). "Continuous relaxation and retardation spectrum method for viscoelastic characterization of asphalt concrete." Mechanics of Time-Dependent Materials, 16(3), 287-305.

Birgisson, B., Roque, R., and Page, G. (2003). "Evaluation of water damage using hot mix asphalt fracture mechanics." Journal of the Association of Asphalt Paving Technologists (AAPT), 73, 424-462.

Branthaver, J. F., Petersen, J., Robertson, R., Duvall, J., Kim, S., Harnsberger, P., Mill, T., Ensley, E., Barbour, F., and Scharbron, J. (1993). "Binder characterization and evaluation. Volume 2: Chemistry."

Callister Jr, W. D., and Rethwisch, D. G. (2012). Fundamentals of materials science and engineering: an integrated approach, John Wiley & Sons.

Caro, S., Masad, E., Bhasin, A., and Little, D. (2010). "Micromechanical modeling of the influence of material properties on moisture-induced damage in asphalt mixtures." Construction and Building Materials, 24(7), 1184-1192.

Caro, S., Masad, E., Bhasin, A., and Little, D. N. (2008). "Moisture susceptibility of asphalt mixtures, Part 1: mechanisms." International Journal of Pavement Engineering, 9(2), 81-98.

Cheng, D., Little, D.N., Lytton, R.L. and Holste, J.C. (2003). “Moisture damage evaluation of asphalt mixtures by considering both moisture diffusion and repeated-load conditions.” Transportation research record, 1832(1), pp.42-49.

Cheng, D. (2003). "Surface free energy of asphalt-aggregate system and performance analysis of asphalt concrete based on surface free energy."

Cheng, D., Little, D. N., Lytton, R. L., and Holste, J. C. (2002). "Use of surface free energy properties of the asphalt-aggregate system to predict moisture damage potential." Journal of the Association of Asphalt Pavement Technologists (AAPT), 71, 59-88.

Christensen, D. W. (1992). Mathematical modeling of the linear viscoelastic behavior of asphalt cements (PhD dissertation). Pennsylvania State University, State College.

Christensen, D. W., and Anderson, D. A. (1992). "Interpretation of dynamic mechanical test data for paving grade asphalt cements (with discussion)." Journal of the Association of Asphalt Paving Technologists, 61.

Christensen Jr, D., Pellinen, T., and Bonaquist, R. (2003). "Hirsch model for estimating the modulus of asphalt concrete." Journal of the Association of Asphalt Paving Technologists, 72.

Collop, A., Choi, Y., Airey, G., and Elliott, R. "Development of the saturation ageing tensile stiffness (SATS) test." Proc., Proceedings of the Institution of Civil Engineers-Transport, Thomas Telford Ltd, 163-171.

Cooper, J., Ns, L. E., and Dooley, R. (2007). "International Association for the Properties of Water and Steam."

Copeland, A., Youtcheff, J., and Shenoy, A. (2007). "Moisture sensitivity of modified asphalt binders: Factors influencing bond strength." Transportation Research Record: Journal of the Transportation Research Board(1998), 18-28.

Crank, J. (1979). The mathematics of diffusion, Oxford university press, Oxford, UK.

Cucalon, L. G., Yin, F., Martin, A. E., Arambula, E., Estakhri, C., and Park, E. S. (2015). "Evaluation of moisture susceptibility minimization strategies for warm-mix asphalt: Case study." Journal of Materials in Civil Engineering, 28(2), 05015002.

Garcia Cucalon, M. L. (2016). "Physicochemical interactions at the binder-aggregate interface." Doctoral Dissertation, Texas A&M University.

Claine Petersen J. (1998). A dual, sequential mechanism for the oxidation of petroleum asphalts. Petroleum Science and Technology. 1998;16(9-10):1023-59.

Elwardany, M. D., Yousefi Rad, F., Castorena, C., and Kim, Y. R. (2017). "Evaluation of asphalt mixture laboratory long-term ageing methods for performance testing and prediction." Road Materials and Pavement Design, 18(sup1), 28-61.

Glover, C. J., Davison, R. R., Domke, C. H., Ruan, Y., Juristyarini, P., Knorr, D. B., and Jung, S. H. (2005). "Development of a new method for assessing asphalt binder durability with field validation." Texas Dept Transport, 1872.

Han, R., Jin, X., and Glover, C. J. (2011). "Modeling pavement temperature for use in binder oxidation models and pavement performance prediction." Journal of Materials in Civil Engineering, 23(4), 351-359.

Herrington, P. (1998). "Oxidation of bitumen in the presence of a constant concentration of oxygen." Petroleum science and technology, 16(7-8), 743-765.

Hicks, R. G., Santucci, L., and Aschenbrener, T. (2003). "Introduction and seminar objectives." Moisture Sensitivity of Asphalt Pavements: A National Seminar, San Diego, California.

Hicks, G. R. (1991). "Synthesis of Highway Practice 175: Moisture Damage in Asphalt Concrete." Transportation Research Board, National Research Council, Washington, D.C.

Houston, W. N., Mirza, M., Zapata, C. E., and Raghavendra, S. (2005). "Environmental effects in pavement mix and structural design systems." NCHRP, Project, 9-23.

Huang, S.-C., Glaser, R., and Turner, F. (2012). "Impact of water on asphalt aging: Chemical aging kinetic study." Transportation Research Record: Journal of the Transportation Research Board(2293), 63-72.

Hu, H., Zhang, J., Guo, S., and Chen, G. (1999). "Extraction of Huadian oil shale with water in sub-and supercritical states." Fuel, 78(6), 645-651.

Huang, T., and Luo, R. (2018). "Investigation of effect of temperature on water vapor diffusing into asphalt mixtures." Construction and Building Materials, 187, 1204-1213.

Kanitpong, K., and Bahia, H. (2005). "Relating adhesion and cohesion of asphalts to the effect of moisture on laboratory performance of asphalt mixtures." Transportation Research Record: Journal of the Transportation Research Board(1901), 33-43.

Kassem, E., Masad, E., Bulut, R., and Lytton, R. (2006). "Measurements of moisture suction and diffusion coefficient in hot-mix asphalt and their relationships to moisture damage." Transportation research record: journal of the transportation research board(1970), 45-54.

Kiggundu, B. M., and Roberts, F. L. (1988). "Stripping in HMA mixtures: State-of-the-art and critical review of test methods." Rep. No. NCAT 88-02, National Center for Asphalt Technology (NCAT), Auburn, Alabama.

Kim, Y. R., Castorena, C., Elwardany, M. D., Rad, F. Y., Underwood, S., Gundla, A., Gudipudi, P., Farrar, M. J., and Glaser, R. R. (2018). Long-Term Aging of Asphalt Mixtures for Performance Testing and Prediction, Transportation Research Board.

Kim, Y.R., Little, D. and Lytton, R., 2004. “Effect of moisture damage on material properties and fatigue resistance of asphalt mixtures.” Transportation Research Record: Journal of the Transportation Research Board, (1891), pp.48-54.

Kringos, N., Scarpas, A., and De Bondt, A. (2008a) "Determination of moisture susceptibility of mastic-stone bond strength and comparison to thermodynamical properties." Proc., Annual Meeting of the Association of Asphalt Paving Technologists, AAPT; Philadelphia, PA; 25 April 2008 through 30 April 2008, 435-478.

Kringos, N., Scarpas, A., Kasbergen, C., and Selvadurai, P. (2008b). "Modelling of combined physical-mechanical moisture-induced damage in asphaltic mixes, part 1: Governing processes and formulations." International Journal of Pavement Engineering, 9(2), 115-118.

Kringos, N., Scarpas, A., Copeland, A., and Youtcheff, J. (2008c). "Modelling of combined physical–mechanical moisture-induced damage in asphaltic mixes Part 2: moisture susceptibility parameters." International Journal of Pavement Engineering, 9(2), 129-151.

Kutay, M. E., Aydilek, A. H., and Masad, E. (2007a). "Computational and experimental evaluation of hydraulic conductivity anisotropy in hot-mix asphalt." International Journal of Pavement Engineering, 8(1), 29-43.

Kutay, M. E., Aydilek, A. H., and Masad, E. (2007b). "Estimation of directional permeability of HMA based on numerical simulation of micro-scale water flow." Transportation Research Record: Journal of the Transportation Research Board, 2001, 29-36.

Liu, C. (2005). "Van der Waals force and asphalt concrete strength and cracking." Journal of engineering mechanics, 131(2), 161-166.

Ling M, Luo X, Gu F, Lytton RL.(2017). "Time-temperature-aging-depth shift functions for dynamic modulus master curves of asphalt mixtures. " Construction and Building Materials. 157:943-51.

Luo, R., Liu, Z., Huang, T., and Tu, C. (2018). "Water vapor passing through asphalt mixtures under different relative humidity differentials." Construction and Building Materials, 165, 920-930.

Luo, R., and Huang, T. (2018). "Development of a three-dimensional diffusion model for water vapor diffusing into asphalt mixtures." Construction and Building Materials, 179, 526-536.

Luo X, Gu F, Lytton RL. (2017). Kinetics-based aging prediction of asphalt mixtures using field deflection data. International Journal of Pavement Engineering, 1-11. https://doi.org/10.1080/10298436.2017.1293262

Luo X, Gu F, Lytton RL. (2015). Prediction of field aging gradient in asphalt pavements. Transportation Research Record: Journal of the Transportation Research Board. (2507):19-28. https://doi.org/10.3141/2507-03

Luo, X., Luo, R., and Lytton, R. (2013). "Modified Paris's law to predict entire crack growth in asphalt mixtures." *Transportation Research Record: Journal of the Transportation Research Board*(2373), 54-62.

Lytton, R. L., (2015). "Micromechanics of Civil Engineering Materials, Class Notes." Zachry Department of Civil Engineering, Texas A&M University, College Station.

Lytton, R. L., Masad, E. A., Zollinger, C., Bulut, R., and Little, D. N. (2005). "Measurements of surface energy and its relationship to moisture damage."

Masad, E., Al-Omari, A., and Chen, H.-C. (2007). "Computations of permeability tensor coefficients and anisotropy of asphalt concrete based on microstructure simulation of fluid flow." Computational Materials Science, 40(4), 449-459

Masad, E., Tashman, L., Little, D., and Zbib, H. (2005). "Viscoplastic modeling of asphalt mixes with the effects of anisotropy, damage and aggregate characteristics." Mechanics of Materials, 37, 1242-1256.

Mensching, D. J., Rowe, G. M., and Sias Daniel, J. (2017). "A mixture-based Black Space parameter for low-temperature performance of hot mix asphalt." Road Materials and Pavement Design, 18(sup1), 404-425.

Mirza M.W., Witczak M.W. (1995). "Development of a global aging system for short and long term aging of asphalt cements (with discussion). " Journal of the Association of Asphalt Paving Technologists. 1995;64.

Moraes, R., Velasquez, R., and Bahia, H. (2011). "Measuring the effect of moisture on asphalt-aggregate bond with the bitumen bond strength test." Transportation Research Record: Journal of the Transportation Research Board(2209), 70-81.

Newcomb, D., Martin, A. E., Yin, F., Arambula, E., Park, E. S., Chowdhury, A., Brown, R., Rodezno, C., Tran, N., and Coleri, E. (2015). Short-term laboratory conditioning of asphalt mixtures.

Oshone, M., Dave, E., Daniel, J. S., and Rowe, G. M. (2017). "Prediction of phase angles from dynamic modulus data and implications for cracking performance evaluation." Road Materials and Pavement Design, 18(sup4), 491-513.

Pan, J., Tarefder, R. A., and Hossain, M. I. (2016). "Study of Moisture Impact on Asphalt Before and After Oxidation Using Molecular Dynamics Simulations." Transportation Research Record: Journal of the Transportation Research Board(2574), 38-47.

Pauli, A. T. (2014). "Chemomechanics of damage accumulation and damage-recovery healing in bituminous asphalt binders."Delft, Netherlands.

Petersen, J. C. (2009). "A review of the fundamentals of asphalt oxidation: chemical, physicochemical, physical property, and durability relationships." Transportation Research E-Circular(E-C140).

Petersen J. C. (1998). "A dual, sequential mechanism for the oxidation of petroleum asphalts." Petroleum Science and Technology. 16(9-10):1023-59.

Petersen, J. C., Barbour, F., Dorrence, S. (1974). "Catalysis of asphalt oxidation by mineral aggregate surfaces and asphalt components." Association of Asphalt Paving Technologists Proc.

Reed, J. "Evaluation of the effects of aging on asphalt rubber pavements." Proc., Masters Abstracts International.

Rowe, G. (2009). "Phase angle determination and interrelationships within bituminous materials." Advanced Testing and Characterization of Bituminous Materials, Two Volume Set, CRC Press, 59-68.

Ruan Y, Davison RR, Glover CJ. (2003)."The effect of long-term oxidation on the rheological properties of polymer modified asphalts. " Fuel. 82(14):1763-73.

Sato, T., Adschiri, T., Arai, K., Rempel, G. L., and Ng, F. T. (2003). "Upgrading of asphalt with and without partial oxidation in supercritical water☆." Fuel, 82(10), 1231-1239.

Schlepp, L., Elie, M., Landais, P., and Romero, M. (2001). "Pyrolysis of asphalt in the presence and absence of water." Fuel processing technology, 74(2), 107-123.

Schmidt, R.J. and Graf, P.E., 1972. “Effect of Water on Resilient Modulus of Asphalt-Treated Mixes.” Association of Asphalt Paving Technologists Proc. Vol. 41.

Sias Daniel, J., Gibson, N., Tarbox, S., Copeland, A., and Andriescu, A. (2013). "Effect of long-term ageing on RAP mixtures: laboratory evaluation of plant-produced mixtures." Road Materials and Pavement Design, 14(sup2), 173-192.

Song, I., Little, D. N., Masad, E., and Lytton, R. L. (2005). "Comprehensive evaluation of damage in asphalt mastics using X-ray CT, continuum mechanics, and micromechanics." Journal of the Association of Asphalt Paving Technologists (AAPT), 74, 885-920.

Sousa, P., Kassem, E., Masad, E., and Little, D. (2013). "New design method of fine aggregates mixtures and automated method for analysis of dynamic mechanical characterization data." Construction and Building Materials, 41, 216-223.

Tong, Y. (2013). "Fatigue resistance of asphalt mixtures affected by water vapor movement." PhD dissertation, Texas A&M University.

Thomas, K. P. (2002). "Impact of water during the laboratory aging of asphalt." Road Materials and Pavement Design, 3(3), 299-315.

Van Gooswilligen, G., Berger, H., and De Bats, F. T. "Oxidation of bitumens in various tests." Proc., 3rd Eurobitume Symposium, 95-101.

Vasconcelos, K. L., Bhasin, A., Little, D. N., and Lytton, R. L. (2010). "Experimental measurement of water diffusion through fine aggregate mixtures." Journal of Materials in Civil Engineering, 23(4), 445-452.

Yin, F., Cucalon, L. G., Martin, A. E., Arambula, E., Chowdhury, A., and Park, E. S. (2011). "Laboratory conditioning protocols for warm-mix asphalt."

Yin, F., Epps Martin, A., and Arámbula-Mercado, E. (2016). "Warm-Mix Asphalt Moisture Susceptibility Evaluation for Mix Design and Quality Assurance." Transportation Research Record: Journal of the Transportation Research Board(2575), 39-47.

Yin, F., Arámbula-Mercado, E., Epps Martin, A., Newcomb, D., and Tran, N. (2017). "Long-term ageing of asphalt mixtures." Road Materials and Pavement Design, 18(sup1), 2-27.

Zhou, F., Lydon, F., and Barr, B. (1995). "Effect of coarse aggregate on elastic modulus and compressive strength of high performance concrete." Cement and Concrete Research, 25(1), 177-186.